國 立 交 通 大 學

材料科學與工程學系

博士論文

多壁碳奈米管輔助聚合物氣體感測器陣列於電子
鼻系統之應用

Multi-walled CNT-assisted polymer gas sensor array for electronic nose system

研 究 生：王立群 (Wang, Li-Chun)

指導教授：郭正次 博士 (Dr. Kuo, Chen-Tzu)

潘扶民 博士 (Dr. Pan, Fu-Ming)

中 華 民 國 101 年 1 月
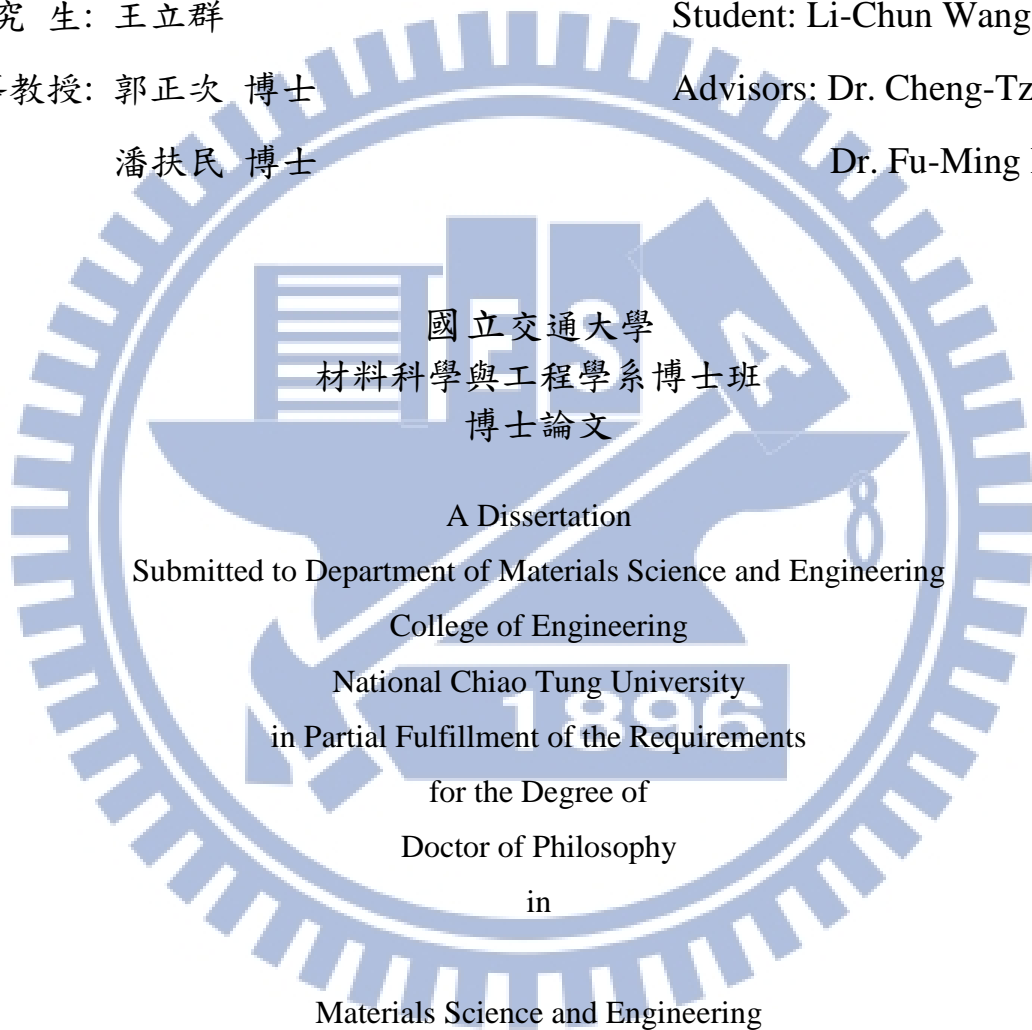
多壁碳奈米管輔助聚合物氣體感測器陣列於電子鼻系統之應用

Multi-walled CNT-assisted polymer gas sensor array for electronic nose system

研 究 生: 王立群　　　　　　　　　　Student: Li-Chun Wang

指導教授: 郭正次 博士　　　　　　　　Advisors: Dr. Cheng-Tzu Kuo

　　　　　潘扶民 博士　　　　　　　　　　　　　　Dr. Fu-Ming Pan

國立交通大學

材料科學與工程學系博士班

博士論文

A Dissertation

Submitted to Department of Materials Science and Engineering

College of Engineering

National Chiao Tung University

in Partial Fulfillment of the Requirements

for the Degree of

Doctor of Philosophy

in

Materials Science and Engineering

Jan 2012

Hsinchu, Taiwan, Republic of China

中華民國 101 年 1 月

多壁碳奈米管輔助聚合物氣體感測器陣列
於電子鼻系統之應用

研究生：王立群　　　　　　　　　　　　　　指導教授：郭正次 教授
　　　　　　　　　　　　　　　　　　　　　　　　　　潘扶民 教授

國立交通大學
材料科學與工程學系博士班

摘　要

　　本研究的目的為開發具八個多壁碳奈米管(MWCNT)輔助之聚合物氣體感測陣列晶片，並以此提昇電子鼻系統在室溫下感測毒化物氣體的靈敏度以及對於多種氣體之辨識能力。此氣體感測晶片共分成兩類，分別是直接以 MWCNTs+PVP 複合材料感測器(MWCNTs+PVP polymer composite sensors)及以聚合物溶液與多壁奈米碳管(MWCNTs)組成之雙層膜堆疊式感測器(polymer / CNTs stacked sensors)。本研究中所使用之測試氣體有三種化學戰劑模擬劑氣體、六種工業毒化物(toxic industrial compound)氣體，以及四種不同酒類等十三種氣體，分別為二甲基甲基磷酸酯(DMMP)、二氯甲烷(DCM)、氰甲烷(ACN)、四氯化碳(CCl_4)、氯仿($CHCl_3$)、四氫呋喃(THF)、甲苯(Toluene)、二甲苯(Xylene)、甲乙酮(MEK)、清酒(Japanese sake)、高粱酒(Kinmen sorghum)、 藥酒(medicinal liquor)、威士忌(Scotch whisky)，在室溫下針對不同濃度的目標氣體進行測試。

　　而多壁碳奈米管與 PVP 聚合物複材感測器(MWCNTs+PVP polymer composite sensors)及以聚合物與多壁奈米碳管(MWCNTs)形成之雙層膜堆疊式感測器(polymer / CNTs stacked sensors)所使用之多壁奈米碳管(MWCNTs)材料，是在熱化學氣相沉積(thermal CVD)系統中，以鐵鈷(FeCo)合金濺鍍於矽基板上當觸媒並於其上覆蓋一層氧化鎂材料輔助成長，再以乙烯(C_2H_2)及氫氣(H_2)為成長氣體所獲得。之後並以掃瞄式電子顯微鏡(SEM)及拉曼光譜儀(Raman spectroscopy)來檢測其材質特性。另外亦將多壁奈米碳管(MWCNTs)由試片上刮下以穿透式電子顯微鏡(TEM)進行檢測。而所使用的八種高分子是根據線性溶合方程式(linear salvation energy relationship (LSER) theory)理論，及其物理吸附鍵結(physical absorption bonding)性質所挑選。兩個類型的氣體感測器均是以液滴滴定的方式製作以便簡化氣體感測膜的製程。

　　此類元件用來進行氣體感測的原理是因為感測膜吸附目標氣體之後其電性會產生變化，從而了解其對氣體的感測行為並將所獲得數據加以整理呈現。而聚合物與多壁奈米碳管(MWCNTs)形成之雙層膜堆疊式感測器(polymer / CNTs stacked sensors)對各種氣體接觸後產生多組不同的電阻改變量，接著歸納反應情形為長條圖及雷達圖，進而建立各類型化學氣體感測資料庫。之後再使用兩種主要的辨識方法：主成分分析法(principal

component analysis (PCA))於電腦上運算以及最近鄰演算法(k-nearest neighbor (k-NN))於電子鼻系統上進行辨識，進而判定所感測的氣體。

　　與多壁碳奈米管與 PVP 聚合物複材感測器(MWCNTs+PVP polymer composite sensors)比較，此種雙層式堆疊的氣體感測元件最大的好處是碳奈米管層可以被聚合物層包覆及保護，避免其直接與反應氣體接觸以延長其使用時間、元件壽命及其氣體感測靈敏度。另外實驗結果亦顯示，本研究所使用的十三種氣體，於主成分分析法(PCA)以及最近鄰演算法(k-NN)上的辨識結果均非常好。此外，針對部份氣體的感測結果亦與其氣體濃度呈現線性關係，且如加以控制環境及減少外界的干擾，其感測靈敏度應可達到ppm 等級，是十分值得發展的氣體感測系統。

關鍵字: 多壁碳奈米管、氣體感測元件、電子鼻系統。

Multi-walled CNT-assisted polymer gas sensor array
for electronic nose system

Student: Li-Chun Wang

Advisors: Professor Cheng-Tzu Kuo

Professor Fu-Ming Pan

Department of Materials Science and Engineering

National Chiao Tung University

Abstract

For room temperature toxic gas sensing and gas specificity improving, two system chips with two different sensor configurations of a multiwalled carbon nanotube (MWCNT) - assisted polymer gas sensor array of eight sensor types were successfully developed and compared their performance. One chip employed MWCNTs + polyvinylpyrrolidone (PVP) polymer composite sensors and another chip polymer/carbon-nanotubes stacked sensors. Gases tested include three simulants of chemical warfare agents, six toxic industrial compound gas and four commercial liquors, i.e. including dichloromethane, acetonitrile, dimethyl- methyl phosphonate, carbon tetrachloride, chloroform, tetrahydrofuran, toluene, xylene, methyl-ethyl ketone, Japanese sake, Kinmen sorghum, medicinal liquor, and Scotch whisky, respectively.

The chip with composite sensors used a mixture of MWCNTs + PVP polymer as sensing material. The chip with stacked sensors employed sensing materials of MWCNTs as the base layer and one of the eight polymer types as the top layer materials. MWCNT powders were scratched from Si wafer, which were prepared by thermal chemical vapor deposition on MgO/FeCo/Si substrate with C_2H_2 + H_2 as source gases, where FeCo acts as catalyst.

Morphology and bonding structure of the as-deposited MWCNTs were characterized by SEM, TEM and Raman spectroscopy to identify their metallic properties. The eight polymer types were selected according to their linear salvation energy relationship, and physical absorption bonding property differences with respect to different gases in the group for greater gas specificity improvement. Both chips were prepared on Si (001) wafer by solution drop casting method to simplify the process. The principle of gas sensing is basically to measure the different degrees of resistivity changes of the eight sensor types upon contact with a target gas. The sensing responses of eight sensor types on a chip were recorded as a function of time to form a so-called "sensor radar plot". These data were then analyzed by two different mathematical analysis methods, including principal component analysis (PCA) on a personal computer or laptop, and k-nearest neighbor (k-NN) classification algorithm on an electronic nose system.

By comparing the chip with the composite sensors, one of the advantages of the chip with the stacked sensors having a polymer overlayer above the MWCNT layer is to protect the MWCNT from direct interaction with the gas to improve sensor life and sensitivity. The results also indicate that the specificity for one of the three analyte groupss can be determined by its specific radar plot pattern at room temperature for each testing run, using the chip with the stacked sensors made of eight different selected polymer types. The pattern analyses of the radar plots can be simplified through PCA and k-NN analyses. By extrapolation and careful process monitoring, the maximum sensitivity of few ppm among the eight different sensor types is likely. The results also show that a linear relationship between the resistance response and analyte concentration is clearly evident for these toxic gases. The gas sensing mechanisms are discussed in the text.

Keywords: Carbon nanostructures; Gas-sensing devices; Sensing mechanism.

Acknowledgements (致謝)

Contents

List of Symbols

A	Cross section area of a diffusion tube in gas generator
ACN	Acetonitrile (solvent)
C	Concentration of testing gas
CNT	Carbon nanotube
CCl_4	Carbon tetrachloride (solvent)
$CHCl_3$	Chloroform (solvent)
CVD	Chemical vapour deposition
d	Inter-electrode spacing
d	plane spacing of a crystal lattice
D	Diffusion coefficient
D-band	Disorder-induced feature in Raman spectra
dc-PECVD	Direct current plasma-enhanced chemical vapour deposition
DCM	Dichloromethane (solvent)
DMMP	Dimethyl- methyl phosphonate (solvent)
$\Delta R/R_b$	Electrical resistance ratio
E	Electric field
EDX	Energy dispersive X-ray spectroscopy
ECR	Electron cyclotron resonance
F_c	Total flow rate of the gas mixture
FESEM	Field-emission scanning electron microscopy
FET	Field effect transistor
E-Nose	Electronic nose (system)
G-band	Tangential mode in Raman spectra
GPIB	General-purpose interface bus
HPMC	Hydroxypropyl methyl cellulose (polymer)
HRTEM	High-resolution transmission electron microscopy
I_G/I_D	The G-band and D-band intensity ratio of a Raman spectrum
LSER	Linear salvation energy relationship
k-NN	k-nearest neighbor method (classification algorithm)
MFC	Mass flow controller
MEK	Methyl-ethyl ketone (solvent)
MOSFET	Metal-oxide-semiconductor field effect transistor
MPCVD	Microwave plasma chemical vapour deposition
M_w	Molecular weight
MWCNT	Multi-walled carbon nanotube

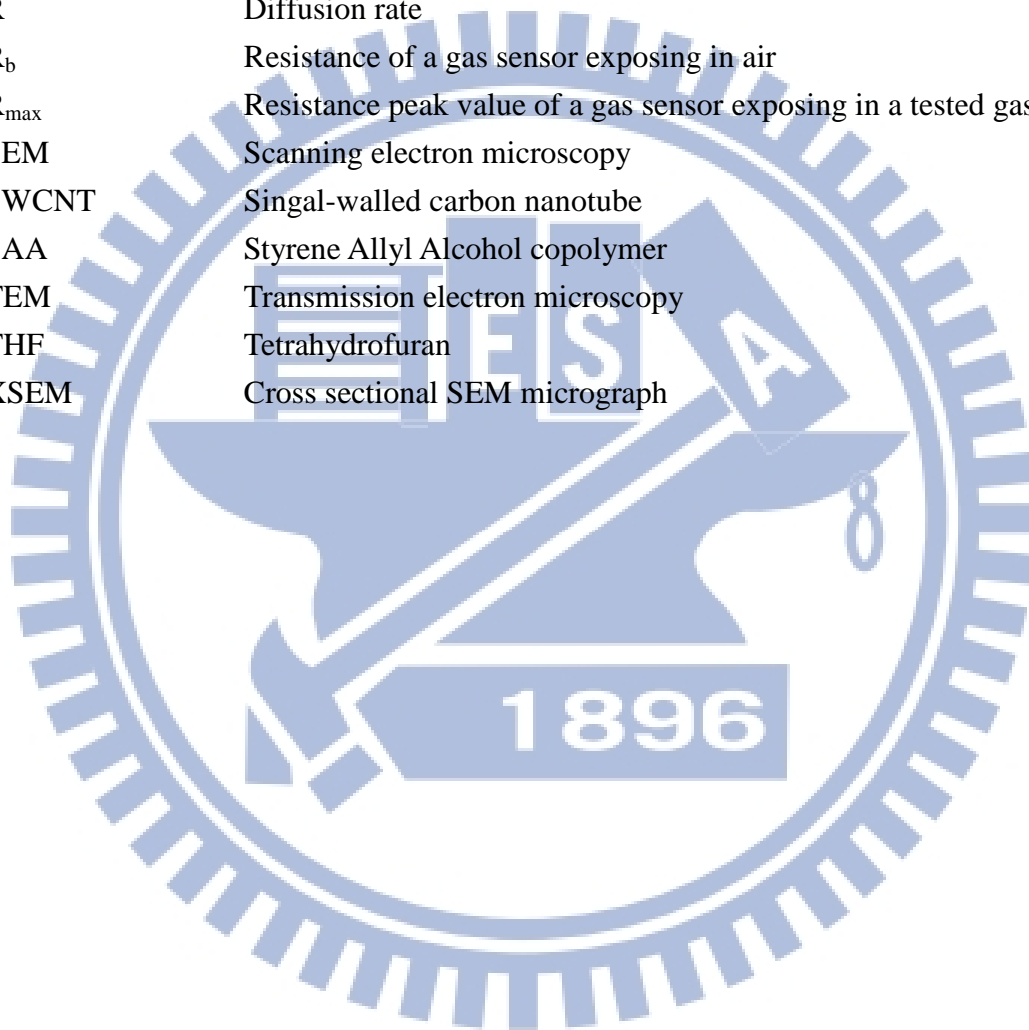| PCA	Principal component analysis method (classification algorithm)
PEA	Poly(ethylene adipate) (polymer)
PMS	Poly(alpha-methylstyrene) (polymer)
PMVEMA	Poly(methyl vinyl ether-alt-maleic acid) (polymer)
PVBC	Poly(vinyl benzyl chloride) (polymer)
P(VDC-AN)	Poly(vinylidene chloride-co-acrylonitrile) (polymer)
PVP	Polyvinylpyrrolidone (polymer)
P	Partial pressure of solvent
R	Diffusion rate
R_b	Resistance of a gas sensor exposing in air
R_{max}	Resistance peak value of a gas sensor exposing in a tested gas
SEM	Scanning electron microscopy
SWCNT	Singal-walled carbon nanotube
SAA	Styrene Allyl Alcohol copolymer
TEM	Transmission electron microscopy
THF	Tetrahydrofuran
XSEM	Cross sectional SEM micrograph

Table Captions

Chapter 3

Chapter 4

Chapter 5

Figure Captions

Chapter 2

Chapter 3

Chapter 4

Chapter 5

Chapter 1

Introduction

Carbon nanostructured materials have attracted considerable research attentions in the past few decades due to their unique physical properties, such as high specific surface area, good corrosion resistance, tailorable pore size, and excellent electronic conductivity. These properties make carbon nanostructured materials suitable for applications as electrodes or as supports for electrode catalysts. For gas sensing applications, CNT-derived high-sensitivity gas sensors for various gases and nerve agents, such as ammonia, ethanol vapor, NO_2, CO, CH_4, and dimethyl methylphosphonate (DMMP) have been reported [Li et al. 2003; Snow et al. 2005; Someya et al. 2003]. In recent years, the various E-Nose (electronic nose) systems[Bartlett et al. 1993; Craven et al. 1996; Gardner 2004; Gardner and Bartlett 1994; Pearce et al. 2003], designing in an effort to microminiaturize the size, were developed to cut down the prices, to offer higher gas sensitivity and higher gas specificity. The sensing materials used for chemical resistors could be divided into two major types: inorganic semiconductors [Gopel and Schierbaum 1995; Meixner et al. 1995] and organic polymers [Gardner and Bartlett 1995; Lonergan et al. 1996; Slater et al. 1993]. The sensing material is essentially to trigger physical reactions with the adsorptive analytes and then to change its resistivity or dielectric constant. The concentration of the analytes can be determined from the amount of property variation. The sensing polymer materials were generally fabricated in the form of thin films, which might provide the following advantages [Doleman et al. 1998; Ryan and Lewis 2001; Severin et al. 2000]. In addition to be readily coupled to microstructure sensor[Hagleitner et al. 2001], the thin film sensors can enhance the gas adsorption and desorption abilities to improve the gas sensitivity and the quick repeating use, respectively.

In this study, MWCNTs and conducting polymers, which used in the chips, were selected according to their linear salvation energy relationship (LSER) and physical absorption bonding properties [Kim et al. 2005; Wang et al. 2010]. These polymer/CNTs stacked sensors are simple to operate and the sensing film quality can be easily controlled through the solution drop casting process. By using the well-controlled gas sensing experiments, the different sensing behaviors of the MWCNT-assisted polymer stacked sensors in the array can be determined.

By collating data, based on different resistance to volume variations of each sensor in the gas sensing array under different gases and concentrations, and summarized the cases in the response bar chart, or called "the radar plots", the selected chemical gas sensing materials library can be established. In other words, the gas specificity can be enhanced by selecting polymer sensing materials with different sensing responses to different gases to form different patterns of the radar plots. By using the method of principle component analysis (PCA) on a PC, or the k-nearest neighbor (k-NN) classification algorithm on the portable system, the analyzing works to determine the gas specificity and concentration can be simplified, and the feasibility has been demonstrated with electronic nose (E-Nose) system. The analytes include three simulants of chemical warfare agents, six toxic industrial compound gas, four commercial liquors and methanol.

Chapter 2

Literature reviews

2.1 Carbon nanostructured materials

Carbon is the fourth most abundant chemical in the universe (by mass). Due to its unique electron structure, it readily forms covalent bonds with itself and other elements. Thus carbon is chemically one of the most flexible elements known to man, as seen in the contrast between diamonds (the hardest material discovered) and graphite (one of the softest materials). Carbon may form a variety of crystals, amorphous and nanostructured materials with extremely different properties. Carbon nanotubes (CNTs) and fullerenes are two of the most attractive nanostructured materials due to their unique electronic, mechanical, optical, and chemical properties[Dekker 1999]. Carbon nanostructured materials have been reported a broad range of applications in the fields of molecular electronics[Avouris 2002], sensing materials[Wang 2004], nano- and micro electromechanic devices[Tombler et al. 2000], field-emission display materials [Choi et al. 1999], energy storage[Che et al. 1998], and composite materials[Moniruzzaman and Winey 2006].

2.1.1   Structure and property of Carbon nanotubes

CNTs, which are formed by rolling the graphene sheets, were first discovered by Iijima in 1991[Iijima 1991]. In early twentieth century, it becomes one of the most exciting new materials in the field of nanoscience and nanotechnology. Various forms of CNTs have been developed over the past few decades by different fabrication

3

approaches. There are different ways of classification of CNTs. Based on number of graphene layers of tube wall[Pillai et al. 2007; Saito et al. 2004], they are called single-, double- or multi-walled CNTs[Bethune et al. 1993; Iijima and Ichihashi 1993; Wei et al. 2003]. In other words, a single-walled carbon nanotube (SWCNT) can be described as a layer of hexagonal graphene sheet rolled into a seamless cylinder, whilst a multi-walled carbon nanotube (MWCNT) is formed with multiple graphene layers. CNTs also could be classified by tube morphology (bamboo-like/hollow, or helix/straight) [Amelinckx et al. 1994], cap morphology (close/open) [Pan et al. 1999], growth mode (tip-/base-growth) [Abdi et al. 2006; Bower et al. 2000; Chen et al. 2004; Chen et al. 2000; Choi et al. 2002; Choi et al. 2001; Dupuis 2005; Fan et al. 1999; Gulino et al. 2005; Hart et al. 2006; Hsu et al. 2002; Kuo et al. 2003; Lee et al. 1999; Lee et al. 2001; Lee and Park 2000; Lee et al. 2004; Lin et al. 2003b; Melechko et al. 2002; Murakami et al. 2000; Ren et al. 1998; Yap et al. 2006; Zhao et al. 2006], or crystal structures (zigzag/chiral/armchair, as shown in Fig. 2-1)[Ge and Sattler 1994; Saito et al. 1992].
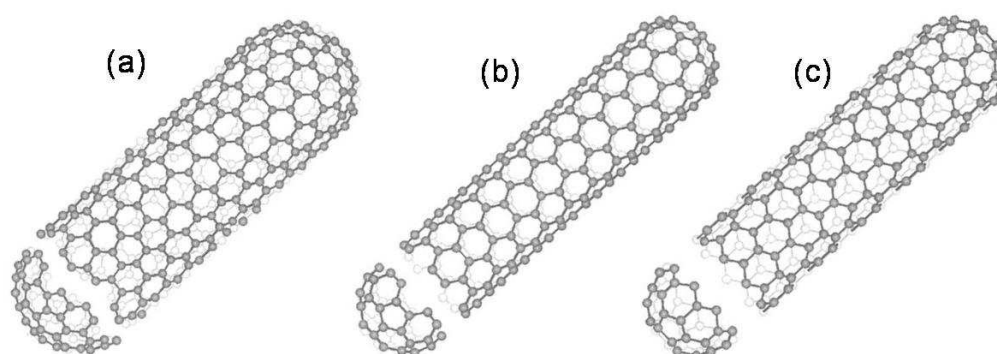
Fig. 2- 1 Schematic drawings of (a) Chiral-type, (b) Armchair, and (c) Zigzag CNTs (Lau and Hui 2002).

These three structural arrangements may be classified as non-chiral and chiral structural types, depending on their rolling direction[Saito et al. 2004] For non-chiral structure of SWCNTs, the honey comb lattices of the nanotube are parallel to the tube axis, which can further be classified as armchair (Fig. 2- 1b) and zigzag (Fig. 2- 1c) arrangements [Saito et al. 1992]. For the armchair structure, two C-C bonds on opposite

sides of each hexagonal lattice are perpendicular to nanotube axis, whereas for the zig-zag structure, the bonds are parallel to nanotube axis. Unlike non-chiral structures, the C-C bonds in chiral structures (Fig. 2- 1a) are with an angle to the nanotube axis.
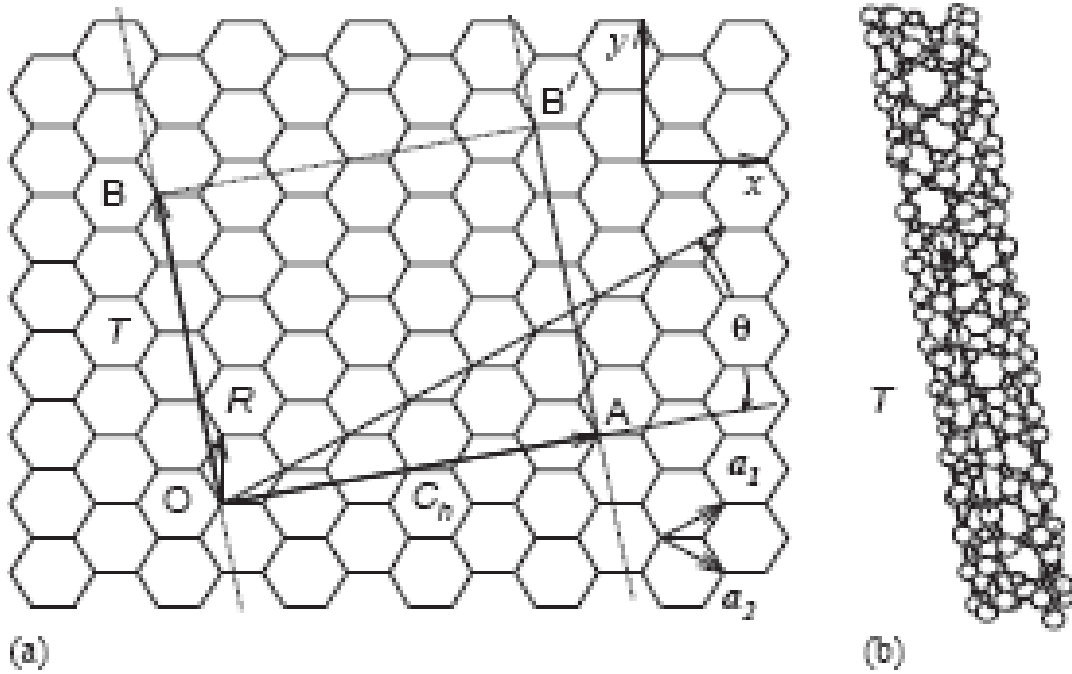
Fig. 2-2 (a) The unrolled honeycomb lattice of a nanotube and (b) (4, 2) SWCNT, showing the translation vector T [Dresselhaus et al. 2005b].

Formation of CNT from a grapheme sheet was analyzed mathematically by Fig.2-2. When sites O and A, and B and B' in Fig. 2-2 are connected, a portion of a graphene sheet can thus be rolled seamlessly to form a SWCNT. Meanwhile, vectors OA and OB are defined as the chiral vector, C_h, and the translational vector T of the nanotube. This rectangle portion, OAB'B, is then defined as a unit cell of the nanotube. Generally, a SWCNT is mathematically specified by a chiral vector, C_h, (Fig. 2-2a), given by the following equation [Dresselhaus et al. 2005b; Saito et al. 2004]:

$$C_h = na_1 + na_2 \equiv (n,m) \qquad \text{(Eq. 2-1)}$$

Where a_1 and a_2 are unit vectors of the two-dimensional (2D) hexagonal lattice, n and m are integers. Meanwhile, chiral vector is often described by a pair of indices (n, m),

5

for example, with a chiral vector $C_h = (n, m) = (4, 2)$, the nanotube in Fig. 2-2 is described as a (4, 2) SWCNT.

The electrical properties of CNTs can either be metallic or semiconducting, depending on their tube diameter and chirality. Nanotubes with n-m = 0 are metallic while all the others are semiconducting. In terms of mechanical properties, CNTs normally exhibit a Young's modulus of 0.8~5.0 TPa and a tensile strength of 10~150 GPa owing to the presence of C-C bonds. They are among the strongest and stiffest fibers known to date. Thermally, CNTs have a high thermal stability both under vacuum and air and an excellent thermal conductivity as high as ca. 3500 W/ (m·K), which is five times higher than copper at room temperature.

2.1.2　Synthesis methods of CNTs

(a) Arc-discharge method

CNTs were first synthesized by arc-discharge method, as reported by Iijima and co-workers in 1991 [Iijima 1991]. Fig. 2-3 shows[Satio 1995] the schematic drawing of the arc-discharge system, in which two graphite rods are used as anode and cathode electrodes, respectively.
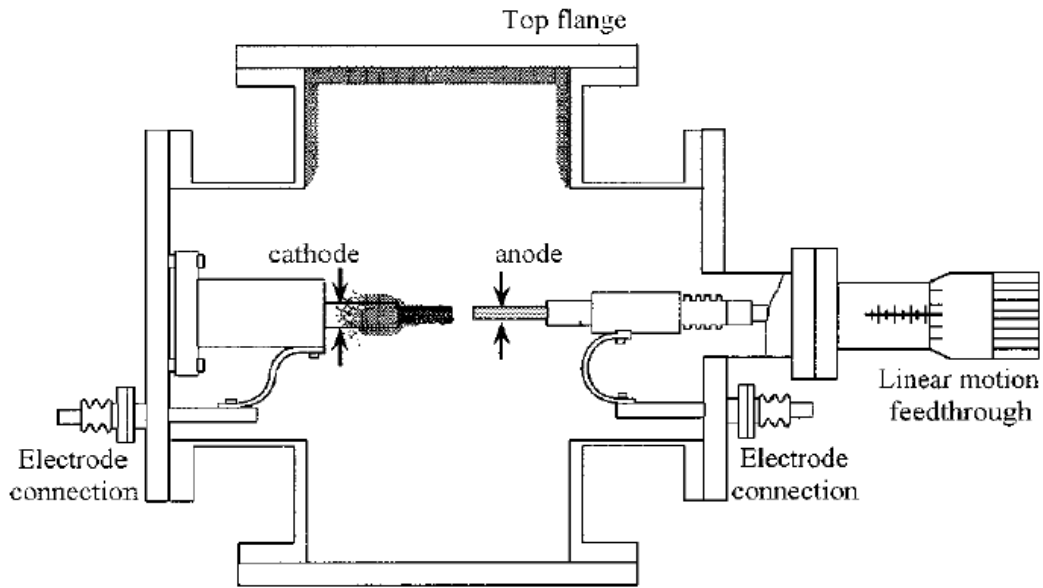
Fig. 2-3 Schematic diagram of arc-discharge system [Saito et al. 1996].

The discharge system is normally operated at a voltage ranging from 20 to 40 V and a current from 40 to 100 Ampere under either He or Ar gas pressure of ca. 10~500 Torr. Carbon clusters emerging from the anodic graphite rod via electron bombardment may be deposited on the cathode surface. These carbon products may include amorphous carbon, fullerenes, carbon cluster, carbon nanotubes, and other carbon structures. During the CNT production process, arcing occurs when DC voltage is applied between these two electrodes. By incorporating a desirable amount of metallic catalysts, such as Fe, Co, Ni, and Y, SWCNTs are formed at the anode [Bethune et al. 1993], while MWCNTs can be fabricated by using pure graphite at both electrodes. Therefore, post treatment is often required to purify the nanostructures for practical applications. In addition, the drawback of this method is its low yield in CNTs.

(b) Laser ablation

Laser ablation was first reported by Guo and co-worker in 1995[(Guo et al. 1995)], as illustrated in Fig. 2-4. An incident laser beam is applied to vaporize a graphite target under helium or argon gas atmosphere at a pressure of 500 Torr. The products are swept out by the flowing gas and eventually deposited on the water cooled collector. As such, it is also named as the laser vaporization method. The graphite target used in this scheme often contains a small amount of Co, Ni, Fe, or Y as catalyst, SWCNTs grow very fast from atoms and molecules within these first few milliseconds, the majority of growth appears to occur from a feedstock of mixed nanoparticles over seconds of annealing time. [(Puretzky et al. 2000)].
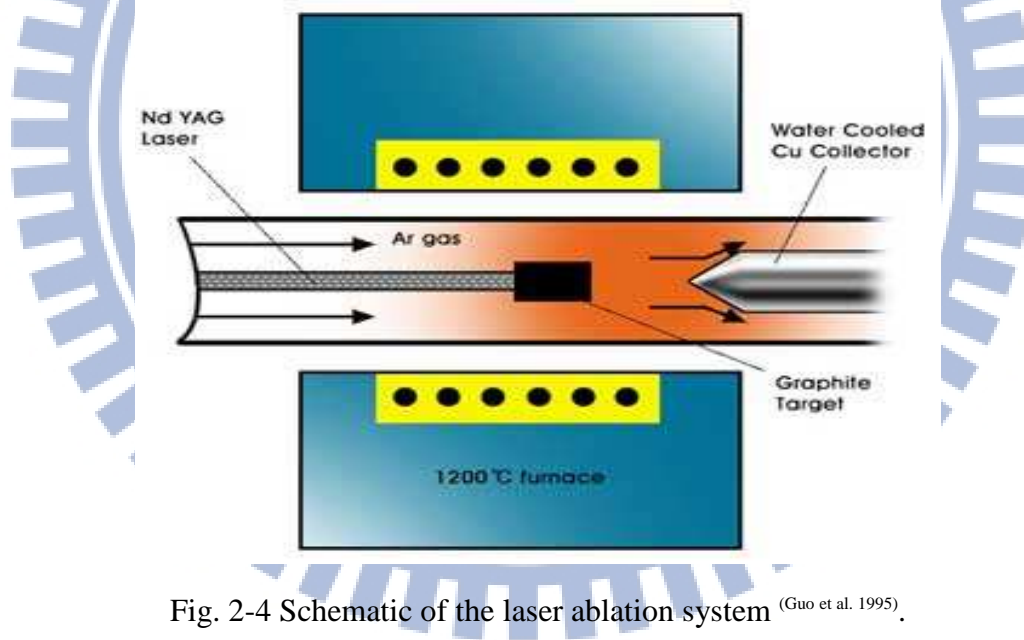
Fig. 2-4 Schematic of the laser ablation system [(Guo et al. 1995)].

(c) Chemical vapor deposition

Chemical vapor deposition (CVD) method has been known to be a mature technique in thin film processing. A variety of different films can be fabricated by CVD method, covering from metals, semiconductors to insulators. By using the CVD method, arrays of CNTs can be produced through decomposition of carbon-containing gaseous species (such as CH_4[Dai 2002], C_2H_2[Wang et al. 2001], C_2H_4[Cheung et al. 2002], C_6H_6[Yang et al. 2003], CO[Dai et al. 1996], etc.) on various substrates containing transition metal catalysts. During the CVD process, it is essential to introduce some forms of energy to decompose the precursor gases and to deposit the reaction product on the substrate surface. The energy introduced may be thermal, microwave, RF power, or other forms of energy, thus, leading to different process names for the production of CNTs. For examples, microwave plasma enhanced CVD (MPE-CVD)[Lin et al. 2003a], electron cyclotron resonance CVD (ECR-CVD)[Kuo et al. 2003], inductively coupled plasma CVD (ICP-CVD)[Delzeit et al. 2002], RF plasma enhanced CVD (rf-PE-CVD)[Kato et al. 2004], DC plasma enhanced CVD (dc-PE-CVD)[Hofmann et al. 2007b], thermal CVD[Lee and Park 2000], hot filament CVD (HF-CVD)[Yang et al. 2004], etc. In general, these CVD systems can be roughly classified as thermal and plasma CVD on the basis of their working principles. Typically, the former process includes a substrate preheating zone and CNTs are grown while the precursor gases are flowing through the catalyst/substrate (shown in Fig. 2- 5). The heat source of plasma CVD mainly arising from the plasma, as illustrated by a dc-PE-CVD system in Fig. 2- 6. Compared with arc-discharge and laser ablation methods, CVD enhanced by plasma is more economical (lower reaction temperature) and the reaction process can also be controlled more easily. Moreover, it is superior compared to other methods in terms of the purity, yield, and controlled alignment of the CNT products. Recent advancements in plasma enhanced CVD have been focusing on the development and fabrication of vertically aligned CNTs.

9
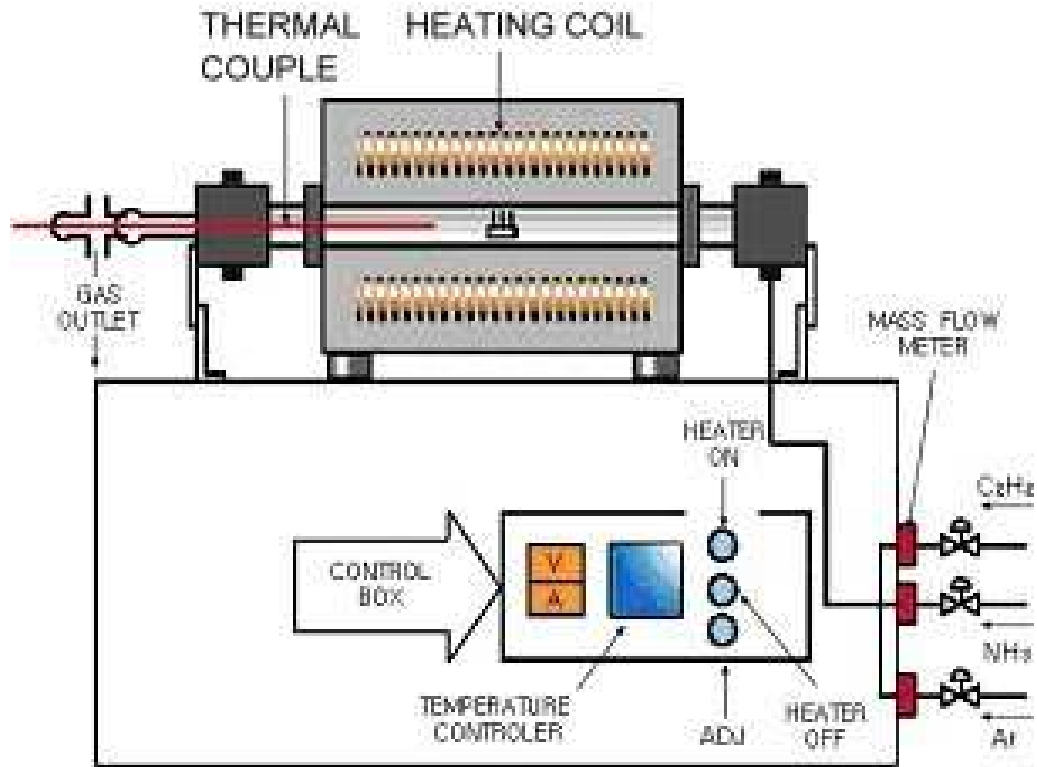
Fig. 2- 5 Schematic illustration of the thermal CVD system [(Lee et al. 2001)].
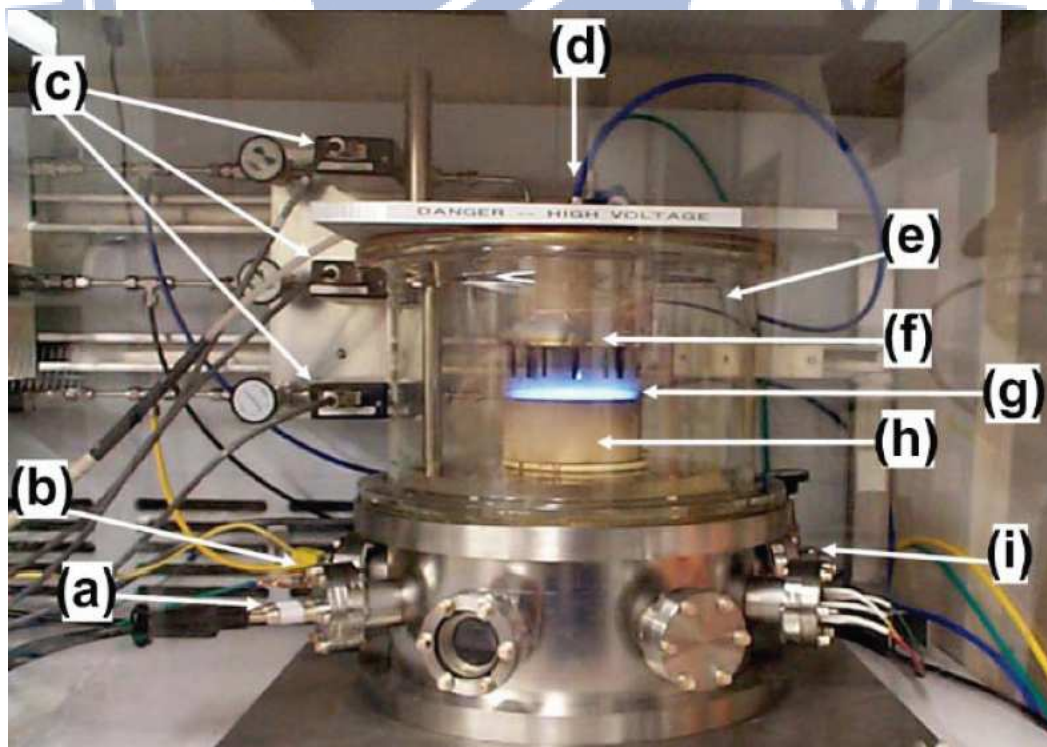
Fig. 2- 6 A dc-PE-CVD reactor for the fabrications of CNTs and nanofibers [(Chen 2005)].

2.2 Structure analyses and property measurements

The principles of typical microstructure examination techniques and Raman spectroscopy property measurement commonly used for characterization of porous and nano carbon materials are summarized below:

2.2.1   Scanning electron microscopy (SEM)

Generally, a scanning electron microscope (SEM) is a type of electron microscope that produces images of a sample by scanning over it with a focused beam of electrons. The electrons interact with electrons in the sample, producing various signals that can be detected and that contain information about the sample's surface topography and composition. The SEM apparatus is consists of an electron gun, which serves to generate electron beams that, in turns, are accelerated under high voltage (0.4-40 keV). SEM can achieve resolution better than 1 nanometer. By deflecting the incident beams with the focusing coils, a two-dimensional image can be obtained by detecting the reflected secondary and backscattered electrons.

All samples must also be of an appropriate size to fit in the specimen chamber and are generally mounted rigidly on a specimen holder called a specimen stub. Several models of SEM can examine any part of a 6-inch (15 cm) semiconductor wafer, and some can tilt an object of that size to 45°. The SEM was often being employed to observe the growth behaviors of carbon nanotubes on the substrates.

2.2.2   Transmission electron microscopy (TEM)

Transmission electron microscopy (TEM) is a microscopy technique where a beam of electrons is transmitted through an ultra thin specimen, interacting with the

specimen as it passes through. An image is formed from the interaction of the electrons transmitted through the specimen; the image is magnified and focused onto an imaging device, such as the fluorescent screen, or to be detected by a CCD camera sensor. Transmission electron microscopy is the most important technique for studying microstructure of materials in great detail. Typically, an electron beam with accelerating voltage of 100-400 keV would illuminate a region of the specimen. The transmitted and diffracted electrons are recombined by the objective lens to form a diffraction pattern in the back focal plane of that lens and a magnified image of the sample in its image plane. A number of intermediate lenses are used to project either the image or the diffraction pattern onto a fluorescent screen for observation. The screen is usually lifted and the image may be printed out on photographic film or stored for recording purposes.

The methods for TEM sample preparation from carbon deposit can be categorized into some main groups: (1) Ultrasonic method, but this carbon nanotube (CNT) preparation method disenables to determine the growth mode and may lead to the structural damage and removal of catalysts from CNTs[Park et al. 2002]. (2) Ion thinning technique, the cutting and ion thinning techniques preserve the CNT structure and enable unambiguous determination of the CNT ends, as well as evaluation of interfacial structure of CNTs –catalyst – substrate[Zhang et al. 2001].

Some researchers also used this instrument to observe dynamic effects before and during catalyst-assisted CVD of CNFs and SWCNTs[Hofmann et al. 2007a]. And they also found data of various stages of SWCNT growth. The TEM images also show the catalyst crystals for which SWCNT nucleation has stopped early. A small-sized carbon cap has emerged on top of each catalyst particle. The carbon network surrounding the deactivated catalyst particle forces a stronger faceting.

2.2.3 Raman spectroscopy

Raman spectroscopy is a spectroscopic technique used to study vibrational, rotational, and other low-frequency modes of the materials in a system. Normally, a monochromatic laser beam is used as the incident light source, upon irradiating on the substrate, photons may be absorbed, scattered, or not interacting with the sample. When the light is elastically scattered from an atom or molecule, the scattered photons have almost the same frequency with the incident photons. However, a small fraction of the light may be scattered during excitation, such scattered photons would have a frequency different from, and usually lower than, the frequency of the incident photons. As such, the energy difference between the monochromatic light and the Raman scattered light should be equal to the energy involved in changing the molecule's vibration state [Dresselhaus et al. 2002; Dresselhaus et al. 2005a; Jorio et al. 2003]. This energy difference is called the Raman shift. Typically several different Raman signals may often be observed; each being associated with different vibration or rotational motions of molecules in the sample.

Typically, Raman spectroscopy is also a popular technique for determining the diameter distribution, chirality, purity, and architecture of CNTs[Dresselhaus et al. 2002]. The most prominent Raman features in CNTs are the radial breathing modes (RBMs), the higher frequency D (disordered), G (graphite), and G' (second-order Raman scattering from D-band variation) modes. The RBM mode is a confirmation for the presence of SWCNTs in a sample, since it is not present in graphite. This mode is located between 75 and 300 cm^{-1} from the excitation line, and is associated with the symmetric movement of carbon atoms in the radial direction. The RBM frequency is inversely proportional to the nanotube diameter with the relationship:

$$\omega r \ (cm^{-1}) = 224 \ (cm^{-1}) \ /d_t \ (nm) \qquad\qquad \text{(Eq. 2-2)}$$

Tube diameters between 0.8 and 1.3 nm give nearly identical results. Most single-grating Raman spectrometers have cutoff frequencies between 100 and 120 cm^{-1}, which restricts the range of tube diameters smaller than 2 to 2.5 nm. The D band, which normally locates at ca. 1300 cm^{-1} is associated with carbons with the sp^3 structures, such as functionalized and amorphous carbons, whereas the G band locates at ca. 1600 cm^{-1} is normally assigned to carbons with the sp^2 structure carbon, such as graphite. The G'-band frequency is close to twice that of the D band and is found from 2500 to 2900 cm^{-1}. The G' band is an intrinsic property of the nanotube and graphite, and present even in defect-free nanotubes for which the D band is completely absent.
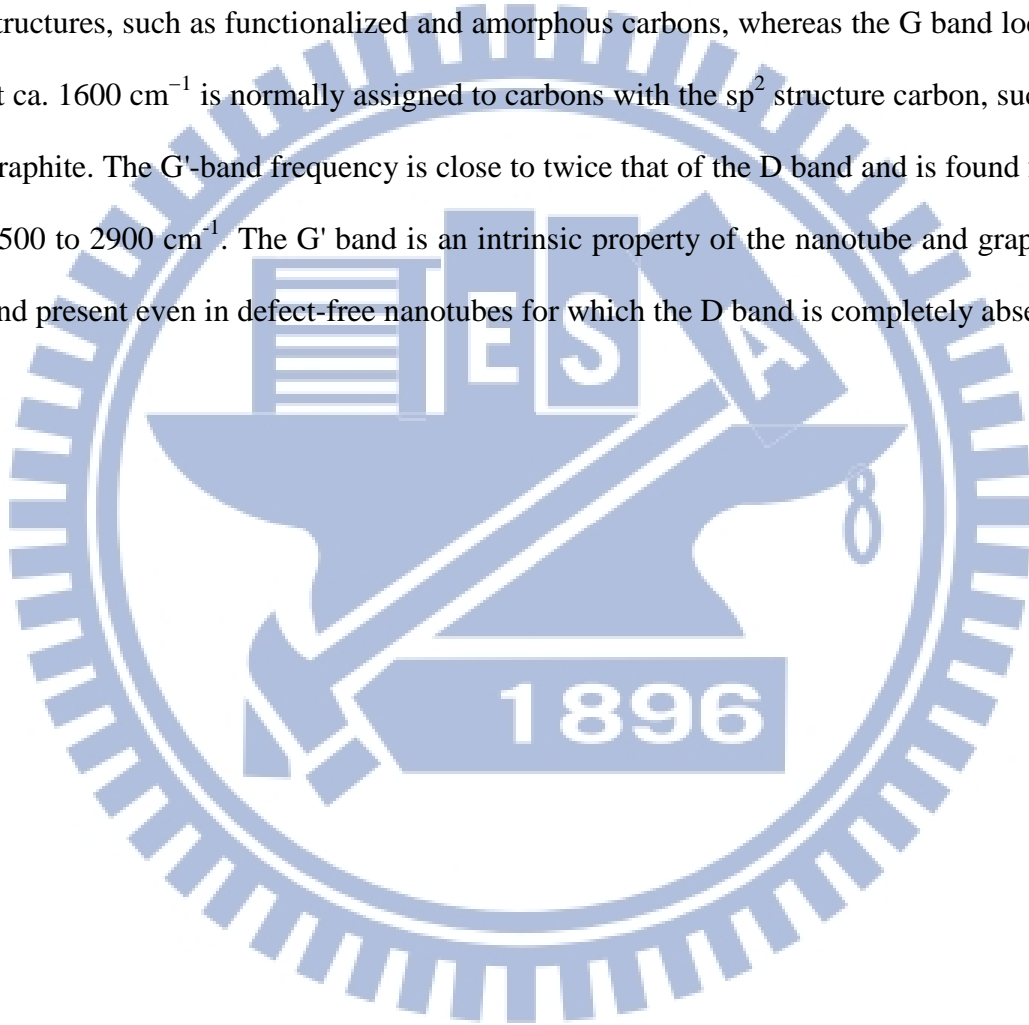
2.3 Gas sensing devices and their working principles

A sensor is a device that measures a physical quantity and converts it into a signal which can be read by an observer or by an instrument. The sensor's sensitivity indicates how much the sensor's output changes when the measured quantity changes. The sensors sorted by type list in the follow: (1) acoustic (2) biological (3) chemical (4) electric (5) magnetic (6) mechanical (7) optical (8) radiation (9) thermal, etc.[ref]

This research will focous on the chemical gas sensor, and will illustrate some of these chemical gas sensors with carbon nanotubes as the sensing materials. The chemical gas sensor contains two or three electrodes, occasionally four, in contact with an electrolyte. The gas diffuses into the sensor, through the back of the porous membrane to the working electrode where it is oxidized or reduced. These sensors features advantages such as compact, light weight, easy to be carried, cheap price, robust and capable of real-time monitoring thus it becomes the research subject for institutes all over the world.

Among all gas sensors, the most representative one is "chemiresistors"[Gardner and Bartlett 1993]. The operating principle of chemiresistor is based on the variation of resistance when a conductive polymer electrode is exposed in chemical gases. The polymer is coated on the circuit board and it will absorb chemical gas and cause swelling of polymer after exposure. This swelling of polymer will then vary the electrode resistance.   The specific resistance variation can be used as signal to estimate the concentration of tested gas. The key to the fabrication of "chemiresistor" is selection of polymer material. There are two major types：(1) Chemiresistor made of ICP (Intrinsically Conducting Polymers), utilizing the semiconductor property of conductive polymer. For the past ten years, this type of sensors was mostly applied to

15

the sensing of chemical and bio-chemical substances. (2) Chemiresistor made of composite material by mixing conductive substances with non-conductive polymers, called LP (i.e. loaded polymers). The conductive substances here are mainly carbon black mixing with inorganic semiconductor or metal powder. The studies on composite sensor array fabricated by mixing different polymers with conductive carbon black were broadly conducted by Lewis[Albert et al. 2000] and the others [Collins et al. 2000; Dekker 1999; Derycke et al. 2002; Postma et al. 2001; Romero et al. 2002; Rosenblatt et al. 2002] for gas specificity applications.
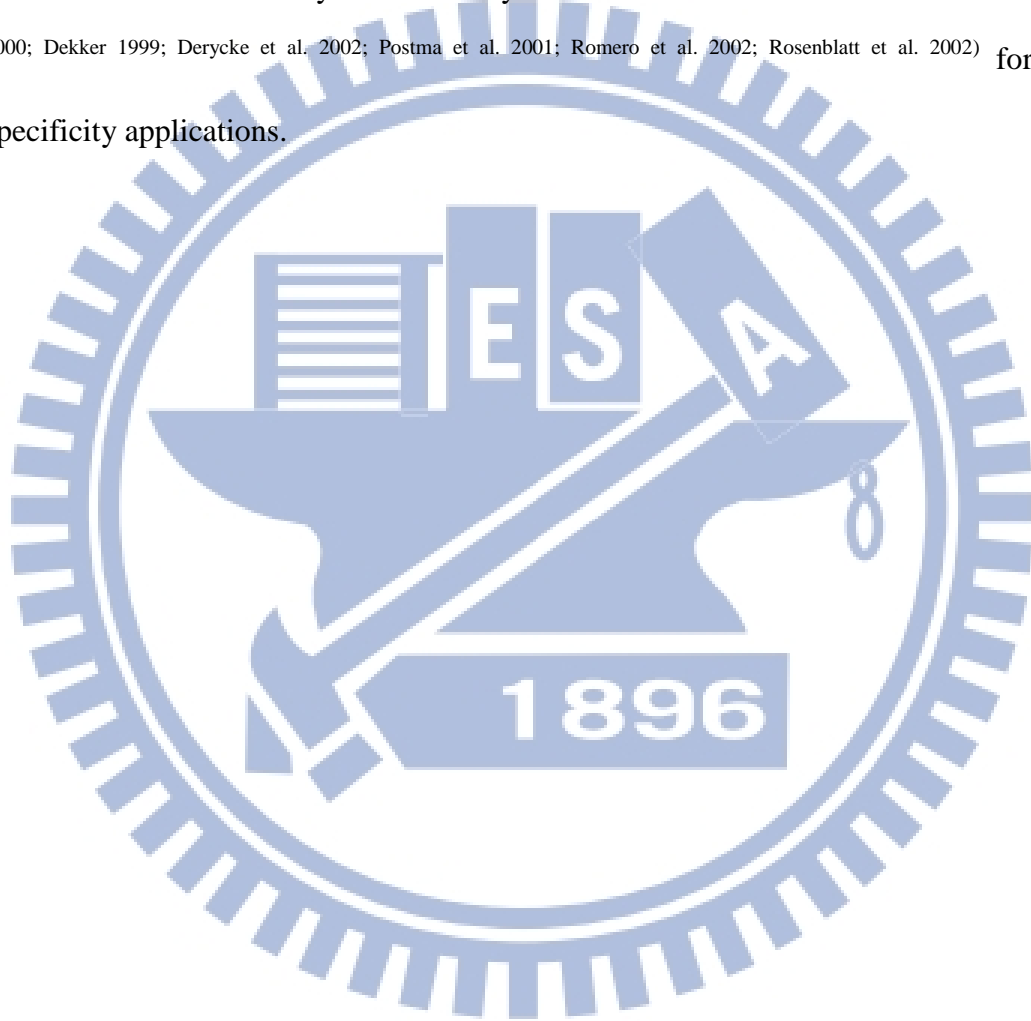
2.4 Carbon nanostructure-based gas sensing devices

Carbon nanotubes (CNTs) are molecular scale quantum wires exhibiting many unique properties for potential nano-devices applications [Chopra et al. 2002; Snow et al. 2003; Snow et al. 2005; Someya et al. 2003]. One of the applications is to act as the gas sensing materials due to its high specific surface area to enhance the gas sensitivity. They also possess high thermal stability to increase possibility to be deployed in most environments. Depending on the types of sensing signals, these devices can be classified into four types, including sensing gas ionization, capacitance, and resistance and field effect changes, as described in the following sections.

2.4.1 Semiconducting CNTs FET Gas Sensors

As addressed in the previous section, SWCNTs can be either semiconducting or metallic. If two metal contacts are connected to each end of an individual semiconducting SWCNT (S-SWCNT), the metal/S-SWCNT/metal device exhibits p-type transistor characteristics. Therefore, the resistance response of CNTs to gas adsorption can be detected with field effect transistors (FETs) by Kong et al [Kong et al. 2000]. Figure 2-7 shows the conductance versus time curves of the transistor upon exposure to NO_2 and NH_3 at room temperature. A sharp increase in conductance of the S-SWCNT FET by about three orders of magnitude was observed after introducing 200 ppm of NO_2 into the testing chamber (Figure 2-7(a)). The response time was about 2–10 seconds, and the sensitivity (the ratio between resistance after and before gas exposure) was about 100 to 1000. Exposure to NH_3 effectively shifts the valence band of the nanotube away from the Fermi level, resulting in hole

depletion and reduced conductance. For the NO$_2$ case, exposure of the initially depleted sample to NO$_2$ resulted in the nanotube Fermi level shifting closer to the valence band. This caused enriched hole carriers in the nanotube and enhanced sample conductance.
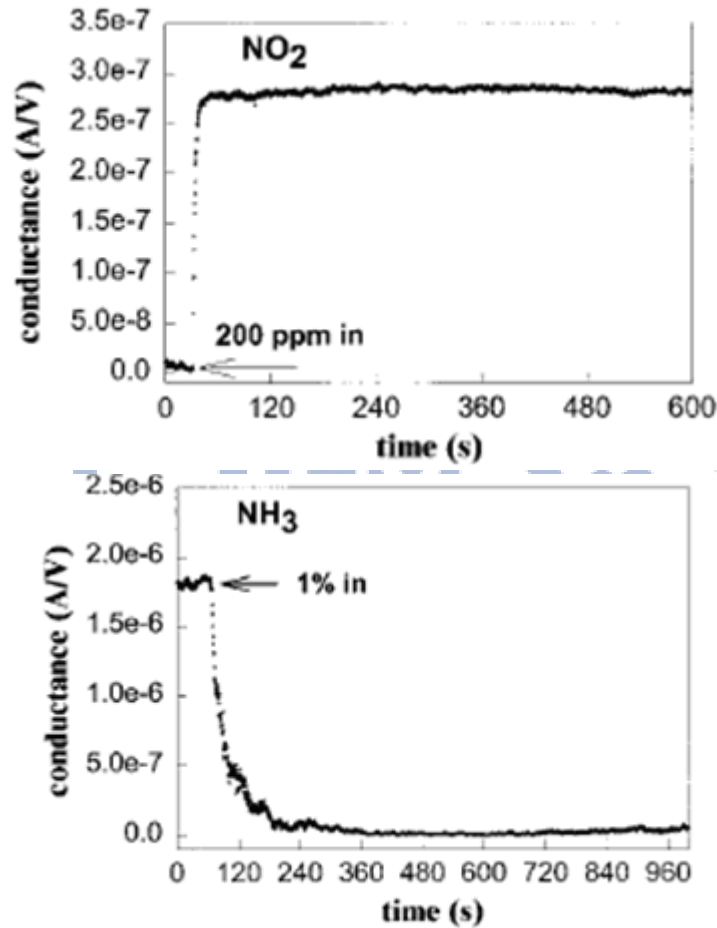
Fig. 2- 7 Conductance change of the CNTs FET sensor when exposed to (a) NO$_2$ and (b) NH$_3$ gases [Kong et al. 2000]

2.4.2 CNTs-Based Resistor Gas Sensors

The resistance change of CNTs under gas exposure can also be detected by resistors with dc voltage. Valentiniet et al [Valentini et al. 2004] designed a CNT serpentine resistor for the detection of various gases including NO$_2$, CO, NH$_3$, H$_2$O, and C$_2$H$_5$OH. The sensor was fabricated by photolithography defining Pt IDEs on Si$_3$N$_4$ substrate,

18

and then CNTs films were grown on the substrate by using radiofrequency plasma enhanced CVD (RF-PECVD) with Ni as the catalyst. Figures 2-8 shows the as-grown CNTs and a scheme of the sensor design.
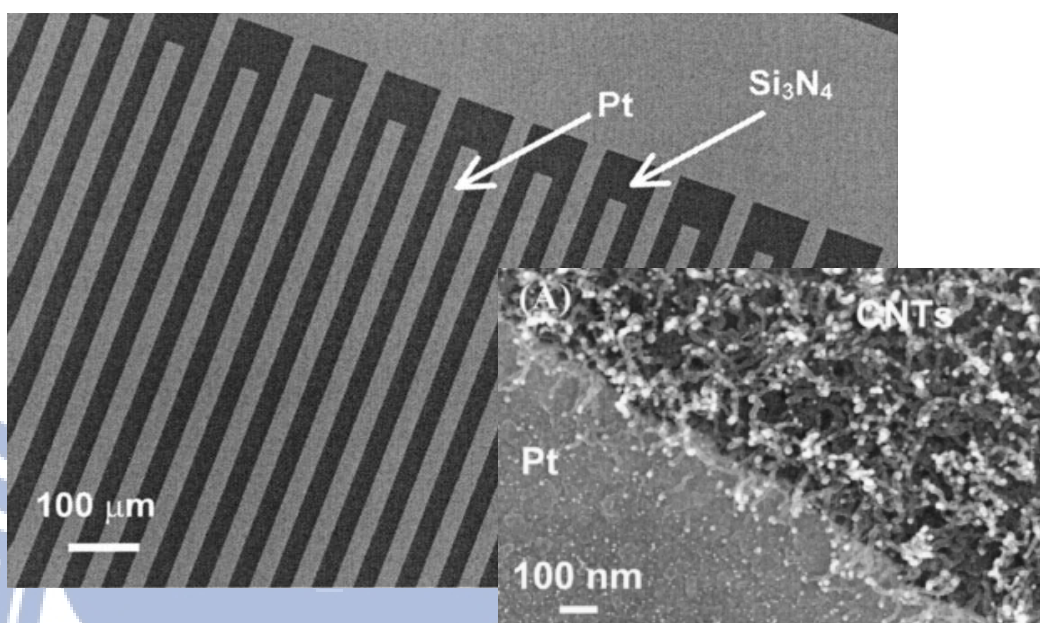
Fig. 2-8 SEM image of prepatterned platinum contacts in resistor geometry [Valentini et al. 2004]

The sensor showed a good sensitivity to NO_2 at room temperature. However, at 165℃, the sensor showed the best response as a tradeoff between the higher resistance variations and the fast and reproducible baseline recovery. The dynamic gas response of CNT films at an operating temperature of 165 °C and NO_2 concentrations ranging from 10 to 100 ppb. From Fig. 2-9 the amazing result is that the CNT film is sensitive to NO_2 at concentrations as low as 10 ppb and that when the NO_2 concentration is increased and decreased stepwise in this range, the sensor response is reproducible and stable. In order to explain the obtained results, the chemical nature of the NO_2 molecule has to be considered. Recent experimental results refer to the electrical conductance of an individual semiconducting single-walled tube strongly increasing upon NO_2 gas exposure and that the NO_2 is identified as an electron

19

acceptor. A possible interpretation of the electrical response of CNT films to NO_2 gas could be the physical absorption of this molecule. NO_2 has an unpaired electron and is known as a strong oxidizer. Upon NO_2 adsorption, a charge transfer is likely to occur from CNTs to NO_2 due to the electron–acceptor character of NO_2 molecules.
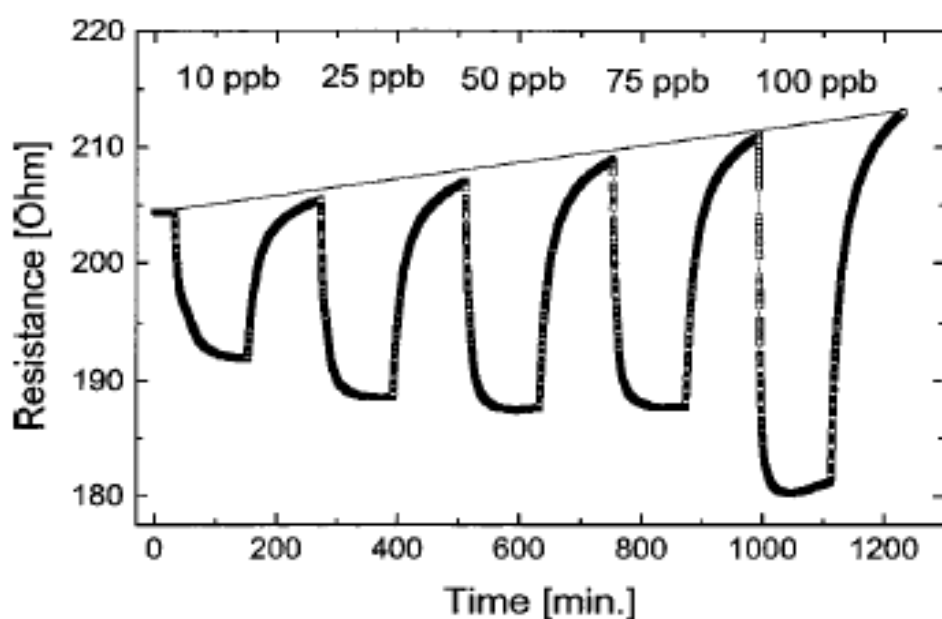
Fig. 2-9 Time-dependence change of the CNTs' resistance at an operating temperature of 165 °C and NO_2 concentrations ranging from 10 to 100 ppb [Valentini et al. 2004]

2.4.3 CNTs-Based capacitance Gas Sensors

Snow et al demonstrated the use of SWCNTs as chemicapacitors for sensing of both polar and non-polar gas molecules at room temperature [Snow et al. 2005]. The SWCNT-based chemicapacitors were fabricated by a CVD-grown SWCNT network on a 250 nm thick thermally grown silicon oxide on a highly doped silicon substrate. The capacitance was measured at 30 kHz and 0.1 V_{AC} bias between the SWCNTs and the heavily doped silicon substrate with 250 nm thick SiO_2. Under the applied bias, strong fringing electric fields radiate outward from the SWCNTs surface and the polarization of the adsorbates can be detected as an increase in capacitance. This

capacitance change was fast (< 4 s response time), sensitive, completely reversible, and with low electrical noise. This approach enables detection of a wide range of analytes including less polar chemical vapors such as dimethyl formamide (DMF) and DMMP (figure 2-10).
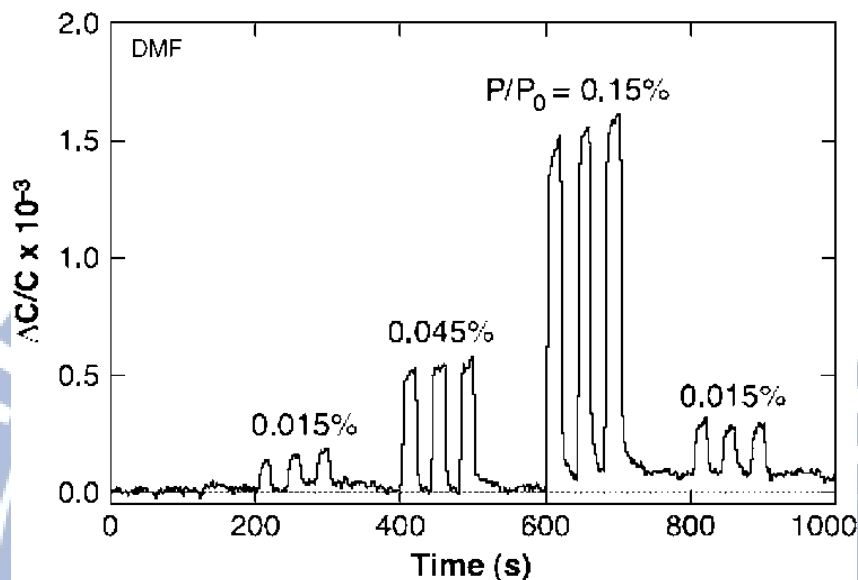
Fig. 2-10 The measured relative capacitance change of a SWCNT chemicapacitor in response to repeated 20 s pulses of dimethyl formamide (DMF) at varying concentrations [Snow et al. 2005].

2.4.4 Carbon Nanotubes Enhanced Ionization Chamber for Gas Sensing

A miniaturized gas ionization sensor with aligned MWCNT film as anode was developed by Ashish Modi et al. in 2003 [Modi et al. 2003]. Figure 2-11 shows a diagram of the sensor structure. It consists of MWCNT film anode, Al plate cathode and a 150 μm thick glass insulator between them. The vertically aligned MWCNT film was prepared by CVD on SiO_2 substrate with tip diameter in the range of 25 ~ 30nm and 30 μm in length (Figure 2-11 (c)). This results in the formation of a "corona" or conduction filament of high ionized gas that surrounds the MWNT tips, and thereby promotes the formation of a self-sustaining interelectrode discharge at very low

21

voltage. Compared with ionization chamber with metal anode (without CNTs), the breakdown voltage of air was brought down dramatically from 960V to 346V. Different gases including NH_3, CO_2, N_2, O_2, He, Ar, and air were tested and showed distinct and precise breakdown voltage.
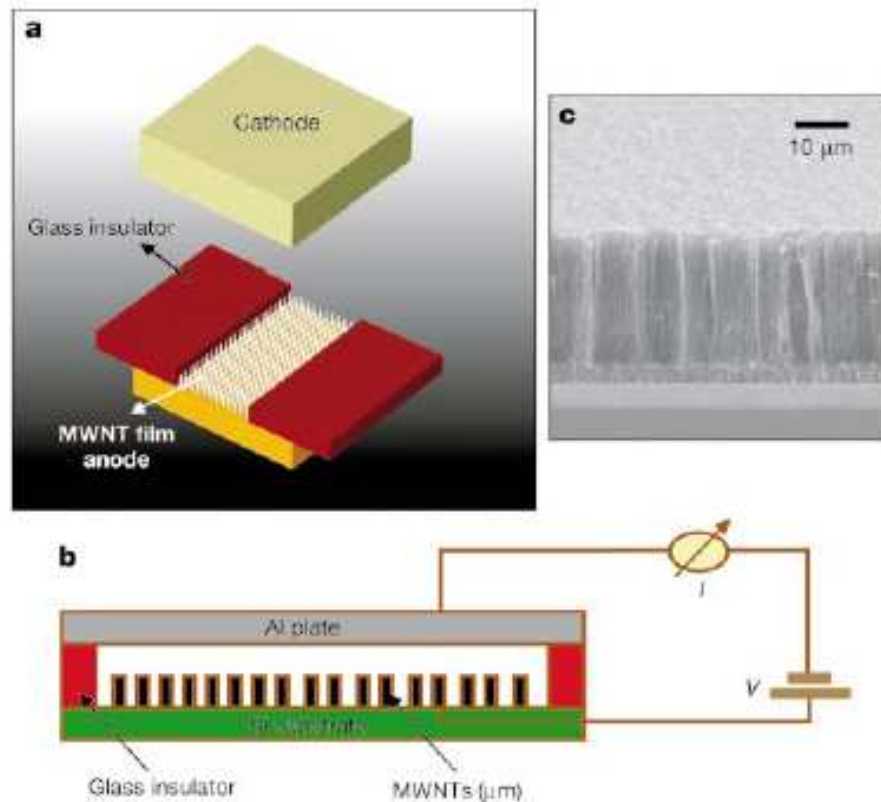
Fig. 2-11 (a) Schematic diagram of the nanotube sensor device; (b) diagram of actual test set-up; (c) SEM micrograph of vertically aligned MWCNT film used as the anode (Modi et al. 2003)

The single-walled carbon nanotubes (SWCNTs), multi-walled carbon nanotubes (MWCNTs) and randomly oriented nanotube networks for detecting chemical gases and vapors have been a subject of active research [Park et al. 2010]. But slow response and recovery is a challenge to be addressed for CNTs-based gas sensors, which are caused by the nature of nanotubes materials. However, with the increasing interests and development of related technologies, CNTs-based gas sensors have a promising opportunity and will bring a giant change to the current life.

2.5 Carbon nanostructure-assisted gas sensing devices

Non-conductive polymers causing the bulk dissolution of gas into the film can bring about changes of their physical properties. The feasibility of using MWCNTs/Nylon-6 nanofiber materials for gas sensing at room temperature has been demonstrated by Neeta L. Lala et al. in 2009 [Lala et al. 2009]. The nanofiber based device has shown the significant reproducibility and responsiveness to organic analytes, especially to polar and non-polar molecules. Fig 2-12 shows the comparative response of MWCNTs/Nylon-6 nanofiber composite towards various polar organic analytes, clearly indicates that the nanofiber composite is responding to the various type of analytes used.
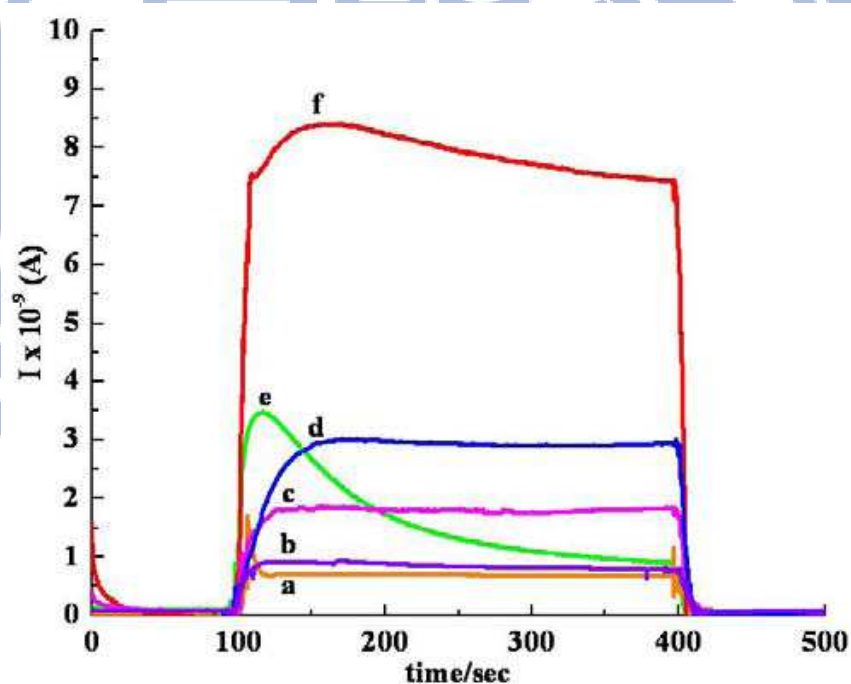
Fig. 2-12 Response profile obtained for all analytes by MWCNT/Nylon-6 nanofibers at room temperature: (a) trichloromethane, (b) THF (c) EA, (d) ethanol, (e) acetone, (f) DCM [Lala et al. 2009].

Hargsoon Yoon et al. in 2006 [Yoon et al. 2006] measured the responses of f-CNT/PMMA composite sensors for different gas concentrations by using

conventional resistance measurement methods. As shown in figure 2-13, the resistance of CNT/PMMA composite thin film rapidly increased with dichloromethane vapor concentration. It is observed that the resistance of the composite in figure increased with gas concentration and reached saturated values within 10 min. The resistance increase is regarded as being caused by the free volume change of the PMMA polymer matrix. The volume change is determined by the exposure time and concentration of dichloromethane vapor. Because lateral expansion of polymer is negligible compared to the vertical direction, the volume change of swollen polymer can be described as the increase in thickness of the polymer matrix. Due to the matrix swelling, the gap between the electrical junctions and the conducting carbon nanotubes increases and becomes wider.
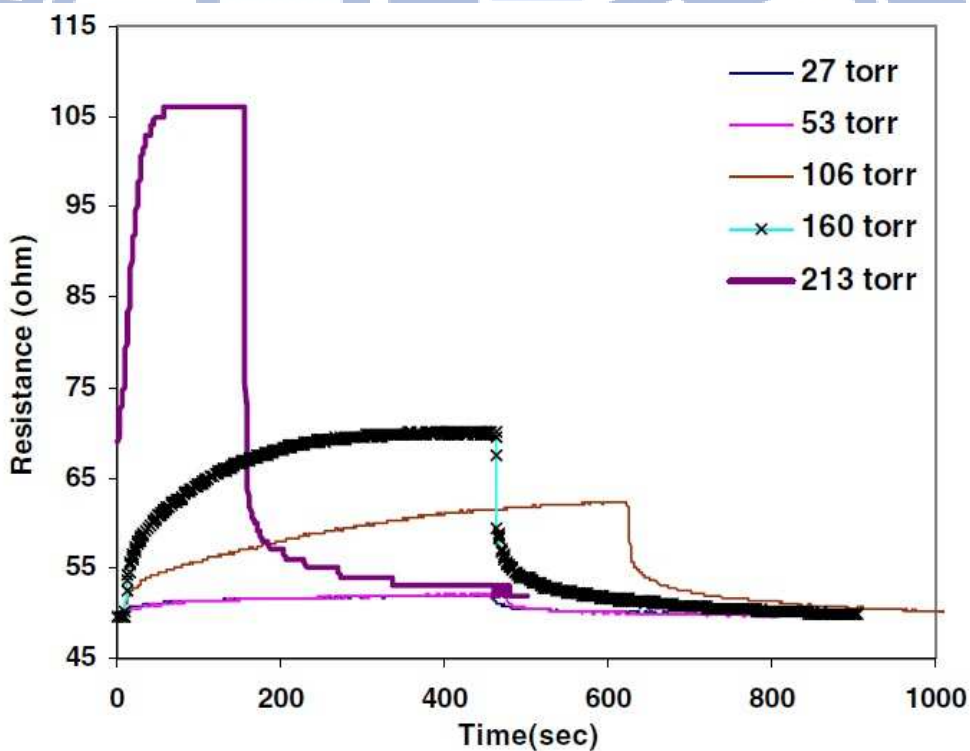
Fig. 2- 13 Response of CNT/PMMA composite thin film sensor to different dichloromethane vapor concentration [Yoon et al. 2006]

2.6 Introduction to olfaction

Smell is a primal sense for humans as well as animals. From an evolutionary standpoint it is one of the most ancient of senses. Smell (or Olfaction) allows vertebrates and other organisms with olfactory receptors to identify food, mates, and predators.[ref] Accordingly, it provides both sensual pleasure (the odor of flowers and perfume) as well as warnings of danger (e.g., spoiled food, chemical dangers). For both humans and animals, it is one of the important means by which our environment communicates with. Olfaction is a prime example; the discovery of the gene family encoding vertebrate olfactory receptors (ORs) [Buck and Axel 1991] has led to a relatively detailed understanding of the molecular and neurological bases for how organisms can smell volatile compounds. Linda B. Buck and Richard Axel won the 2004 Nobel Prize in Physiology or Medicine for their work on the study of "Odorant receptors and the organization of the olfactory system".

The olfactory area of two nasal passages in humans is a small area containing in total approximately 50 million primary sensory receptor cells. The olfactory regions be made of cilia down out of the olfactory epithelium into a 60 microns thick layer of mucous. This mucous layer is a lipid-rich secretion at the epithelium surface. Therefore, they can interact with the olfactory receptors and produce the signals that our brain interprets as odor. Humans have several hundred distinct genes that encode olfactory receptor proteins and rodents have an increase of 500 to 1000 separate genes, that is, as much as 1% of the genome. This extremely broad range of receptor types permits the detection of odor sources comprised of unpredictable mixtures of molecular species, and even allows detection of newly synthesized compounds with unknown functions.

2.7 Artificial electronic nose system

An artificial electronic nose (E-Nose) system is a biomimetic system for odor detection, analysis, and recognition. Since it was first developed in 1987 [Gardner and Bartlett 1994; Gardner 1987], the E-Nose has been adapted in a wide range of applications, such as environmental monitoring [Baby et al. 2000; Lamagna et al. 2008], food product quality control [Balasubramanian et al. 2008; Capone et al. 2000; Panigrahi et al. 2006], agricultural evaluation [Gomez et al. 2006; Pathange et al. 2006], the automotive industry [Morvan et al. 2000; Park et al. 2009; Sobanski et al. 2006], health management, and medical diagnosis [Bernabei et al. 2008; D'Amico et al. 2010; Lin et al. 2001; Pavlou et al. 2002].

Recent efforts have yielded a miniaturized and inexpensive chemical gas sensor [Guerin et al. 2005; Tang et al. 2006; Yamaguchi and Yang 2004] with high reproducibility and a rapid reaction rate. Research, including that from our own group working under size and price restraints, has produced a portable E-Nose based on a carbon black-polymer composite sensor array [Kim et al. 2005; Tang et al. 2010], shown in fig 2-14.
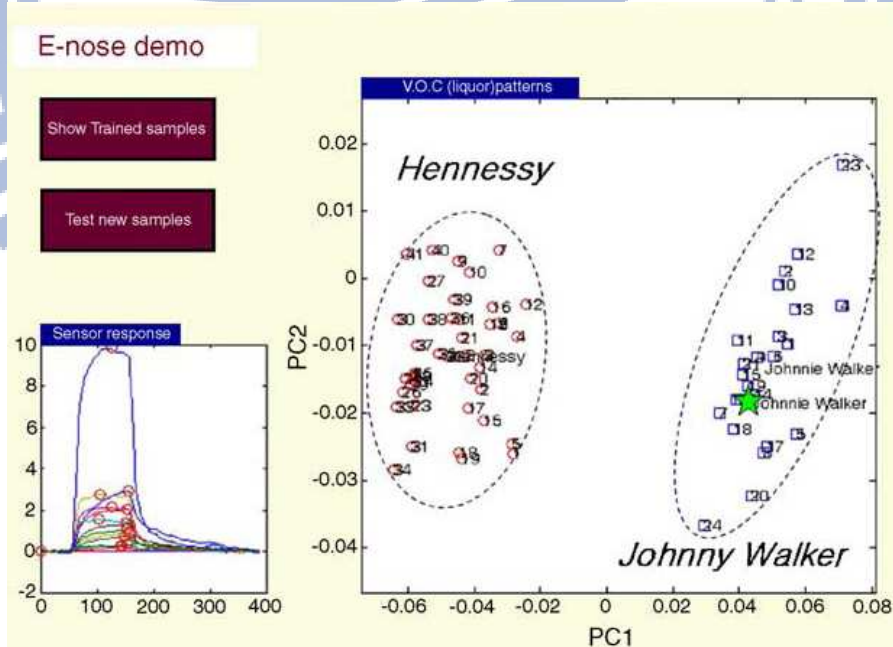
Fig. 2-14 (a) Pictures for the E-Nose system realized by using PDA as personal digital apparatus (b) the identification of tested liquor sample when Hennessy and Johnny Walker are used as test sample [Kim et al. 2005].

Compared those of with carbon black, the electrical conduction properties of carbon nanotubes (CNTs) have drawn considerable interest [Park et al. 2009], and multiple-walled carbon nanotube (MWCNTs)–polymer composite sensors show very good performance with respect to sensitivity, response time, reproducibility, and long-term stability [Alig et al. 2007; Wu and Lin 2006].

To improve sensor performance further, researchers have studied biological olfaction as a reference. Mammalian olfactory receptor cells distributed in the olfactory epithelium contain a mucous covering layer. The surface of an olfactory cell consists of tens of cilia, which extend into the mucus. As gas molecules enter the nose, they first dissolve in the mucus before being captured by the cilia. The mucus filters out dust and impurities that could otherwise damage the cilia. The receptor cells then transmit neural signals to the cerebrum. This two-layer structure inspired researchers to investigate the use of artificial mucosa to emulate this mechanism, and the use of artificial mucosa as shown in Fig. 2-15, resulted in a five-fold increase in sensitivity [Gardner and Covington 2007]. The artificial mucosa approach uses GC columns with a 10 mm thick layer of Parylene C (polymonochloroparaxylylene C) to emulate the mucosa and 40 polymer-composite sensors to emulate the cilia.
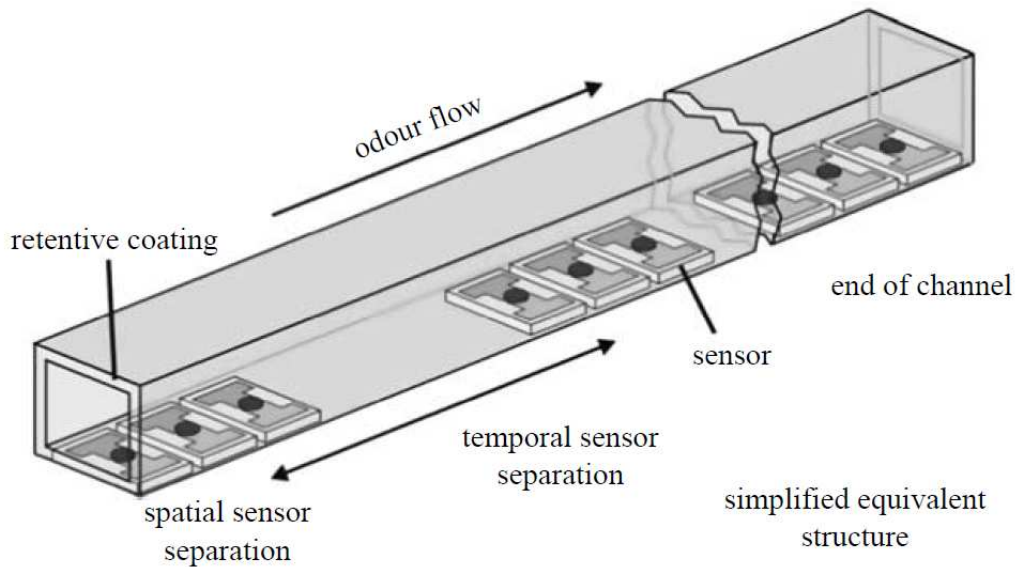
Fig. 2-15 The artificial mucosa comprises multiple chemical sensors distributed along the length of a gas chromatograph channel [Gardner and Covington 2007]

This artificial mucosa is capable of generating both spatial and temporal signals which, when combined, create a novel spatio-temporal representation of an odor. Such a system not only offers improved odor discrimination over a sensor array-based electronic nose, but also shorter analysis times than conventional gas chromatographic techniques. Future work will be directed towards the analysis of more challenging odor discrimination problems (e.g. odor segmentation) and this will require the development of more advanced topologies and nonlinear spatio-temporal signal processing techniques.

Chapter 3

Experimental details

3.1 Experimental flow chart

The flow chart for the experiments in this work is shown in Fig. 3-1. In brief, CNTs were prepared by thermal CVD with C_2H_2 and H_2 as source gases, FeCo as catalyst and MgO as capping layer on catalyst layer. The CNTs were then mixed with sensing polymer materials and drop cast on Si wafer to act as gas sensor. The CNTs were also used as the base layer and followed by drop casting sensing polymer on the top to act as gas sensor. The gas sensing chip with eight different sensors was then installed on a gas testing stand for gas sensing experiments and followed by data analyses with one of two mathematical methods (PCA, k-NN), as will be described in the following text. The structures and properties of as-grown CNTs were characterized by SEM, TEM and Raman spectroscopy.
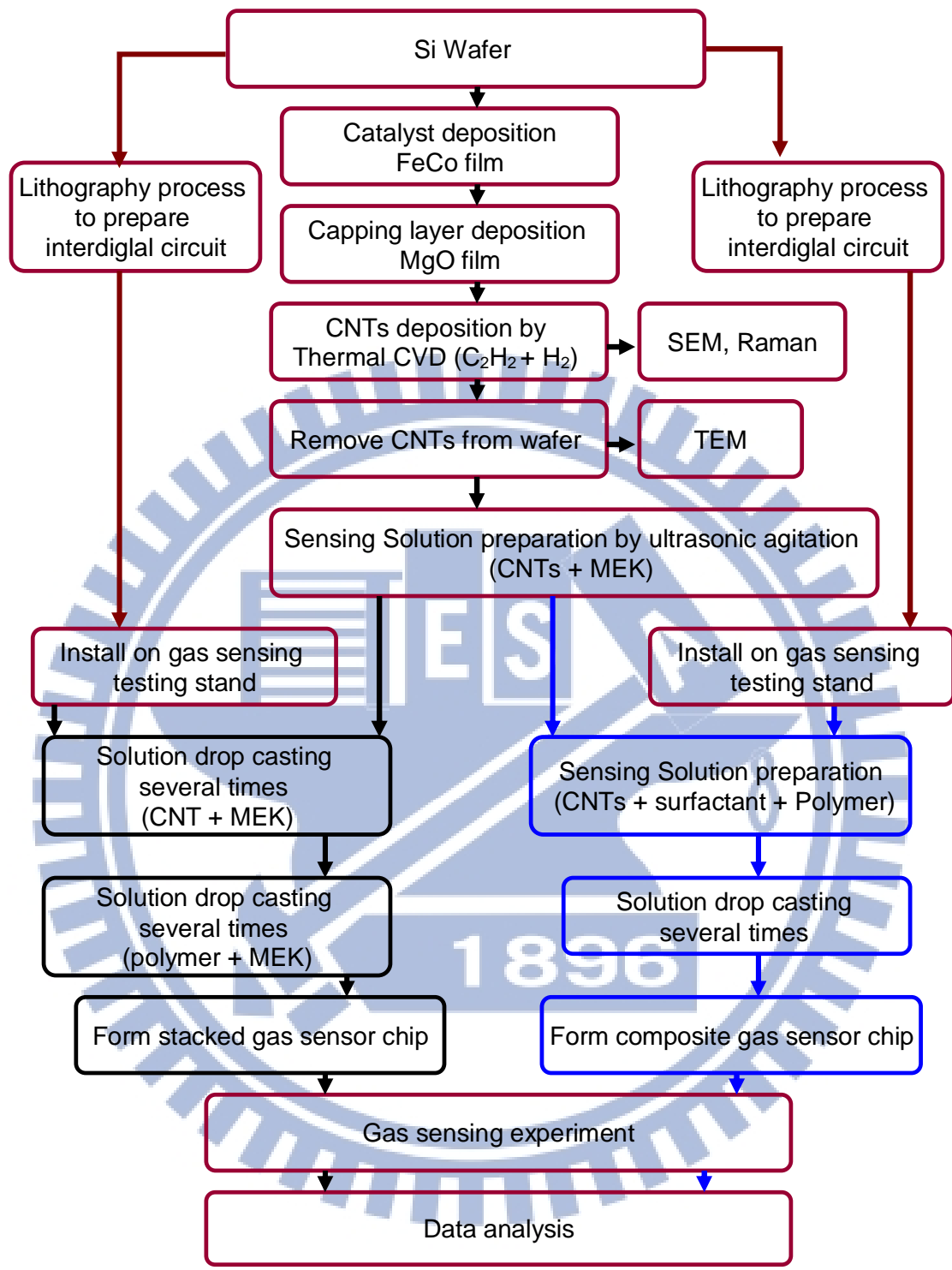
Fig. 3-1 Flow chart of the experiments.

3.2 Raw materials

The raw materials used in this work, including wafer, alloy, oxide, gas, chemical, and polymer materials are listed in Table 3-1.

Table 3-1 Raw materials, including chemicals, used in this work

*Material (purpose)	Formula	Supplier
P-type (100) silicon wafer (substrate)	99.9999%	Tekatarter Co.
Iron Cobalt (catalyst for CNTs growth)	FeCo (99.99%)	Tekatarter Co.
Magnesium Oxide (capping layer for CNT growth)	MgO (99.99%)	Summit-Tech. Co.
Acetylene (source gas for CNT growth)	C_2H_2 (purity 99.9995%)	San Fu
Argon (carrier gas for CNT growth)	Ar (purity 99.998%)	San Fu
Hydrogen (source gas for CNT growth)	H_2 (purity 99.9995%)	San Fu
Acetonitrile(ACN) (analyte)	CH_3CN (Anhydrous, 99.8%)	Sigma-Aldrich
Carbon tetrachloride (analyte)	CCl_4 (Reagent grade, 99.9%)	Sigma-Aldrich
Chloroform(analyte)	$CHCl_3$ (Anhydrous, ≥99%)	Sigma-Aldrich
Dichloromethane(DCM) (analyte)	CH_2Cl_2 (ACS reagent, ≥99.5%)	Sigma-Aldrich
Dimethyl-methyl phosphonate (DMMP)(analyte)	$CH_3PO(OCH_3)_2$ (Purum, ≥97.0% (GC))	Fluka
Methyl-ethyl ketone (MEK) (analyte and solvent)	$C_2H_5COCH_3$ (ACS reagent, ≥99.0%)	Sigma-Aldrich
Tetrahydrofuran (THF) (analyte)	C_4H_8O (Anhydrous, ≥99.9%)	Sigma-Aldrich
Toluene (analyte)	$C_6H_5CH_3$ (Anhydrous, 99.8%)	Sigma-Aldrich
Xylene (analyte)	$C_6H_4(CH_3)_2$ (ACS reagent, ≥98.5%)	Sigma-Aldrich
Acetone (solvent for wafer cleaning)	$(CH_3)_2CO$ (HPLC, ≥99.9%)	Sigma-Aldrich
Isopropanol (solvent for wafer cleaning)	$(CH_3)_2CHOH$ (≥99.7%)	Aldrich
Polymer (gas sensing)	shown in Table 3.2	

3.3   Thermal CVD system

In this work, thermal CVD system was used for synthesizing MWCNTs, as schematically shown in Fig. 3-2. It mainly consists of three gas tanks (for H_2, C_2H_2, Ar, respectively), corresponding mass flow controllers (Matheson, Model 5850E), mechanical pump, a quartz tube reaction chamber and the electrical heating circuit. In the reaction tube chamber, a net of quartz wools and a thermocouple are installed to act as specimen holder and temperature measurement, respectively. This arrangement is to ensure better gas distribution around the specimens and temperature monitoring. The effective sizes of quartz tube are 63.5 mm in diameter and 120 cm in length.
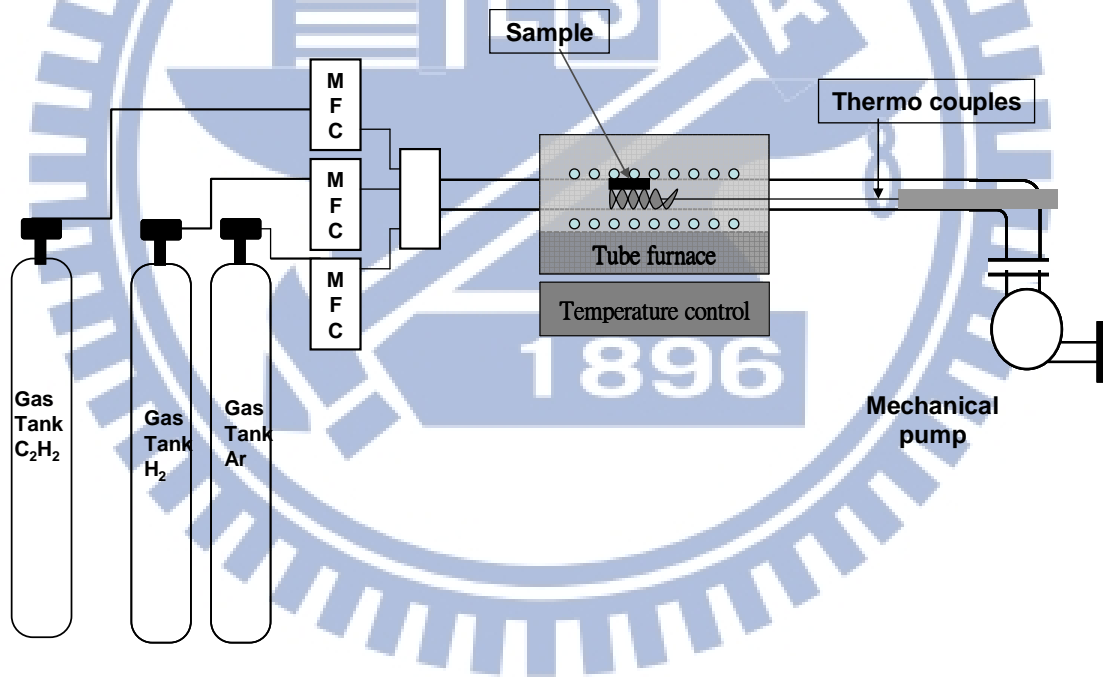
Fig. 3-2 Schematic diagram of the thermal CVD system.

3.4 Preparation of MWCNTs by thermal CVD

MWCNTs (multi-walled carbon nanotubes) were synthesized on Si wafer by thermal CVD with C_2H_2 and H_2 as source gases, Ar as carrier gas, FeCo as catalyst and MgO as capping layer for catalyst layer. The Si wafer was cleaned first and 2 nm FeCo film was then sputtered on the wafer with Ar as carrier gas and FeCo alloy as target (six targets magnetron sputter, Chinese United Semiconductor Equipment Manufacturing, Inc.). The coated wafer was then deposited with 0.5 nm MgO by the same sputter using MgO as target. The double deposited substrates were then pretreated at 700℃ for 5 min by hydrogen plasma in the thermal CVD system with Ar as carrier gas. Subsequently, MWCNTs were deposited on the pretreated specimens under C_2H_2/H_2 = 10/10 sccm/sccm flow ratio for 5 min. MWCNTs powders were finally scratched from the substrate.

3.5　Structure and property characterization

The structures and properties of MWCNTs were characterized by the following techniques.

3.5.1　Scanning electron microscopy (SEM)

Scanning electron microscopy is a very useful tool for observing surface morphology of specimen. SEM has secondary electrons (SE) or backscattered electrons (BSE) detectors passing the signal to computer and forming image. In this study, scanning electron microscopy (SEM, JEOL JSM-6700, point resolution 1.5 nm) under 15 kV was employed to examine the cross sectional secondary electron images of the as-deposited specimens.

3.5.2　Transmission electron microscopy (TEM)

Transmission electron microscopy (TEM) is a powerful tool to investigate the structural features and crystallographic defects of nanostructures down to the nanoscale, and is a critical technique to reveal material phenomena at atomic level with extremely higher resolution ability. In this study, the structural of the carbon nanostructured materials were carried out by a Hitachi H-7100 operating at 100 kV accelerating voltage to produce high resolution (2 Å) and high contrast images. The TEM specimens were prepared by scratching nanostructures directly from substrates, then sonicating in ethanol and having few drops on copper (Cu) grids coated with a lacey film.

3.5.3 Raman spectroscopy

Raman spectroscopy is known as a reliable characterization tools for obtaining the structural information of CNTs. In this study, Raman spectroscopy (Jobin Yvon LabRam HR with two laser excitation sources 514.5 nm (2.41 eV) and 632.8 nm (1.96 eV)) was employed to identify the bonding structures of as-deposited nanostructures. The laser spot size was about 5 μm in diameter. To obtain better information, each sample was examined on more than six locations.
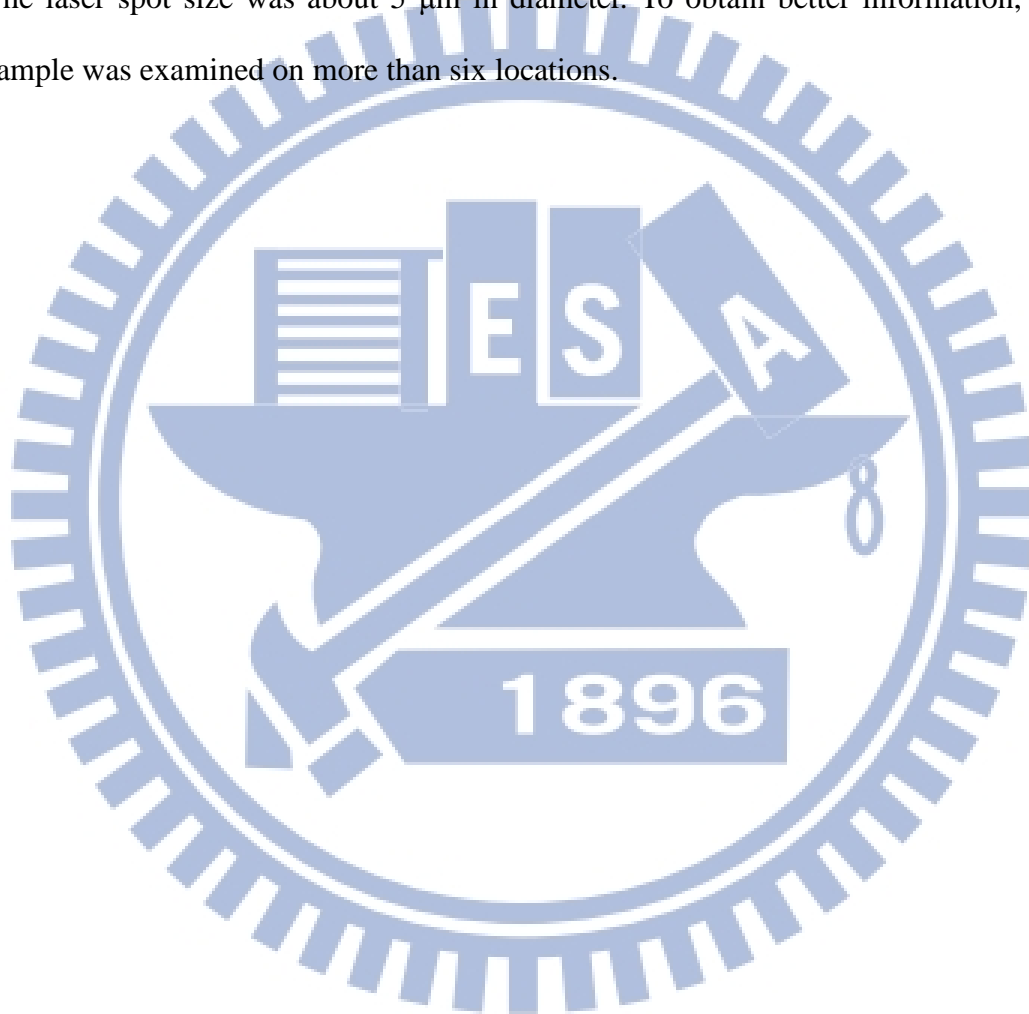
3.6　Preparation of MWCNT-polymer gas sensor-array chip

Figure 3-3 shows a stainless steel testing stand with a Si (001) chip, consisting of eight gas sensors, one humidity sensor, two temperature sensors, one heating device and the corresponding 12 independent sensing electrical leads in a 2×6 arrangement to facilitate measurement of the resistance response of each sensor. The humidity sensors were reserved for future use. The chip is 34 mm× 20 mm in size. Each circular membrane sensor was limited to 2 mm in diameter to minimize heat loss from the silicon substrate [Chang et al. 2004; Chang and Yuan 2009].
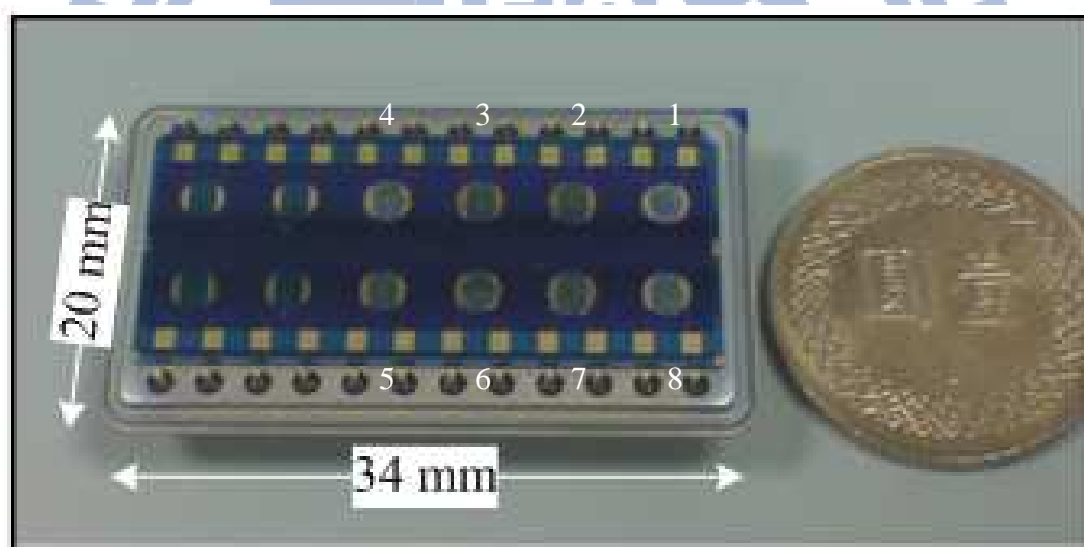
Fig. 3-3 Gas testing stand with a sensing chip

The eight polymer types were selected according to their linear salvation energy relationship (LSER), and physical absorption bonding properties. First, the LSER theory is applying to enhance the device's recognition capability for different odors [Grate et al. 1998; Grate et al. 1995; Liron et al. 1997]. The LSER model has been widely used to explain equilibrium partition coefficients in gas–liquid chromatography (GLC), thermogravimetry [Artzi-Gerlitz et al. 2009], and quartz crystal microbalance (QCM) and

37

surface acoustic wave [(Murugaraj et al. 2010)] sensing experiments [(Star et al. 2006)]. In this model, each interaction term on the right of Eq. (3-1) is expressed as product of two solvation parameters (one for solute and one for solvent) that quantify complementary characteristics of vapor and polymer molecules for a particular interaction process. The LSER is described by the expression:

$$\text{Log } K_p = c + rR + s\pi^H + a\Sigma\alpha^H + b\Sigma\beta^H + l\text{Log } L^{16} \quad \text{------} \quad \text{(Eq. 3-1)}$$

where c, r, s, a, b and l characterize solubility properties of the solvent (polymer), and $\mathbf{R}$、$\boldsymbol{\pi}^{\mathbf{H}}$、$\boldsymbol{\Sigma\alpha}^{\mathbf{H}}$、$\boldsymbol{\Sigma\beta}^{\mathbf{H}}$ and $\mathbf{Log\ L}^{\mathbf{16}}$ are the complementary solute (vapor) parameters for specific solvation processes. These are usually referred to as salvation parameters. The r and R measure abilities to interact with dispersion forces; s and $\boldsymbol{\pi}^{\mathbf{H}}$ measure abilities to solvate with dipole interactions; a measures hydrogen bond basicity of the polymer and $\boldsymbol{\Sigma\alpha}^{\mathbf{H}}$ measures hydrogen bond acidity of the vapor; b measures hydrogen bond acidity of the polymer and $\boldsymbol{\Sigma\beta}^{\mathbf{H}}$ measures hydrogen bond basicity of the vapor; l and $\mathbf{Log\ L}^{\mathbf{16}}$ measure combined effects of dispersion interaction and cavity formation in hexadecane; and c is a regression constant representing residual effects not covered by other terms. LSER equations correlate the log of the partition coefficient of a vapor in a polymer with the vapor salvation parameters using a series of LSER coefficients related to the polymer's solubility properties.

For example, applying LSER equation to estimate the solvation coefficient between ethanol gas and various polymer membranes, and considering parameters such as dispersive interactions, dipole interactions, hydrogen bond acidity, and hydrogen bond basicity, the solvation coefficients would be estimated as PMVEMA < PEA < HPMC < PVBC. A smaller solvation coefficient corresponds to a larger

interaction between ethanol gas and polymer, resulting in a larger resistance variation. Therefore, solvation coefficient provides a good estimation. However, carbon nanotubes may change the physical characteristics of the film (glass transition temperature, rigidity, and density), and possibly the chemical characteristics. Therefore, solvation energies may not be sufficient for complete description of the sensor–analyte interaction.[Hierlemann et al. 2001; Ryan et al. 1998]

When using carbon nanotube-polymer composites as gas sensors, to use the sensors repetitively with a short recovery time, the interaction between the gas and polymer membrane is usually reversible physical absorption bonding. There are five kinds of physical absorption bonding: (1) hydrogen-bond acidic (HBA), (2) hydrogen-bond basic (HBB), (3) dipolar and hydrogen-bond basic (D-HBB), (4) moderately dipolar and weakly H-bond basic or acidic (MD-HB), and (5) weakly dipolar with weak or no hydrogen-bond properties (WD) [Hierlemann et al. 2001; Ryan et al. 1998].

Consequently, eight polymer materials were selected for this work. These were styrene/allyl alcohol copolymer (SAA) (WD), polyvinylpyrrolidone (PVP) (HBB), poly(vinylidene chloride-co-acrylonitrile) (P(VDC-AN)), poly(methyl vinyl ether-alt-maleic acid) (PMVEMA), poly(alpha-methylstyrene)(PMS) (WD), hydroxypropyl methyl cellulose (HPMC) (D-HBB), poly(ethylene adipate) (PEA) (HBA), and poly(vinyl benzyl chloride) (PVBC) (D-HBB). The selected polymer materials used in this work are listed in Table 3-1.

Table 3- 2 Sensing polymer materials selected in this work

Sensor number*	Polymer / acronym	Supplier
S1	Styrene Allyl Alcohol copolymer/SAA	Arcos
S2	Polyvinylpyrrolidone/ PVP	Arcos
S3	Poly(vinylidene chloride-co-acrylonitrile)/ P(VDC-AN)	Arcos
S4	Poly(methyl vinyl ether-alt-maleic acid)/ PMVEMA	Arcos
S5	hydroxypropyl methyl cellulose / HPMC	Arcos
S6	Poly(alpha-methylstyrene)/ PMS	Arcos
S7	Poly(ethylene adipate)/ PEA	Arcos
S8	Poly(vinyl benzyl chloride)/ PVBC	Arcos

*Sensor numbers of S1, S2 … correspond to the sensor position numbers of 1, 2 … in Fig. 3-2, respectively.
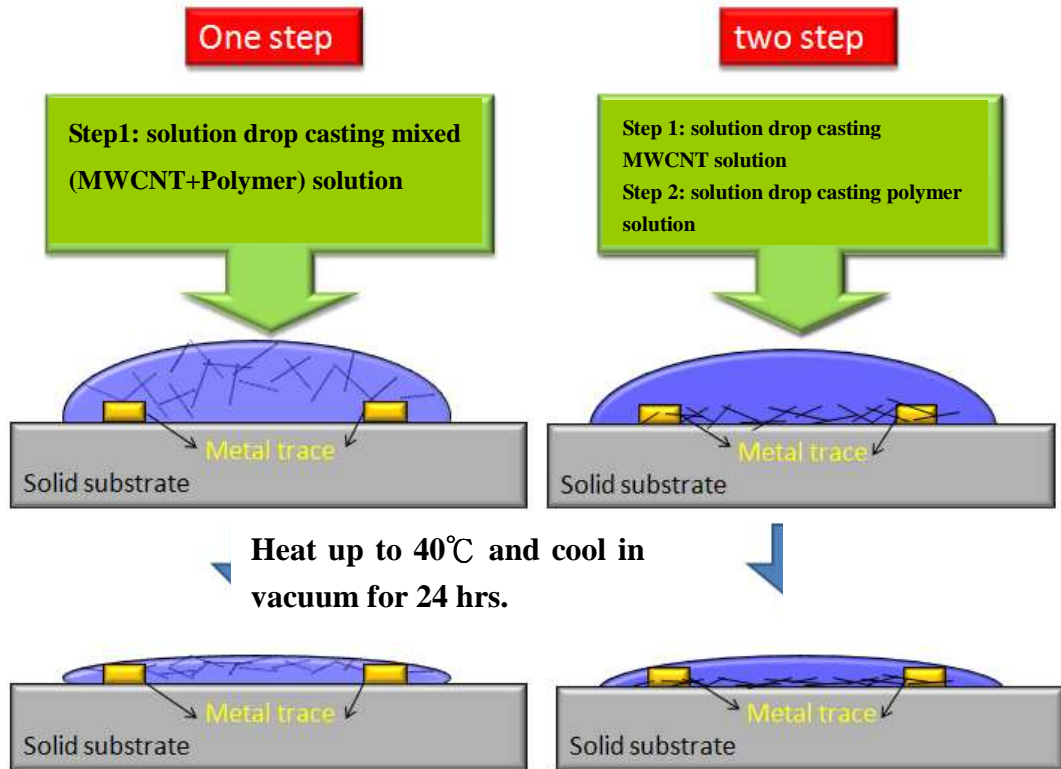
Fig. 3-4 Two different solution drop casting processes to fabricate the gas sensors

Two different solution drop casting processes (Processes 1 and 2) were used to fabricate eight gas sensors on the sensing chip, as shown in Figs. 3-4a and 3-4b, respectively, to illustrate the processing steps.

Process 1: PVP polymer+MWCNT composite film sensor

In this process, the MEK (methyl ethyl ketone) solution was prepared by mixing 1 wt% PVP and 1 wt% MWCNTs. The solution was magnetically and ultrasonically stirred to maximize uniform dispersion. The dispersed composite precursor solution was then drop cast onto the desired spot of an interdigitated microelectrode (IME) on chip using an HPLC syringe, and followed by air drying and monitoring the sensor resistance. The processes were repeated several times to control the sensor resistance within the range of 1 kΩ to 10 kΩ. The remaining solvent in the sensor was finally removed to form composite membrane by cooling in a vacuum oven for 24 hours.

41

Process 2: polymer/MWCNT stacked film sensor

The stacked sensor was fabricated a two-step drop casting method. A MWCNTs-modified electrode layer was prepared by drop-casting a MEK solution with 1 wt% MWCNTs onto the desired spot of an interdigitated microelectrode (IME) on chip using an HPLC syringe. The MEK solvent was finally evaporated in air at room temperature for two hr to yield the MWCNTs film. One of the eight different polymer MEK solutions was then repeatly deposited by drop casting onto the MWCNTs layer, and the sensor resistance after each casting step was monitored to control its value within the range of 1 kΩ to 10 kΩ. The drop cast sensor was followed by a final drying step in vacuum for 24 h to remove the remaining solvent to form a gas stacked sensor.
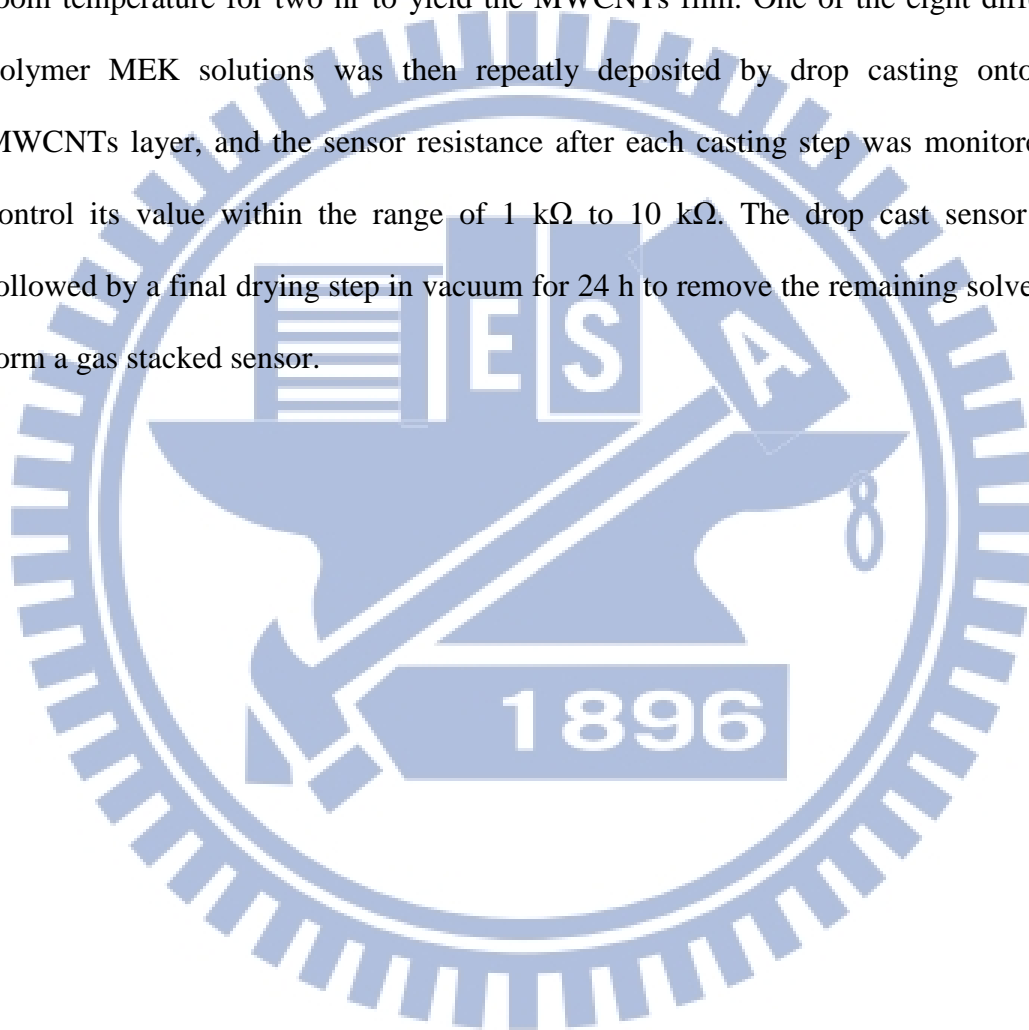
3.7　Gas sensing experiment

Figure 3-5 shows the experimental setup used to characterize the volatile organic compound (VOC)-sensing properties of the sensor devices. The test bench comprises of the gas delivery system, sensor test chamber and the computer controlled electrometer for sensor response acquisition. The gas delivery system includes refrigerating air dryer, pressure regulators, mass flow controllers and required electronics to control flow rate and concentration of testing gas.
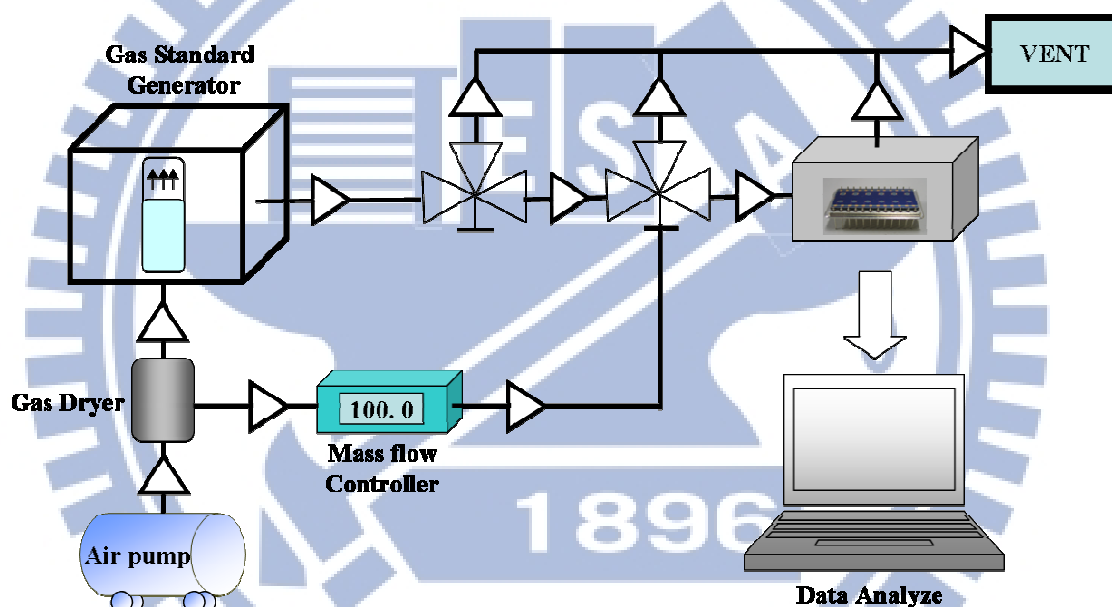
Fig. 3-5 Gas sensing experimental setup

To conduct the gas sensing experiments, the testing stand with sensor array chip was placed in a glass vessel. Analytes with known concentrations were generated by a Standard Gas Generator (made by KIN-TEK Laboratories, Inc.), where the gas concentration was calibrated by measuring the weight loss from the organic solvent solution. The gas flow rate was controlled by a calibrated mass-flow controller (made by Aalborg, Inc.) with air as the carrier gas. For each test, the system stabilized after

about 300 s. Analyte at a flow rate of 100 ml/min was then infused into the chamber

for 300 s (adsorption), followed by infusing dry air for another 300 s (desorption).

After each testing run, the chamber was purged with dry air. Electrical resistance

outputs ($\triangle$R/R %) from each sensor element were measured through a National

Instrument data acquisition card (Interface card: NI DAQ 6009) with a self-written

Lab-VIEW program.

Gas concentration can be manipulated through the following diffusion rate

equation:

$$R = 2.216 \times 10^6 \left(\frac{DMwPA}{TL} \right) \log \left(\frac{P}{P-p} \right)$$ (Eq. 3-4)

R：diffusion rate，ng/min

D：the diffusion coefficient when temperature is T, pressure is P，cm^2/sec

Mw：Molecular weight

P：total pressure，torr Hg

A：diffusion tube cross section area，cm^2

T：temperature，K

L：diffusion tube length，cm

p：Partial pressure of solvent

This diffusion rate equation (Eq. 3-4) takes into consideration of temperature and

pressure effects on gas volume. In other words, the volume is normalized to

conditions of 25°C and 760 mm Hg (1013.2 MBar). The diffusion rate is then used to

calculate the gas concentration of dynamic carrier flow in the permeation tube by Eq.

3-5:

$$C = (R*K) / F_c \qquad\qquad \text{(Eq. 3-5)}$$

Where concentration C is expressed in ppm by volume, R represents the diffusion rate in ng/min, Fc is the total flow rate of the gas mixture in cc/min, and K is a constant calculated by Eq. 3-6.

$$K = \{22.4(T+273)*760\}/M_w*273*P \qquad\qquad \text{(Eq. 3-6)}$$

M_w is the molecular weight of the pollutant gas, corrected to the reference conditions defined above. 22.4 is the molar volume at the reference conditions.
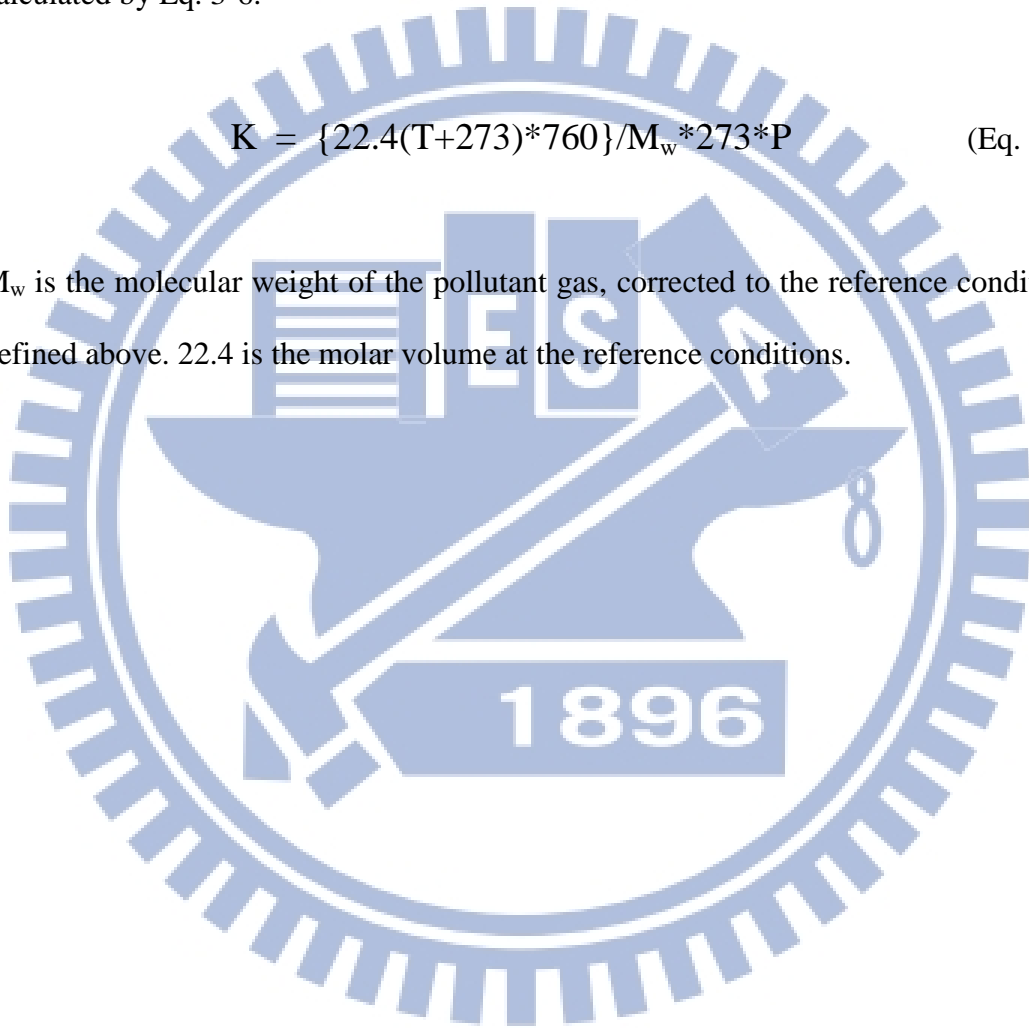
3.8 Analysis of gas sensing response curve

The response of sensors to vapors is generally regarded as a first order time response. The first step in odor analysis is to flush a reference gas (dry air) through the sensor to obtain a baseline. The sensor is then exposed to the target gas, which causes changes in its output signal until the sensor reaches steady-state. It is followed by turning off the gas supply and flushing with dry air to obtain another baseline. The testing process is repeated several times to obtain the desired sensing response data. The typical sensing curve for one cycle is shown in Fig. 3-6 [Arshak et al. 2004]. The time periods - t_1, t_2 and t_3 in the figure are corresponding to testing times by flushing with dry air, testing gas and dry air, respectively. The t_3 is called the recovery time.
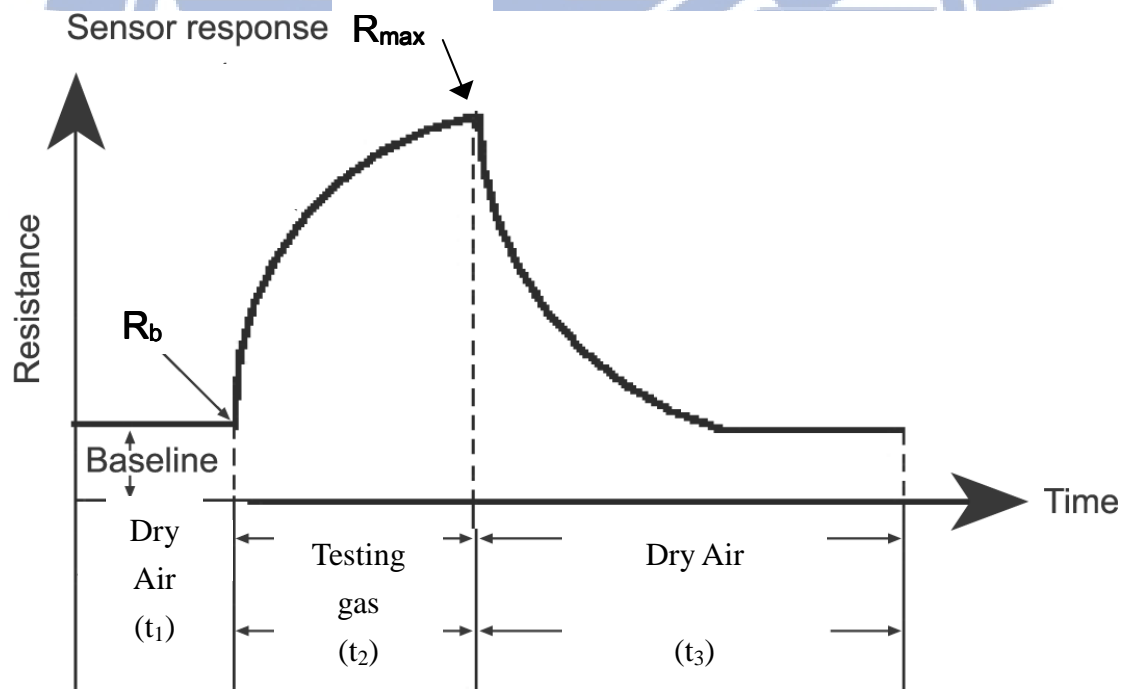
Fig. 3- 6 Typical gas sensing response of a chemiresister sensor [Arshak et al. 2004]

The vertical axis of the sensing curve represents resistance, R, of sensor under the presence of gas, where R_b and R_{max} denote the baseline and maximum resistances

46

of the sensor exposed to air and testing gas, respectively. The gas response can also be recorded by ploting resistance change $\triangle R/R$ versus testing time curve, where $\triangle R/R = (R - R_b)/R_b$.   The maximum value of $\triangle R/R$ on the curve is an index representing the device sensitivity, as indicated in Eq. 3-7.

$$(\Delta R/R)_{max} = (R_{max} - R_b)/R_b \qquad \text{(Eq. 3-7)}$$

Chapter 4

Results and Discussion – comparison between PVP+CNT Composite and Stacked Sensors

4.1. Morphology and structure of MWCNT raw materials

Figure 4-1 shows the cross sectional SEM image of the as-grown carbon nanostructures on an MgO capping layer FeCo/SiO$_2$/Si substrate by thermal CVD. It indicates that the film thickness or the length of the nanostructure is about 48 μm. The scratched carbon nanostructures powders from the substrate were examined by TEM, as shown in Fig. 4-2 for a nanotube. It depicts the tube-like nanostructures with tube thickness of 15 graphine layers.

The Raman spectrum of as-grown nanostructures is shown in Fig. 4-3. Two sharp peaks located at 1347 (D line) and 1575 cm^{-1} (G line) are significant. It depicts a 5 cm^{-1} frequency downshift of the G line with respect to 1580 cm^{-1} for high oriented pyrolitic graphite (HOPG). It may be attributed to sharply curved and closed graphitic structures of CNTs. It I$_D$/I$_G$ ratio is about 1.0, indicating a poor graphilization of the tubes. In addition, the significant D-band signal may be partly attributed to existence of amorphous carbon on the tube surface, as also shown in Fig. 4-2. As a conclusion, the grown nanostructures are essentially MWCNTs with metallic properties.
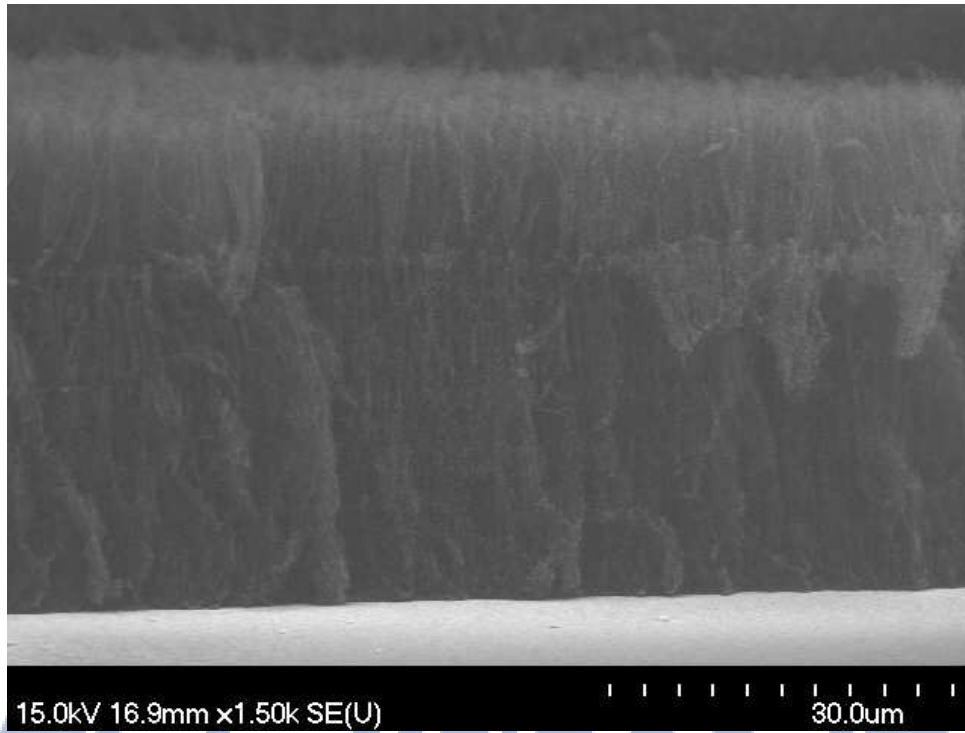
Fig. 4-1 XSEM micrograph of the as-grown MWCNTs.
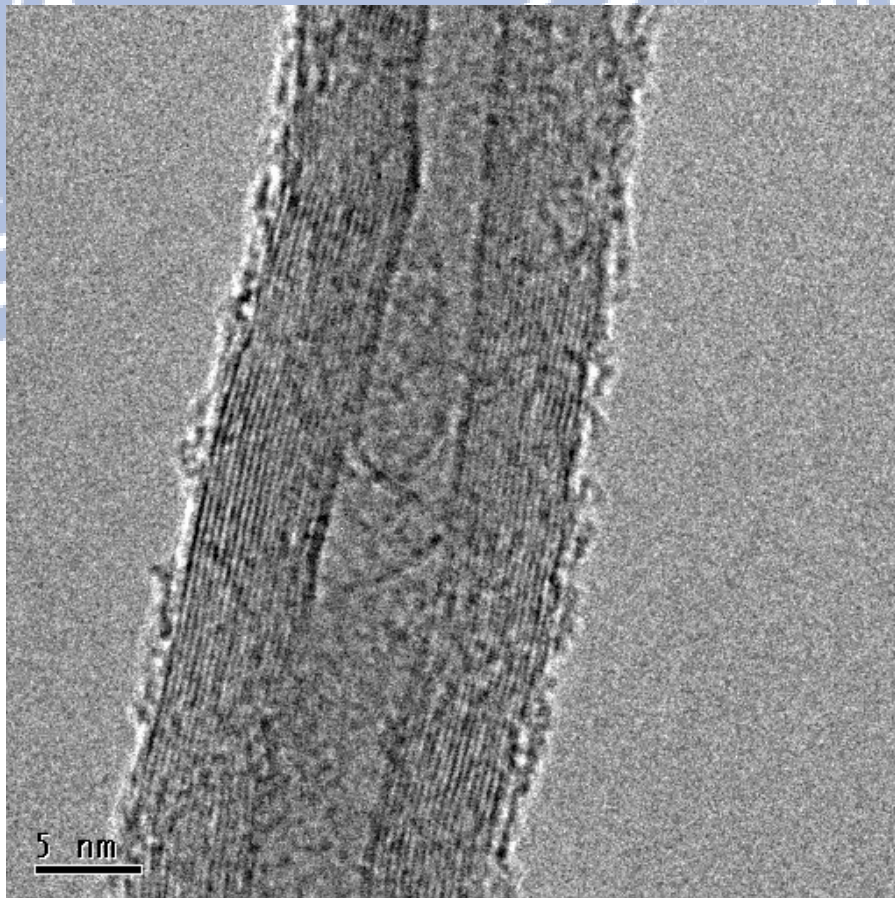
Fig. 4-2 TEM image of a scratched MWCNT tube
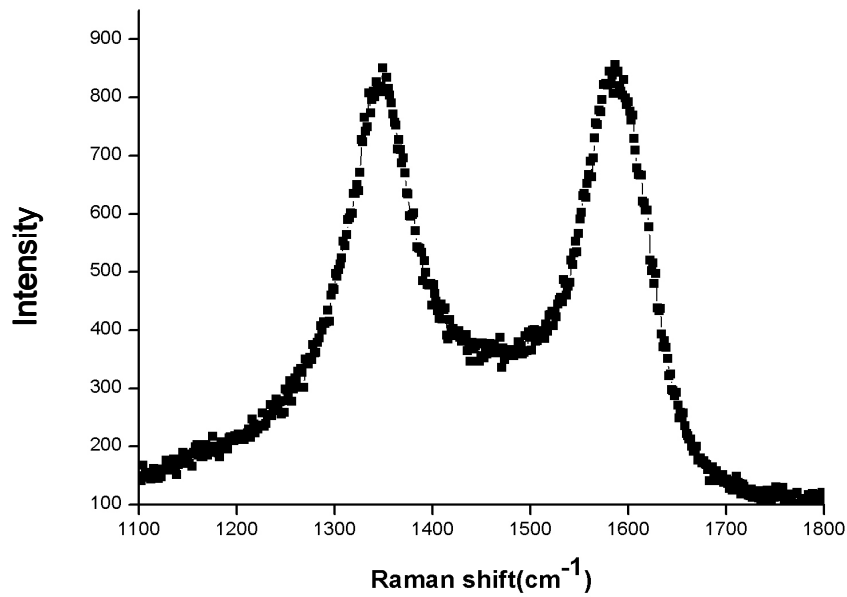
Fig. 4-3 Raman spectrum of the as-grown MWCNTs.

4.2. Performance of composite and stacked MWCNT - assisted sensors

Figures 4-4(a) and (b) show SEM surface morphologies of MWCNTs+PVP composite and PVP/MWCNTs stacked sensors, respectively. There are significant numbers of MWCNTs (tiny white lines) in Fig. 4-4(a), and not in Fig. 4-4(b). In other words, the MWCNT layer of the stacked sensor of Fig. 4-4(b) is covered by a layer of polymer.   As a consequence, both of MWCNTs and polymer of composite sensors can directly contact with the sensing gas. In contrast, only polymer layer of the stacked sensors can contact with the analyte to protect MWCNT layer from degrading. This will expect to enhance the device life and gas sensitivity.

50
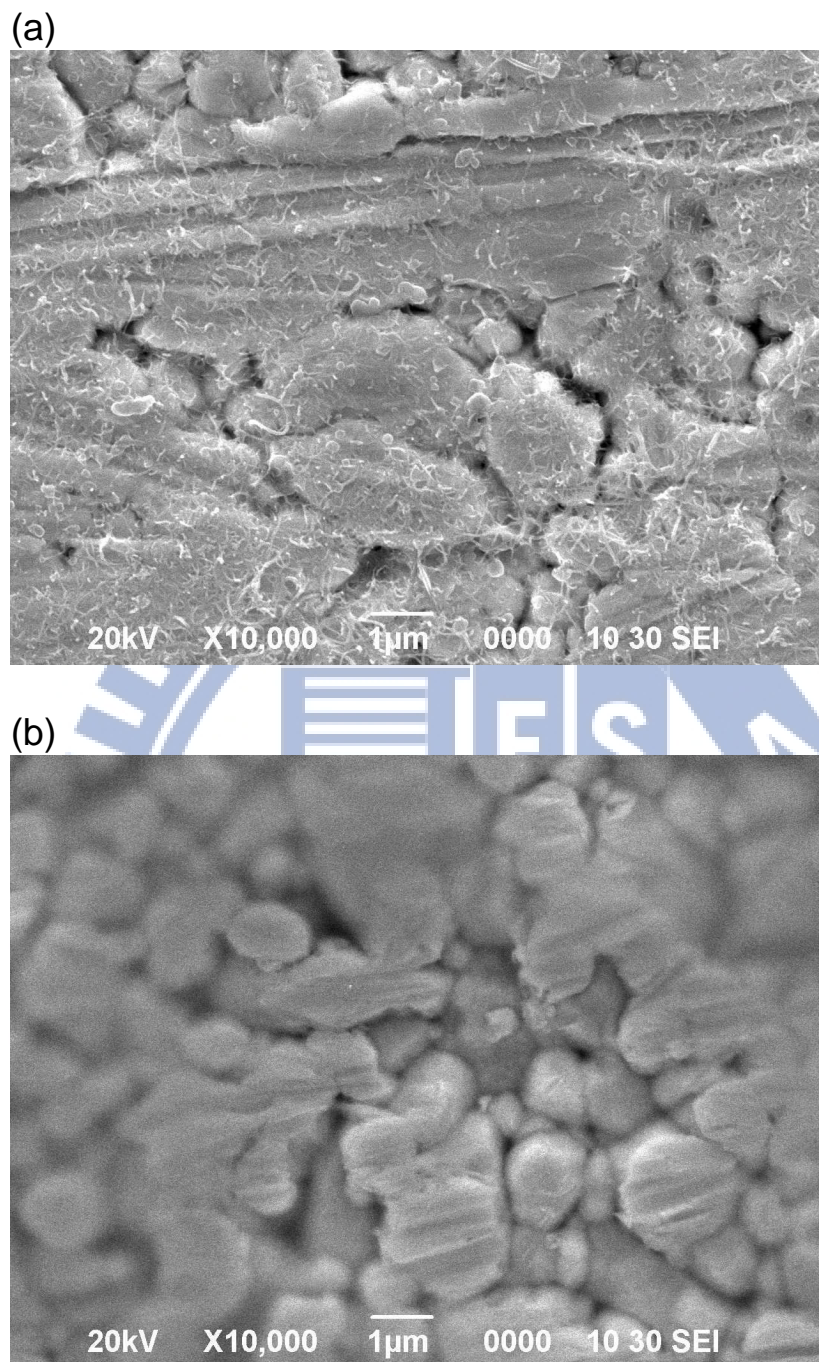
Fig. 4-4 SEM surface morphologies of: (a) MWCNTs+PVP composite, and (b) the PVP/MWCNTs stacked sensors, respectively
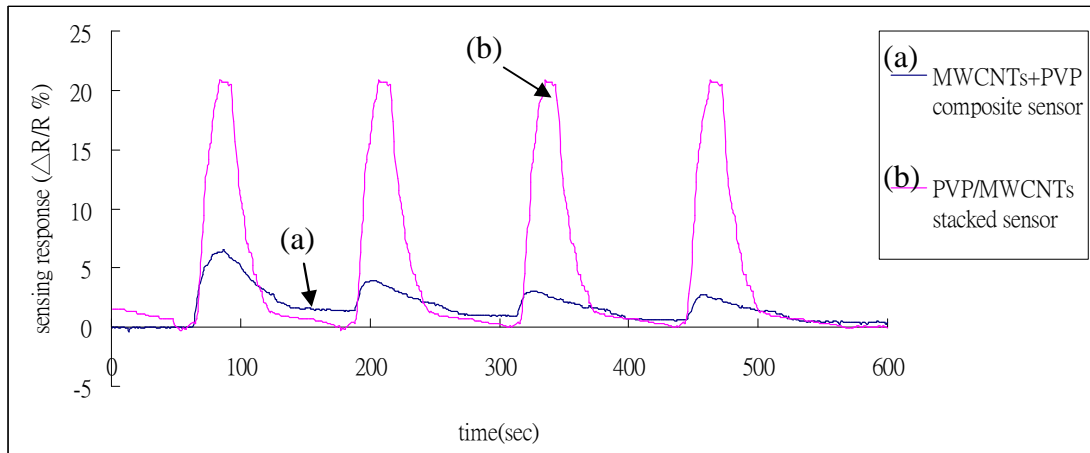
Fig. 4-5 Typical cycle sensing response ($\triangle$R/R %) curves of a gas sensor to methanol gas: (a) for MWCNTs+PVP composite sensor, and (b) for PVP/MWCNTs stacked sensor, respectively.

Gas sensing performance of MWCNTs+PVP composite and PVP/MWCNTs stacked sensors are compared. Figure 4-5 compares the gas response curves for composite and stacked sensors for sensing methanol gas (3.7% v/v) at room temperature, where (a) and (b) curves are for composite and stacked sensors, respectively. The testing sequences are 60 s dry air, 40 s methanol gas, 90 s dry air, and the last two sequences are repeated four times. The results show that the initial gas sensitivity of the stacked sensor is much higher and maintains longer after repeating testing cycles than the composite sensor. The initial peak sensing response ($\triangle$R/R %) values can reach 20.5% and 6% for stacked and composite sensors, respectively. The figure also shows that the gas sensitivity degrads much faster, and the sensitivity recovery rate by dry air is much slower for composite sensor.

The principle of gas sensing is basically to measure the resistivity change of the sensor upon contact with a target gas. When target gas contacts with the conductive polymer and CNTs can swell mainly the volume of polymer to increase device resistance, but not volume of CNTs. In other words, gas contacting specific surface area with composite sensor will be much smaller than stacked sensor due to smaller

52

polymer surface concentration of the former. This may be the reason for a greater gas sensitivity of the stacked sensor. A greater volume swelling for the stacked sensor may also signify a greater pore volume for higher gas desorption rate, which results in a higher sensitivity recovery rate via dry air.   In summary, the stacked sensor has a higher gas sensitivity, and faster sensitivity recovery rate. Consequently, the two-layer stacked sensors were used as the sensors for gas specificity study in this work.
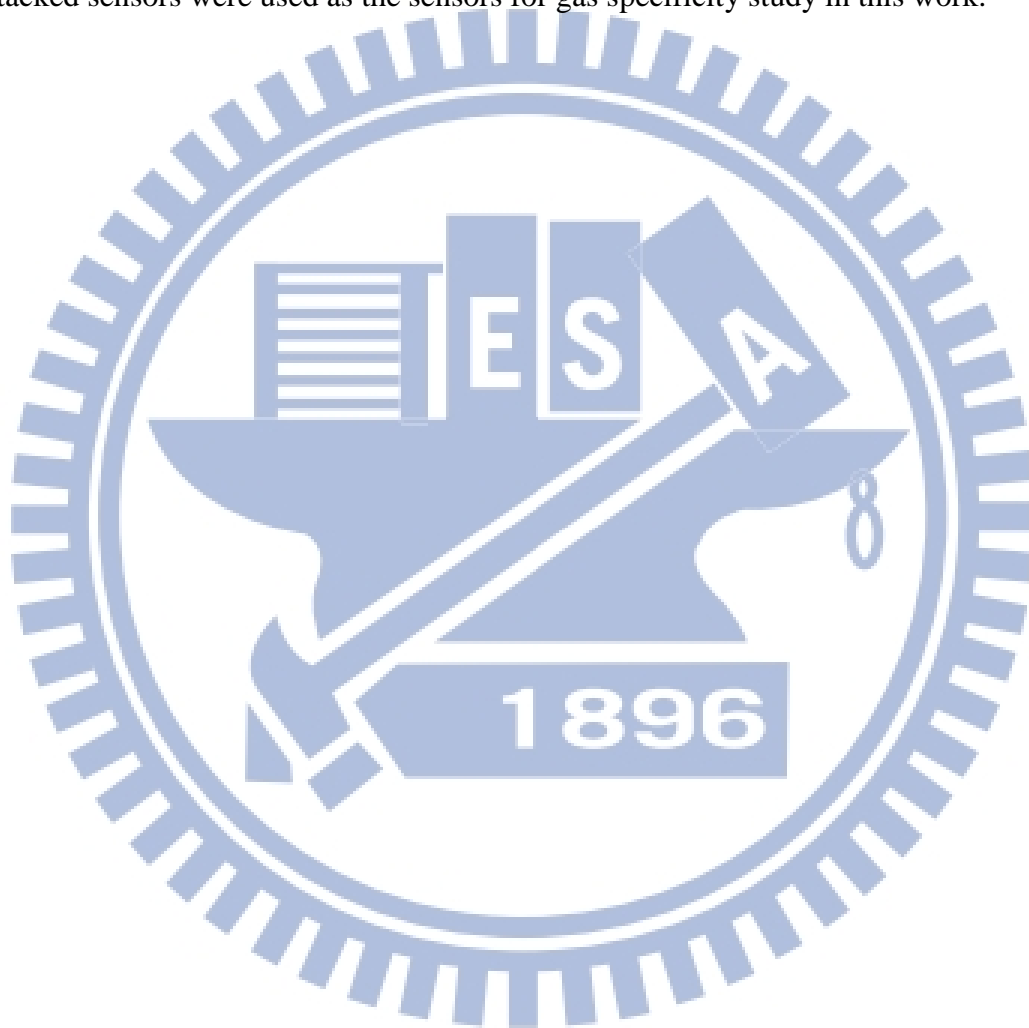
4.3. Effect of polymer layer thickness on performance of PVP/ MWCNT stacked sensors

Performances of the PVP/MWCNT stacked sensors for sensing methanol gas under different PVP polymer thicknesses were examined. Thickness of the top polymer layer was modulated by polymer concentration in the casting solution under the same repeating casting cycles. The typical cycle sensing response ($\triangle$R/R %) curves to methanol gas for different polymer concentrations (or thicknesses) are shown in Fig. 4-7. It indicates that the initial sensing responses ($\triangle$R/R) reach the maximum value after 150 s of gas introduction. However, the peak values are greater for the sensors with a smaller polymer layer thickness (or smaller polymer concentration). It is also noted that there is a greater jump in $\triangle$R/R value between thicknesseses of top layer for 1 ~ 2 wt % PVP. This is probably caused by partial destruction of some contacts between crossing nanotubes in PVP/MWCNT stacked sensing film. The 1.0 wt. % PVP membrane produced the fastest and largest response of the five sample membranes, and this polymer formulation were then be used to produce polymer/MWNCTs stacked sensor membranes for the following sensing experiments.

Table 4-1 compares the sensing responses of the composite and the stacked sensors prepared by solution drop method, including specimen designations, fabrication and sensing conditions, and ($\triangle$R/R)$_{max}$ values at room temperature
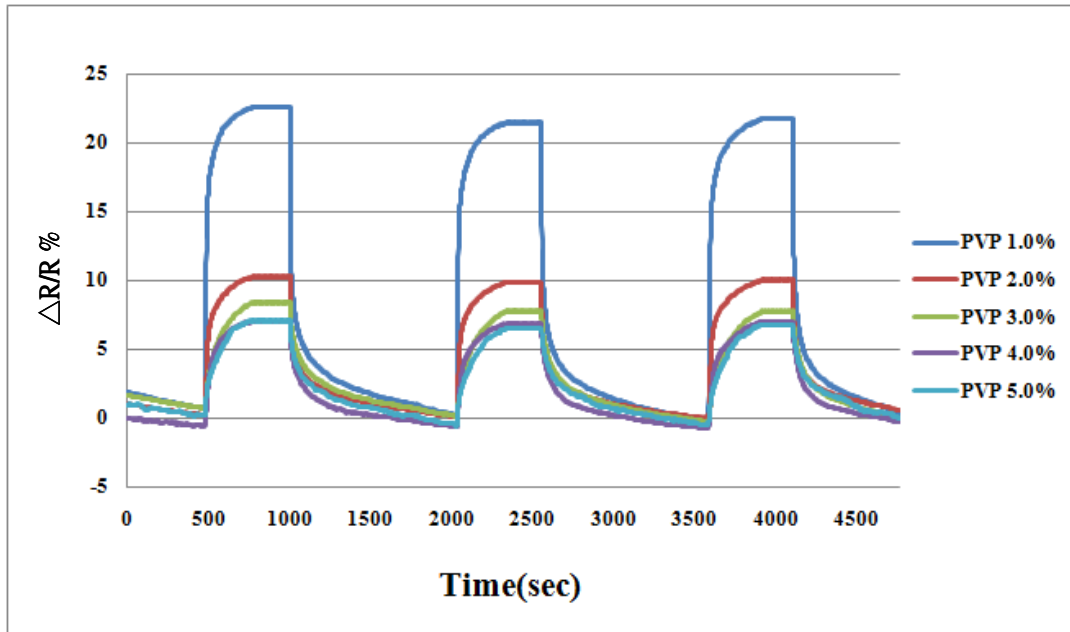
Fig. 4-6: Effect of polymer concentration in MEK solution for drop casting on cycle sensing response ($\triangle$R/R %) curves of PVP/MWCNTs stacked sensor to methanol gas
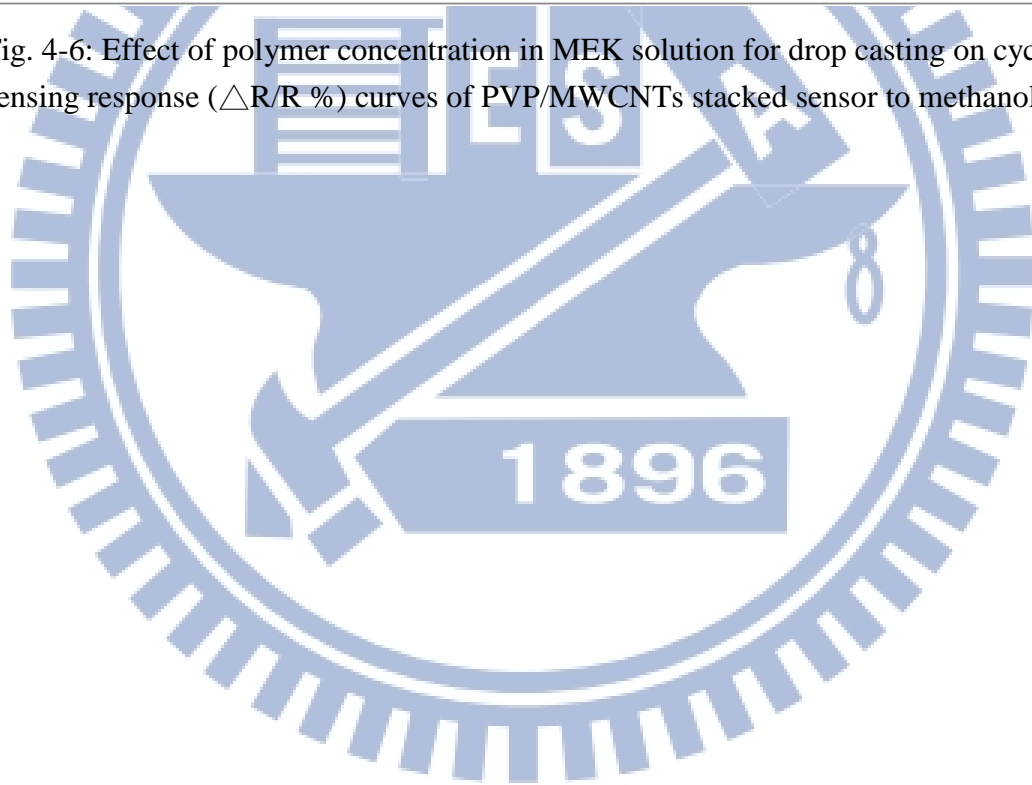
Table 4-1 Specimen designations of the MWCNTs+PVP composite and the PVP/MWCNT stacked sensors prepared by solution drop method, their fabrication and sensing conditions, and $(\triangle R/R)_{max}$ values at room temperature.

***Speci. design	Conc. in MEK solution (wt %)	**Gas conc. (v/v ppm)	*Sensing conditions	$(\triangle R/R)_{max}$ (%)
A1	1	(3.70%, v/v)	60 s (t_1) 40 s (t_2) 90 s (t_3)	6
A2	1			20.5
B1	1		500 s (t_1) 300 s (t_2) 600 s (t_3)	22.5
B2	2			10.0
B3	3	(4.3%, v/v)		7.5
B4	4			6.5
B5	5			6.1

*t1, t2 and t3 represent cycling duration times by introducing dry air, testing gas and dry air, respectively.

**the testing gas = CH_3OH (methanol gas)

***the configuration of A1 is MWCNTs+PVP composite sensor and the others (A2~B5) are PVP/MWCNT stacked sensors

Chapter 5 Results and discussion – polymer/CNT stacked sensors

The purposes of the gas sensing are to determine the gas type and its concentration, i.e. to examine the gas specificity. In this work, the principle of the gas specificity examination is to select different sensor types (i.e. using different sensing polymer materials) to give different degree of responses to different gas types and concentrations. In this chapter, selection of eight different polymer materials to form a sensor array consisting of eight polymer/MWCNT stacked sensors will be examined. In other words, dfferent responses of a sensor array to different gases will give different response pattern. The results show that the sensing patterns can only be used to determine the gas specificity within each group of gases. In this work, the examing groups of gases include (1) six toxic industrial gases (MEK, THF, toluene, xylene, $CHCl_3$, and CCl_4), (2) the three chemical warfare simulant gases (i.e. DMMP, DCM, and ACN), and (3) four liquor gases (Japanese sake, Kin-men sorghum, medicinal liquor, and Scotch whisky). Table 5-1 sumarized the sensing responses of the stacked sensors prepared by solution drop method, including specimen designations, sensing conditions, and $(\triangle R/R)_{max}$ values at room temperature The results for each of the target gas group will be discussed in the following sections.

5.1. Sensing response of six toxic industrial gases

(a) Response of SAA/MWCNTs stacked sensor

The cycle room temperature sensing response ($\triangle$ R/R %) curves for SAA/MWCNTs stacked sensors under three different gas concentrations are shown in

Figs. 5-1(a) and 5-1(b) for two different gases (THF and CHCl$_3$), respectively. The graphs illustrate a time-dependent change of parameter sensor response ($\triangle$R/R %) representing sensitivity of the SAA/MWCNTs stacked sensors. The curves also show the reponses during gas inlet and outlet cycling periods, which is related to gas adsorption/desorption on the sensor. It indicates an advantage of quick repeating usage of the sensor without additional heating to desorp the gas. By comparing Fig. 1(a) with Fig. 1(b), the former gives a quick greater response due to lower polarity of both THF gas and SAA polymer. The interaction of CHCl$_3$ and SAA polymer is slower due to a greater polarity difference of CHCl$_3$ gas and polymer, but it shows to reach more easily to an equilibrium response value, which is more favour to determine the gas concentration. For SAA/MWCNTs stacked sensors, the average values of sensing response change for each gas cycling period are approximately 0.8 % and 0.2 % for THF and CHCl$_3$ gases, respectively, as shown in Table 5-1. These values are defined at time reaching about 95% of total change during gas adsorption or desorption periods. As can be seen from the graphs, the time required is depending on the difference in polarity of gas with SAA polymer. A greater difference in polarity gives rise to a longer time. In other words, the response and recovery times are about 15–30 sec and 200-300 sec for CHCl$_3$ and THF gases, respectively. In general, the response curves demonstrate good reversibility of adsorption/desorption processes, though there are some abnormal sharp peaks in the response curves probably due to partial destruction of some contacts between crossing nanotubes in SAA/MWCNT stacked sensing film[Yoon et al. 2006].

Fig. 5-1 Effect of gas type and concentration on cycle sensing response (△R/R %) curves for SAA/MWCNTs stacked sensors: (a) THF and (b) CHCl$_3$ gases, respectively.

(b) Response of PMVEMA /MWCNTs stacked sensor

The cycle sensing response (△R/R %) curves for PMVEMA /MWCNTs stacked sensors under three different gas concentrations for six different gases: (a) MEK, (b) THF, (c) toluene, (d) Xylene, (e) CHCl$_3$, and (f) CCl$_4$ are presented in Figs. 5-2(a) to 5-2(c) and 5-3(a) to 5-3(c), respectively. The curves also show three cycling responses during the gas inlet and outlet periods. The figures demonstrate the similar

reversibility of adsorption/desorption processes, as compared with the SAA/MWCNT stacked sensor in the previous section, except a greater $(\triangle R/R)_{max}$ value for SAA/MWCNTs stacked sensor under the same gas type. By comparing SAA/MWCNT with PMVEMA/MWCNT stacked sensors, the average values of the maximum sensing response change, $(\triangle R/R)_{max}$, for each gas cycling period are approximately 0.8 % vs 1.2% and 0.2 % vs 0.8% for THF and CHCl$_3$ gases, respectively, as also shown in Table 5-1. In other words, the **PMVEMA**/MWCNT stacked sensor is more sensitive then SAA/MWCNT stacked sensor for these two gases. As to the response and recovery times, the **PMVEMA**/MWCNT stacked sensor gives the same value of 15–30 sec for CHCl$_3$ gas and a faster value of 15-30sec instead of 200-300 sec for THF gases.

For other four gases (MEK, toluene, Xylene, and CCl$_4$), there are no detectable response by SAA/MWCNT stacked sensor; but for the PMVEMA/MWCNT stacked sensor, the corresponding average maximum response values are about 0.2%, 0.4%, 0.6% and 0.2%, respectively, as show in Table 5-1. The faster response and recovery times are apparent and are in the range of 15–30 sec.
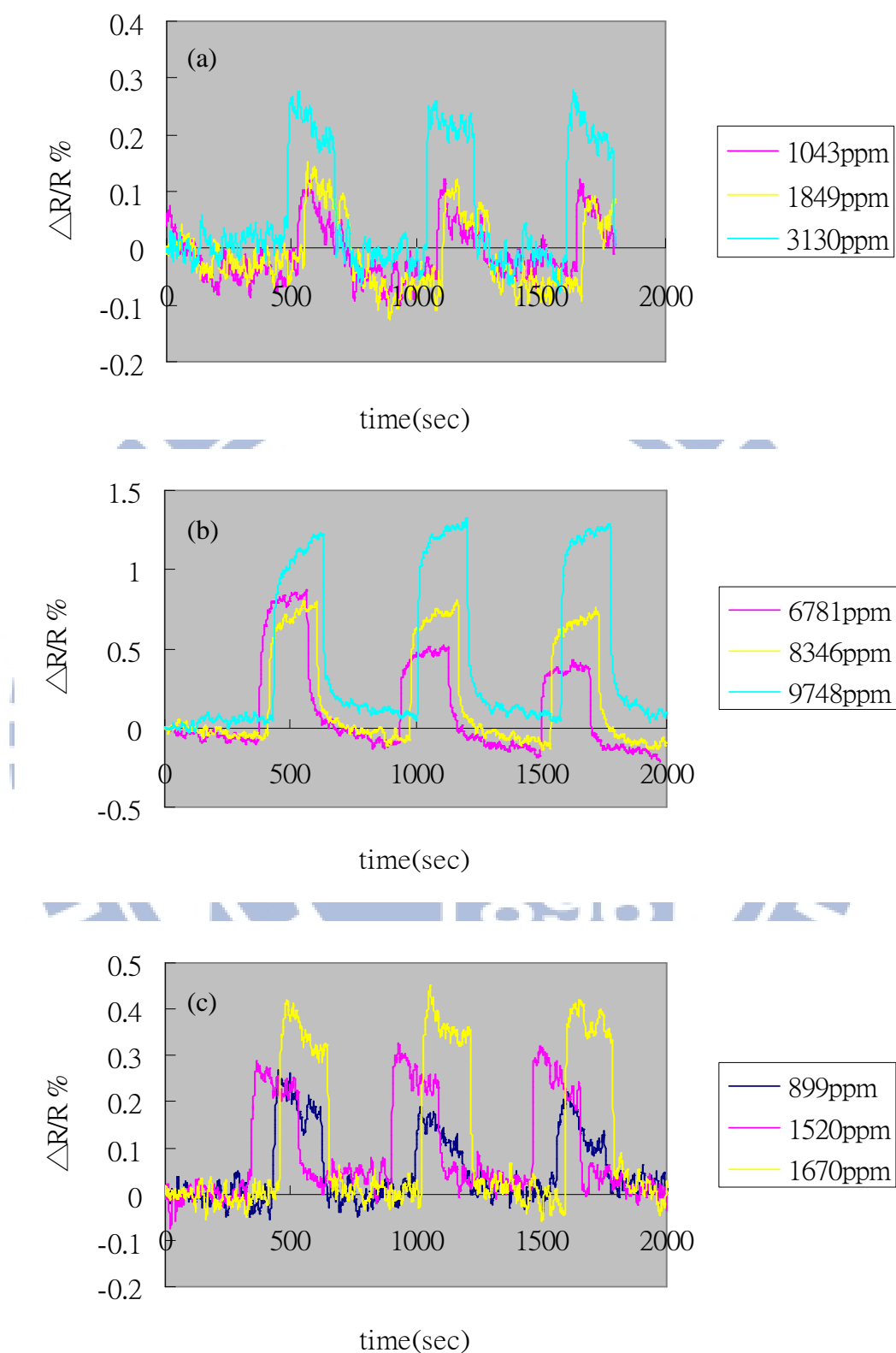
Fig. 5-2 Effect of gas type and concentration on cycle sensing response ($\triangle$R/R %) curves for PMVEMA/MWCNTs stacked sensors: (a) MEK, (b) THF, and (c) toluene
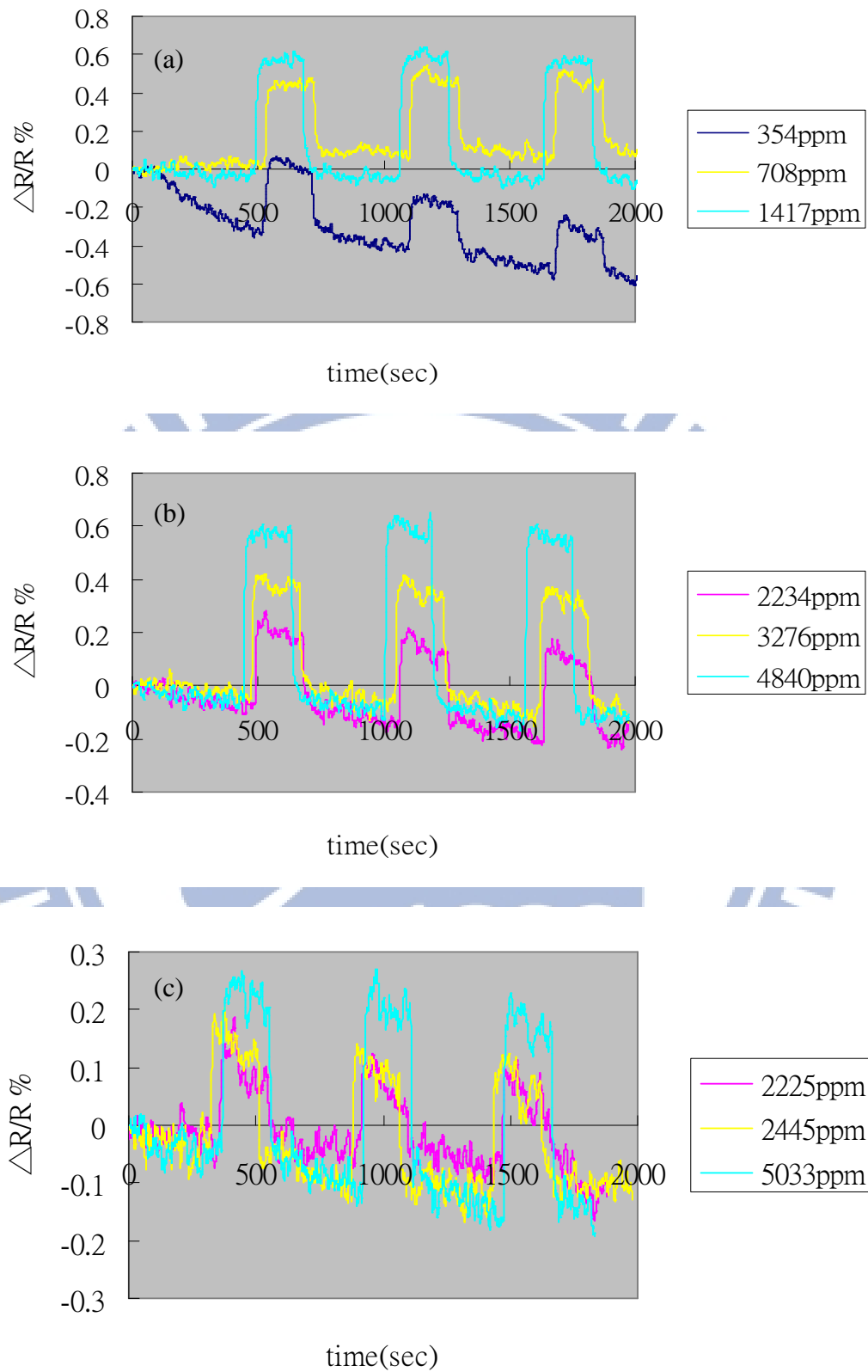
Fig. 5-3 Effect of gas type and concentration on cycle sensing response ($\triangle$R/R %) curves for PMVEMA/MWCNTs stacked sensors: (a) xylene, (b) CHCl$_3$, and (c) CCl$_4$

(c) Response of PMS/MWCNT stacked sensor

The cycle sensing response ($\triangle$R/R %) curves for PMS/MWCNT stacked sensor under three different gas concentrations for six different gases: (a) MEK, (b) THF, (c) toluene, (d) xylene, (e) $CHCl_3$, and (f) CCl_4 are presented in Figs. 5-4(a) to 5-4(c) and Figs. 5-5(a) to 5-5(c), respectively. As shown in Table 5-1, the $(\triangle R/R)_{max}$ values of this sensor are ranging from 0.3% to 1.9%, indicating their sensing sensitivities of the sensors. The minimum and maximum sensitivities are to sense MEK and THF gases, respectivily. It is found that the PMS/MWCNT stacked sensor gives the best sensing sensitivity amoung the eight stacked sensors. Another advantage of this sensor is that the reponse and recovery times are within acceptable range of 15 - 30 sec.
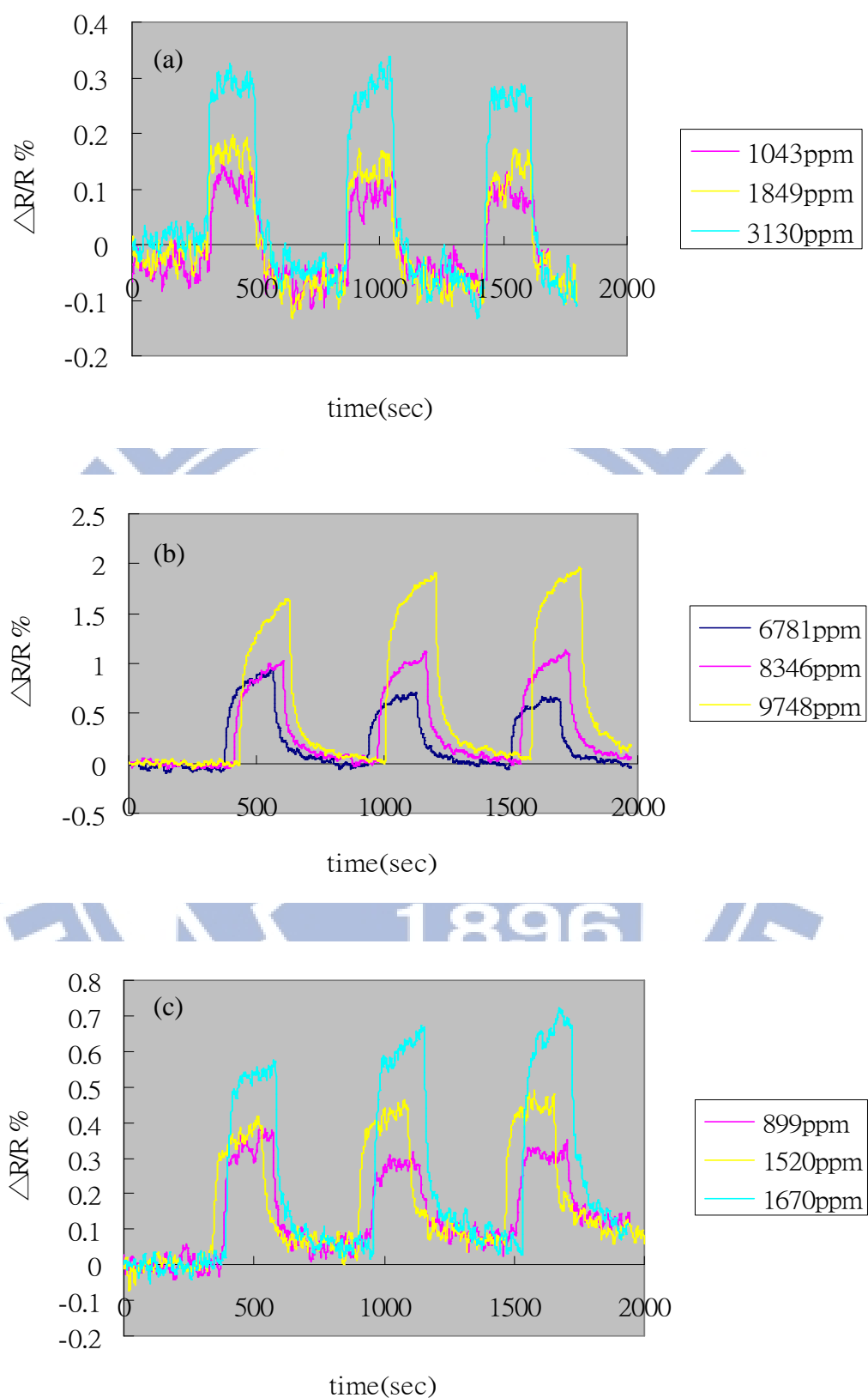
Fig. 5-4 Effect of gas type and concentration on cycle sensing response ($\triangle$R/R %) curves for PMS/MWCNTs stacked sensors: (a) MEK, (b) THF, and (c) toluene
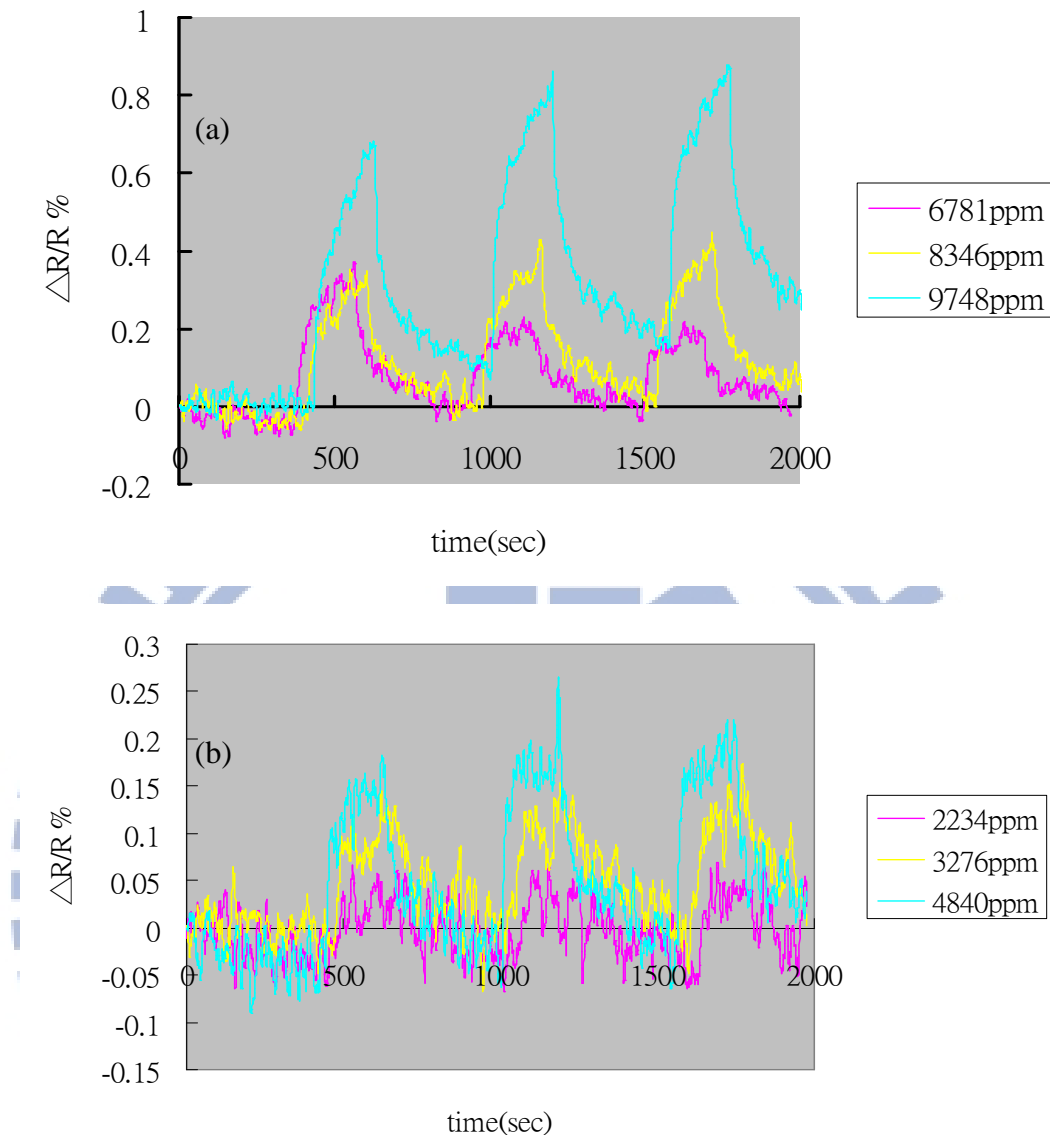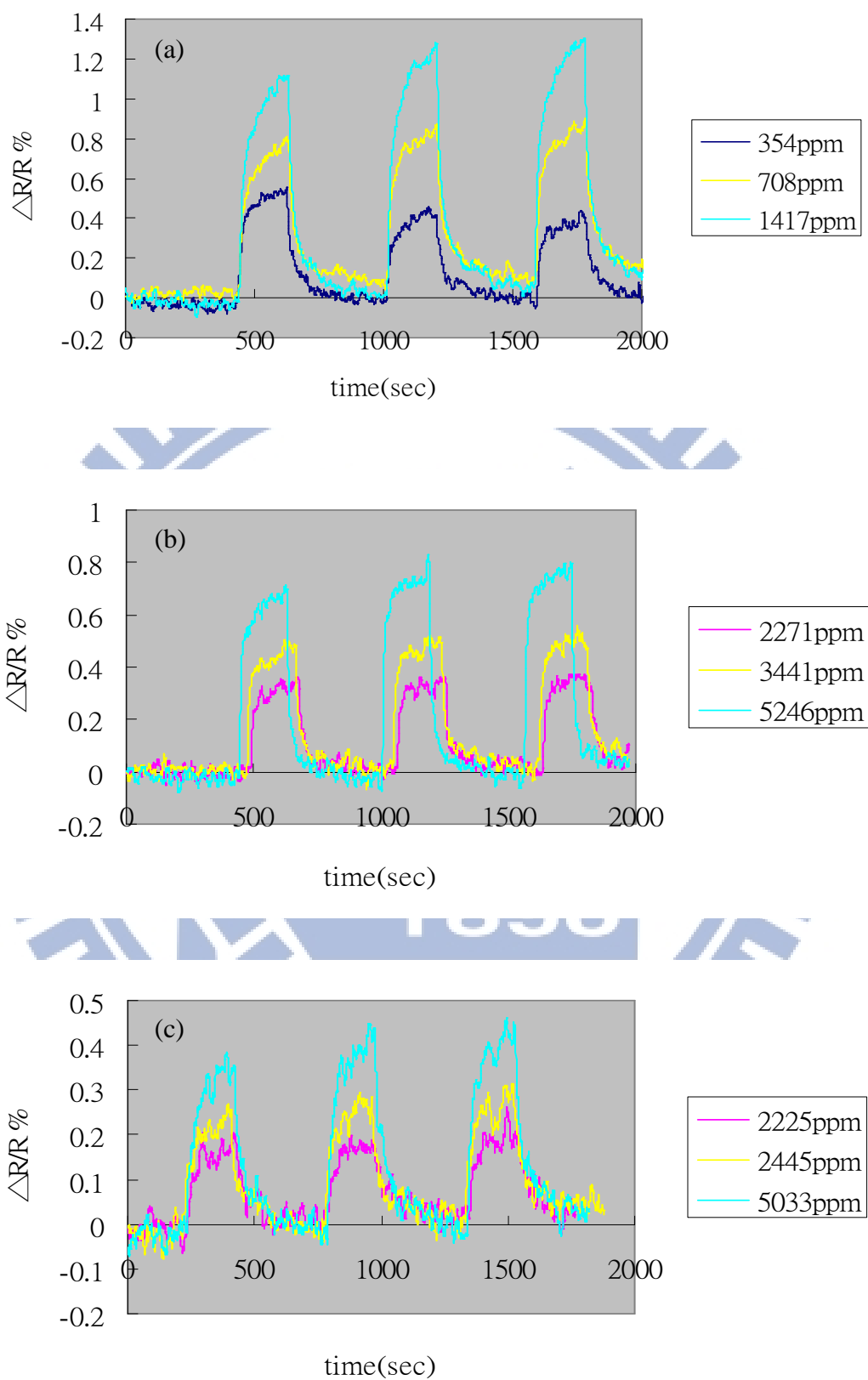
Fig. 5-5 Effect of gas type and concentration on cycle sensing response ($\triangle$R/R %) curves for PMS/MWCNTs stacked sensors: (a) xylene, (b) CHCl$_3$, and (c) CCl$_4$

(d) Response of five other stacked sensors

The five other stacked sensors include PEA/MWCNT, PVP/MWCNT, P(VDC-AN)/MWCNT, HPMC/MWCNT, and PVBC/MWCNT. It is known that polymer selection for fabricating the stacked sensor within a sensing chip depends greatly on the distribution of their chemical functionalities to interact with test gases. If the target polymers possess a broad distribution of chemical functionalities, then it will result in a broad distribution of sensing responses to determine the gas specificity. From Table 5-1, it indicates that the sensing sensitivity is varied from sensor to sensor and from gas to gas. In other words, the eight stacked sensors on a chip in this work possess the ability to differentiate the gas type or gas specificity of the gas group, which consists of six toxic industrial gases. This is the best advantage of this sensor array.

(e) The bar chart and radar plots of the sensing chip for this gas group

Based on $(\triangle R/R)_{max}$ values in Table 5-1, Figs. 5-6, 5-7, and 5-8 show the sensing response bar charts of the sensing chip with eight polymer/MWCNT stacked sensors. The testing group of gases in this case includes six toxic industry compounds (TIC) gas (MEK, THF, toluene, xylene, $CHCl_3$, and CCl_4) under three different concentrations. The corresponding sensing response radar plots are indicated in Figs. 5-9, 5-10, and 5-11, respectively.

From the bar charts, it is noted that the variations of sensing response with respect to gas concentration are nearly linear for most of the sensors, except PVP assisted sensor for toluene gas sensing. In other words, the most of the sensors in the chip can be used to determine the gas concentration. It is also noted that these bar charts or radar plots indicate different patterns under different gas types and

66

concentrations. In other words, selections of polymer group in the sensing chip in this work are good enough for determining the gas specificity of this gas group.

Fig. 5-6: Bar charts of the peak sensing response, $(\triangle R/R)_{max}$, of the sensing chip under different gas concentrations for (a) MEK, and (b) THF gases, respectively.

Fig. 5-7: Bar charts of the peak sensing response, $(\triangle R/R)_{max}$, of the sensing chip under different gas concentrations for (a) toluene, and (b) xylene gases, respectively.
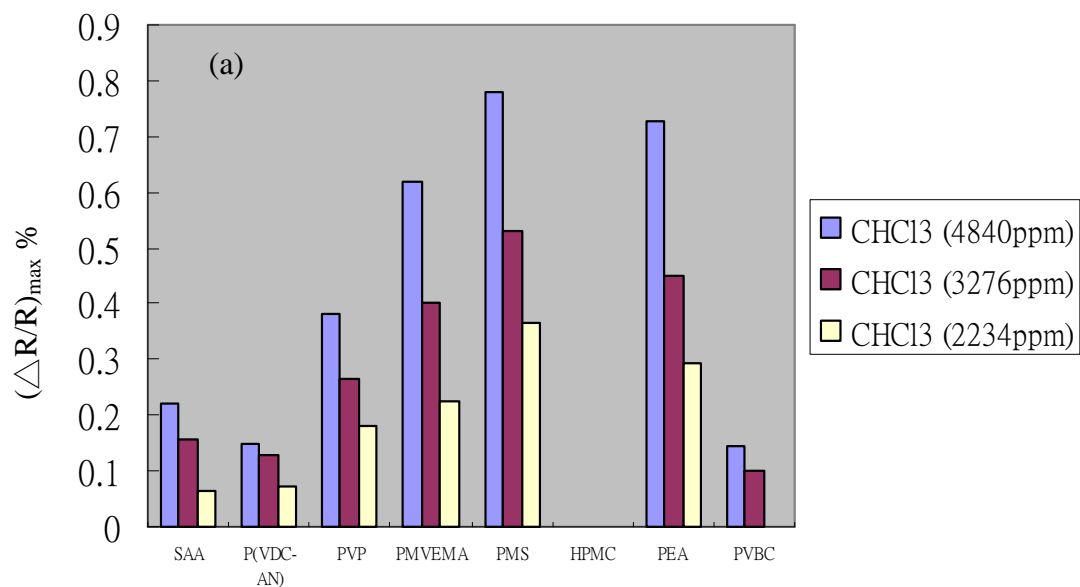
Fig. 5-8: Bar charts of the peak sensing response, $(\triangle R/R)_{max}$, of the sensing chip under different gas concentrations for (a) $CHCl_3$, and (b) CCl_4 gases, respectively.
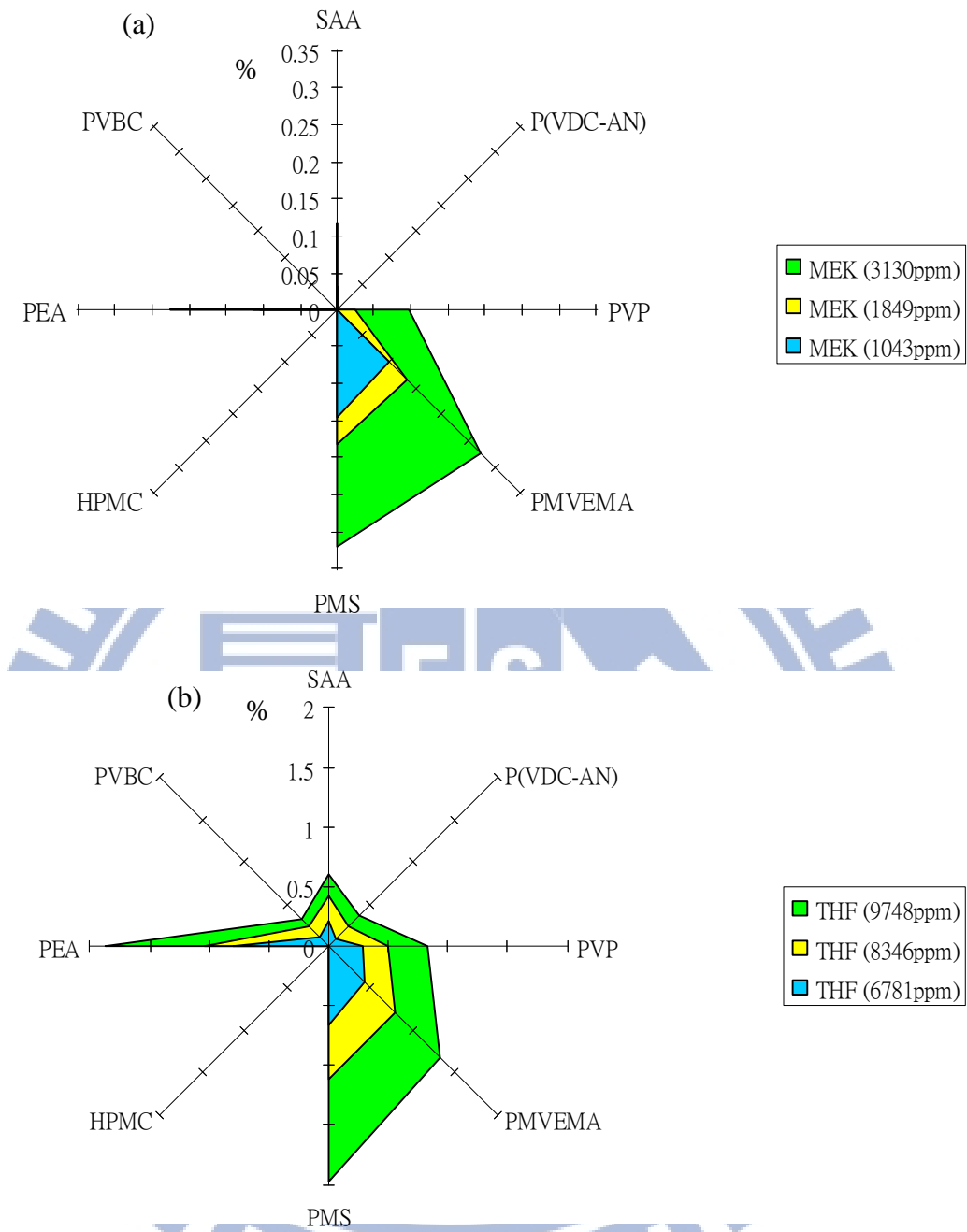
Fig. 5-9: Radar plots of the peak sensing response, $(\triangle R/R)_{max}$, of the sensing chip under different gas concentrations for (a) MEK, and (b) THF gases, respectively.
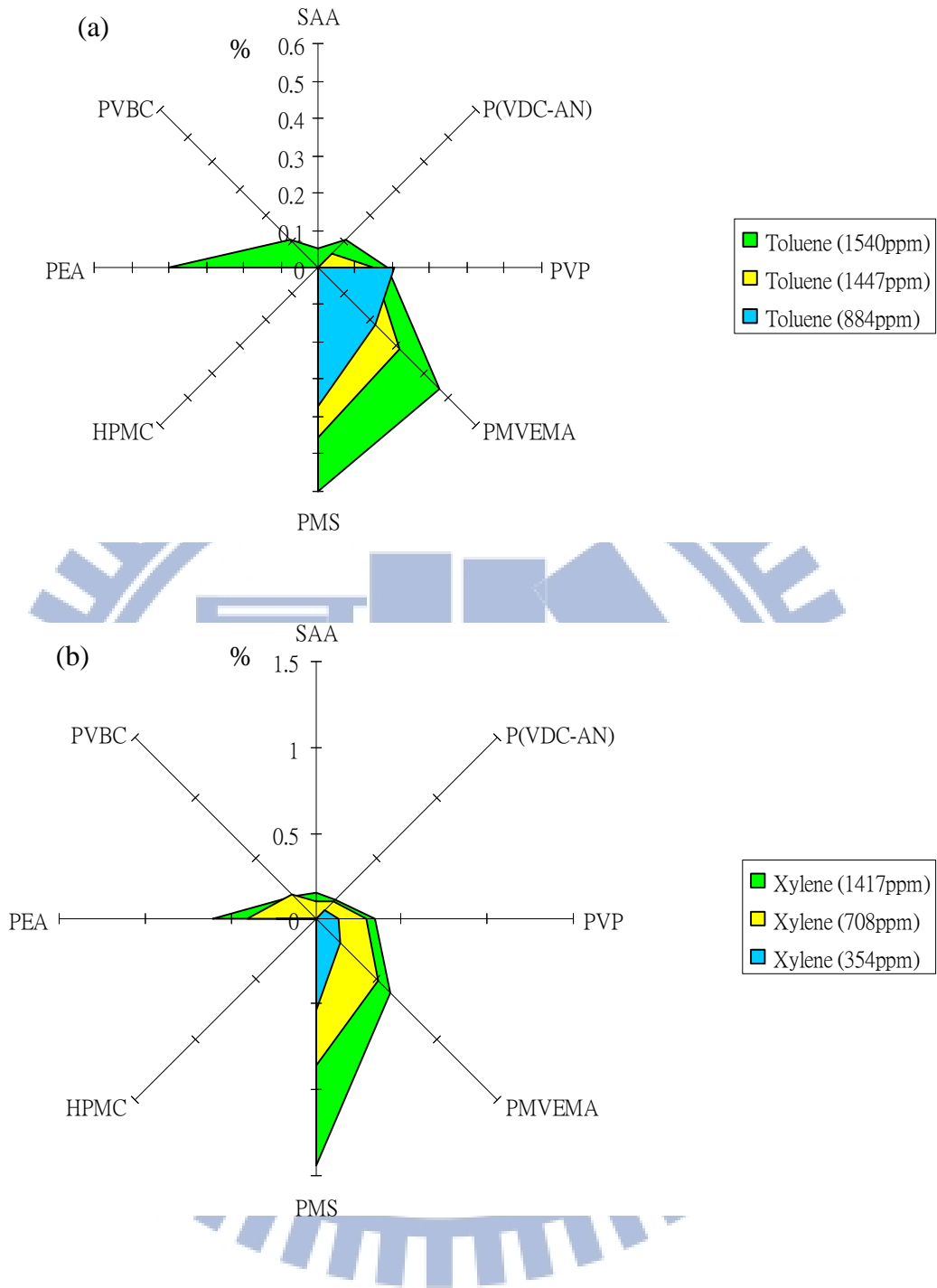
Fig. 5-10: Radar plots of the peak sensing response, $(\triangle R/R)_{max}$, of the sensing chip under different gas concentrations for (a) toluene, and (b) xylene gases, respectively.
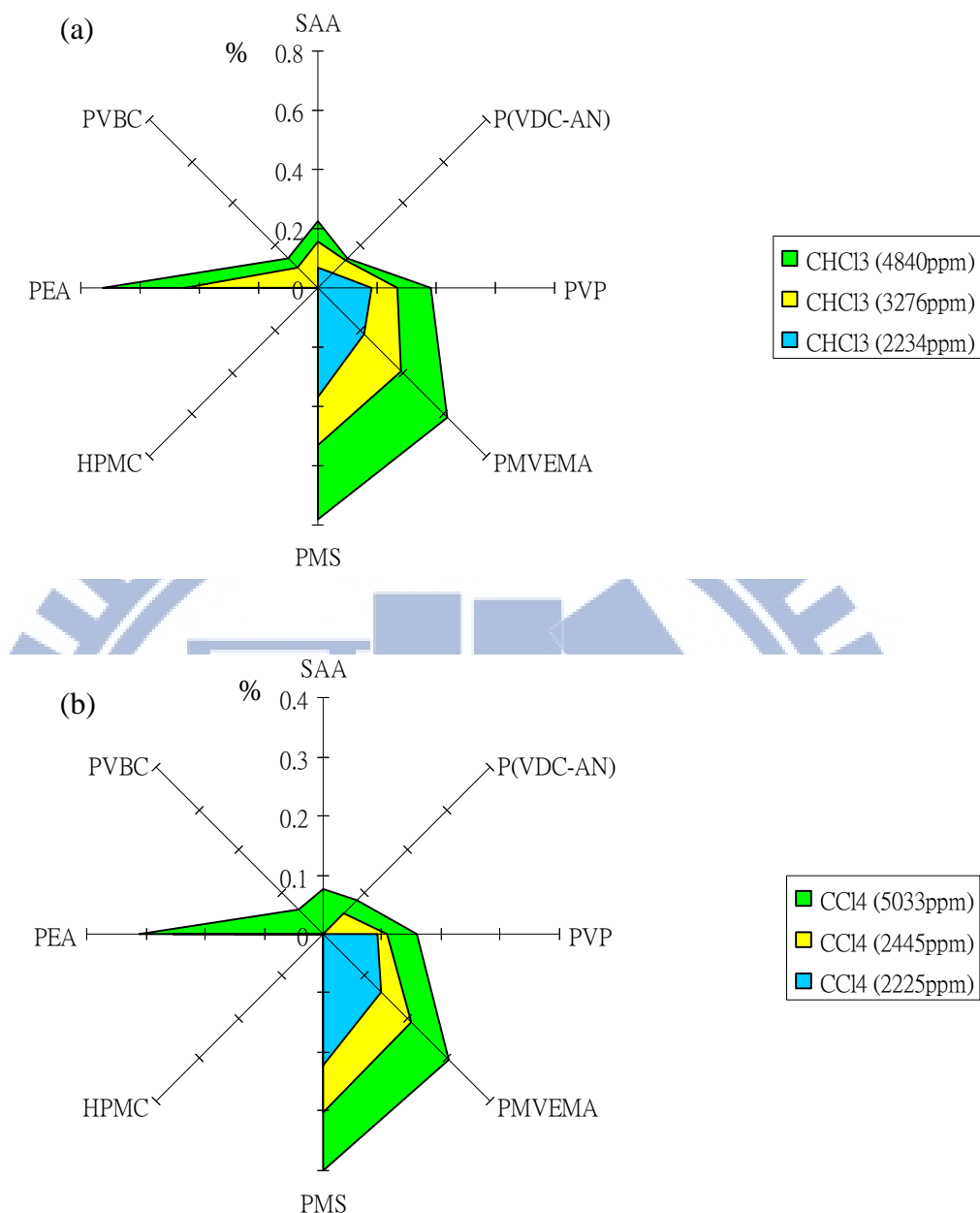
Fig. 5-11: Radar plots of the peak sensing response, $(\triangle R/R)_{max}$, %), of the sensing chip under different gas concentrations for (a) $CHCl_3$, and (b) CCl_4 gases, respectively.

5.2. Sensing response of three chemical warfare agents

The eight different gas sensors on a chip were also used for sensing the warfare gas group, which includes three chemical warfare agent simulants: dimethyl-methyl phosphonate (DMMP), dichloromethane (DCM), and acetonitrile (ACN). Figures

5-12 and 5-13, 5-14 and 5-15, 5-16 and 5-17 show the bar chart and the corresponding radar charts of the peak sensing response $(\triangle R/R)_{max}$, for these three simulant gases, respectively.
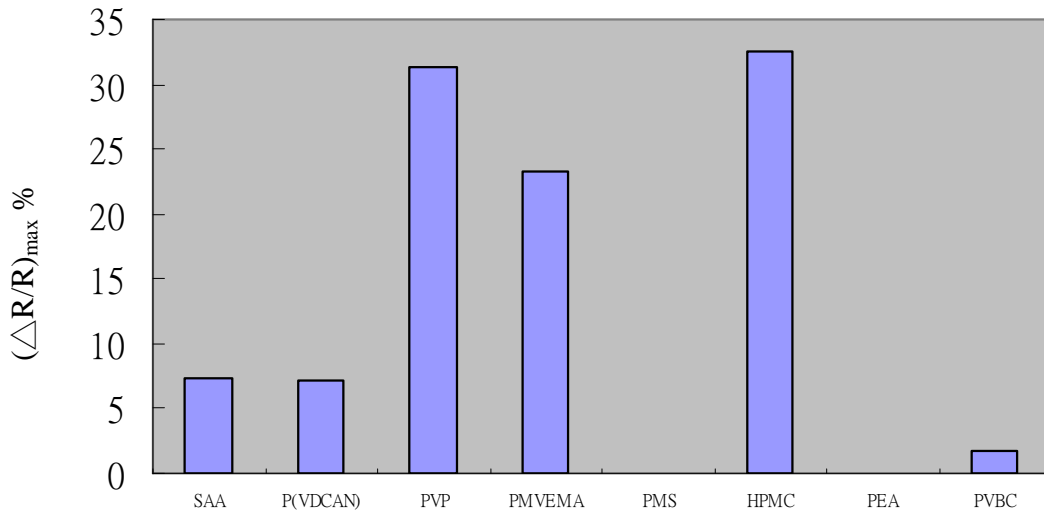
Fig. 5-12 Bar charts of the peak sensing response, $(\triangle R/R)_{max}$, of the sensing chip to DMMP gas, respectively.
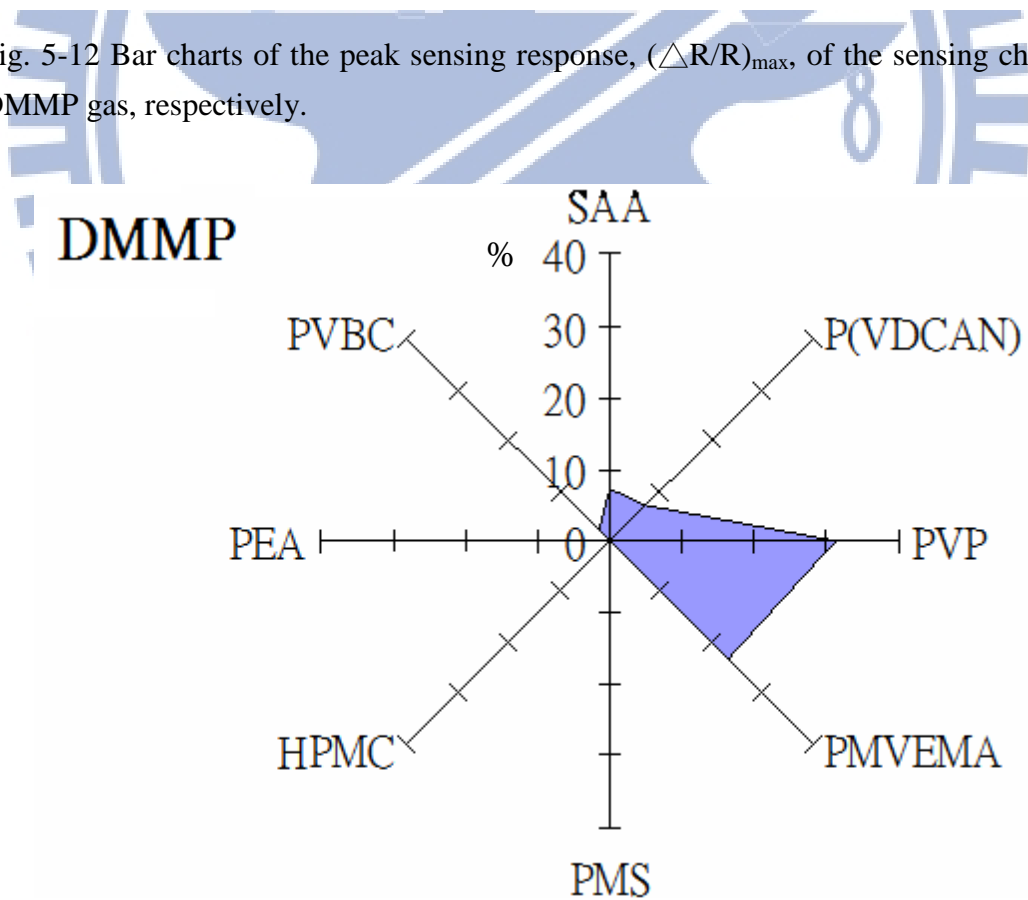
Fig. 5-13 Radar plot of of the peak sensing response, $(\triangle R/R)_{max}$, of the sensing chip to DMMP gas, respectively.
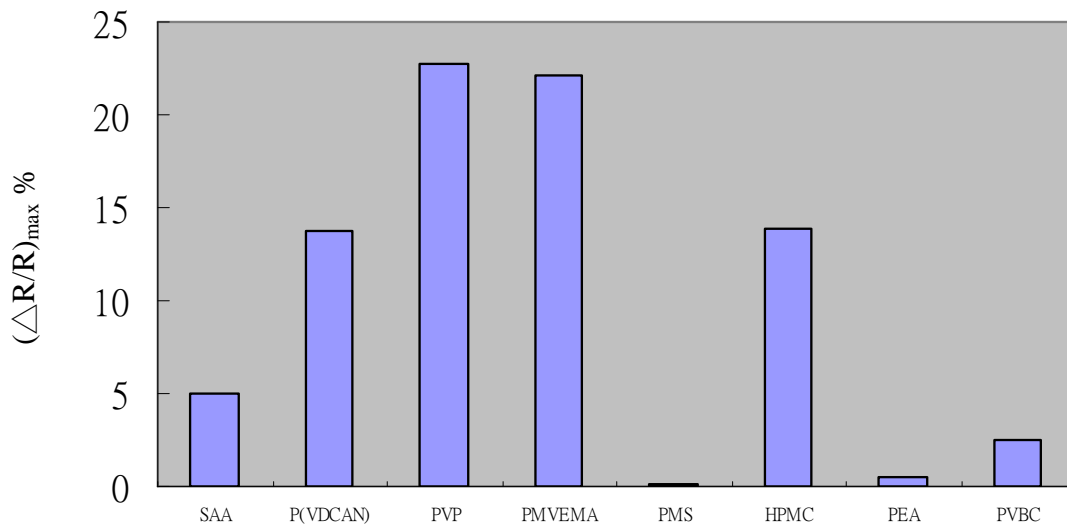
Fig. 5-14 Bar chart of the peak sensing response, $(\triangle R/R)_{max}$, of the sensing chip to DCM gas, respectively.
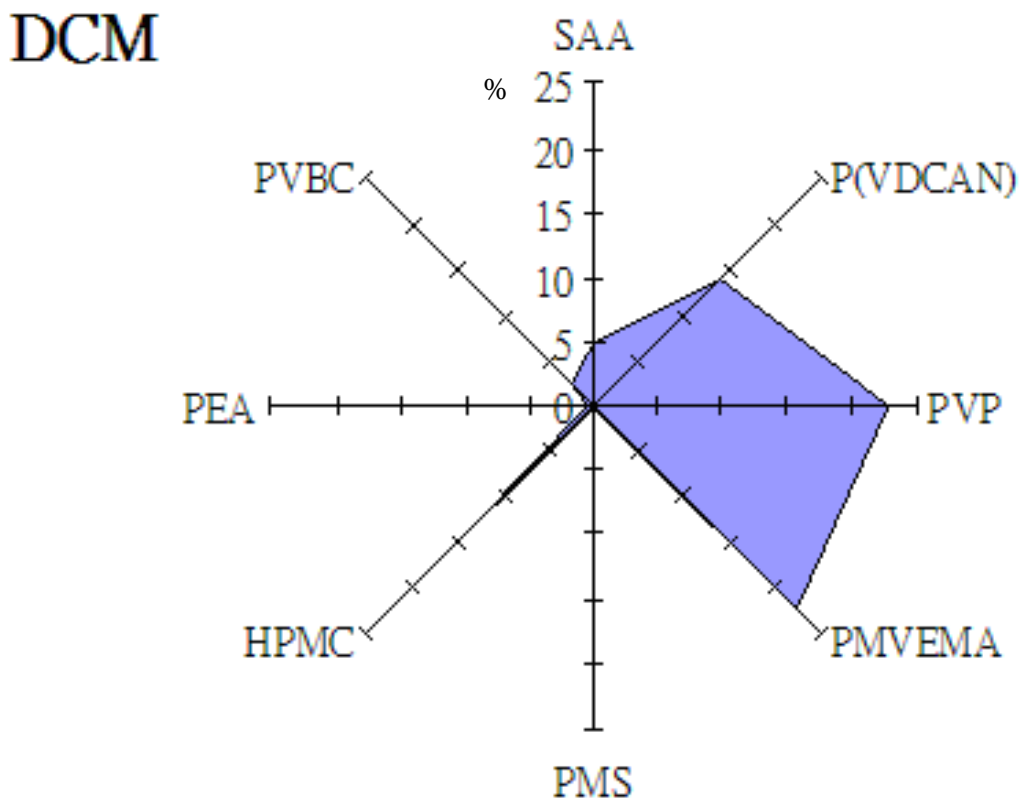
Fig. 5-15 Radar plot of the peak sensing response, $(\triangle R/R)_{max}$, of the sensing chip to DCM gas, respectively.
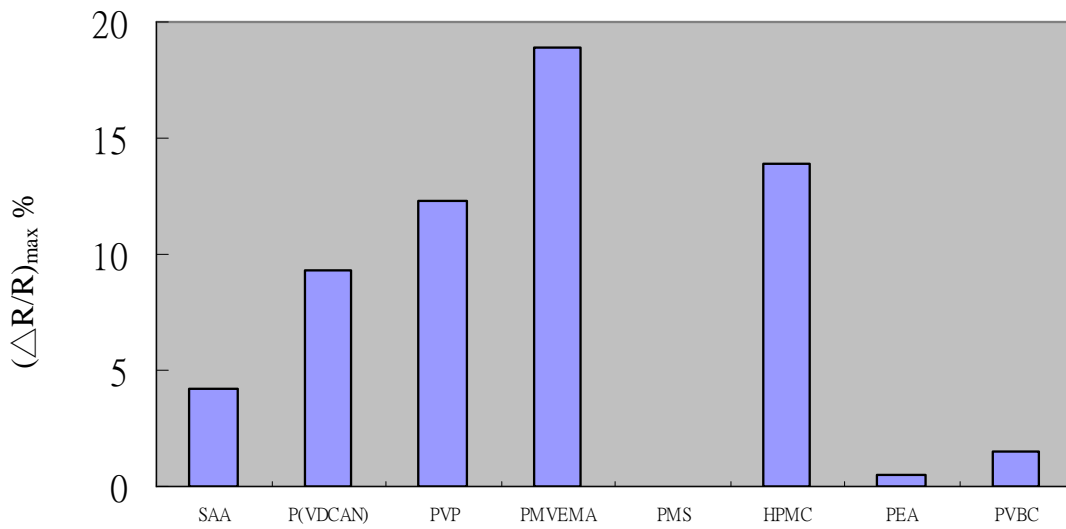
Fig. 5-16 Bar chart of of the peak sensing response, $(\triangle R/R)_{max}$, of the sensing chip to ACN gas, respectively.
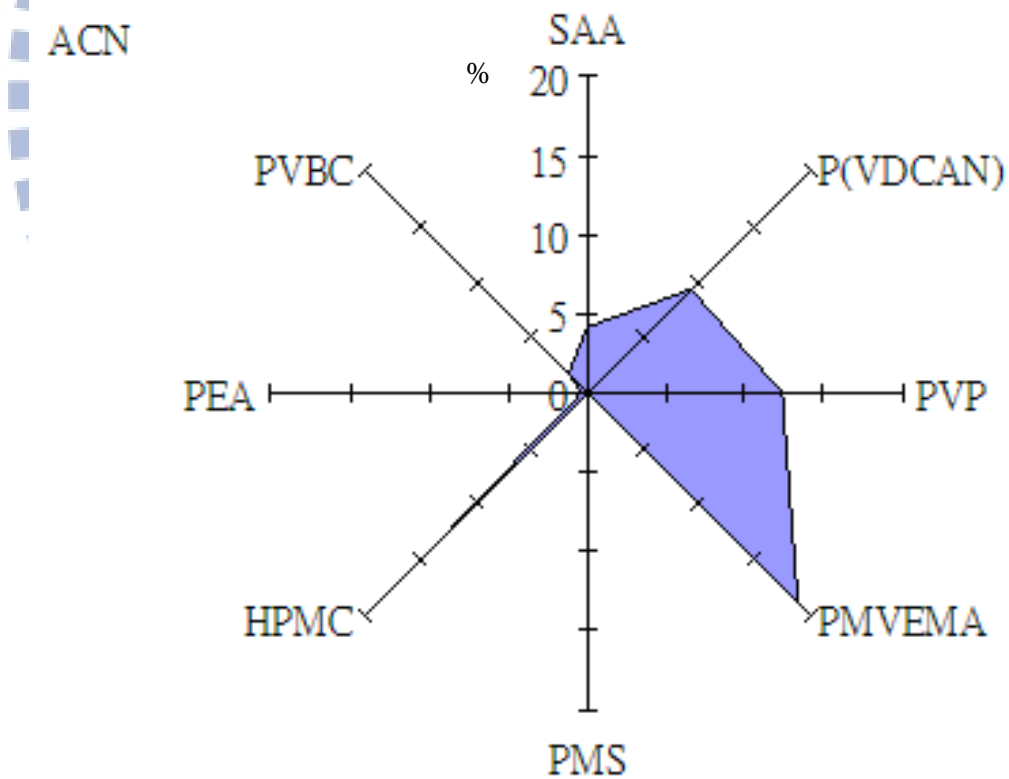
Fig. 5-17 Radar plot of the peak sensing response, $(\triangle R/R)_{max}$, of the sensing chip to ACN gas, respectively.

From the bar chart (Fig. 5-12) and the corresponding radar plots (Fig. 5-13), it shows that PMS and PEA assisted sensors have no detectable response to DMMP gas. The sensing responses of other six sensors are in a broad range and are in order of HPMC > PVP >> PMVEMA >> SAA > PVDCAN >> PVBC.

From the other two bar charts (Fig.s 5-14 and 5-16) and the corresponding radar plots (Figs. 5-15 and 5-17), it reveals that PMS and PEA assisted sensors have no significant response to DCM and ACN gases. The sensing responses of other six sensors are also in a broad range. The greatest response values ($\triangle$**R/R**)$_{max}$) for DMMP (453 ppm), DCM (12.4%) and CAN (1.5%) gases are about 32.5%, 22.8% and 18.7%, respectively, which are corresponding to using the HPMC, PVP and PMVEMA gas sensors, respectively.

By examining these bar charts and the radar plots (Figs. 5-13 ~ 5-17), It indicates that these bar charts or radar plots show significant difference in bar chart and radar plot patterns. In other words, it suggests that the eight kinds of polymers selected by the LSER formula are highly capable of distinguishing these three gases in this gas group.

5.3. Sensing response of four liquor gases

Figures 5-18(a), 5-18(b), 5-19(a) and 5-19(b) show the bar chart of the peak sensing response $(\triangle R/R)_{max}$ values of a sensing chip with eight different stacked sensors under four different gas concentrations for liquor gas group with four liquor gases (Japanese sake, Kin-men sorghum, medicinal liquor, and Scotch whisky gases), respectively. The corresponding radar plots are shown in Figs. 5-20(a) ~ 5-21(b), respectively.
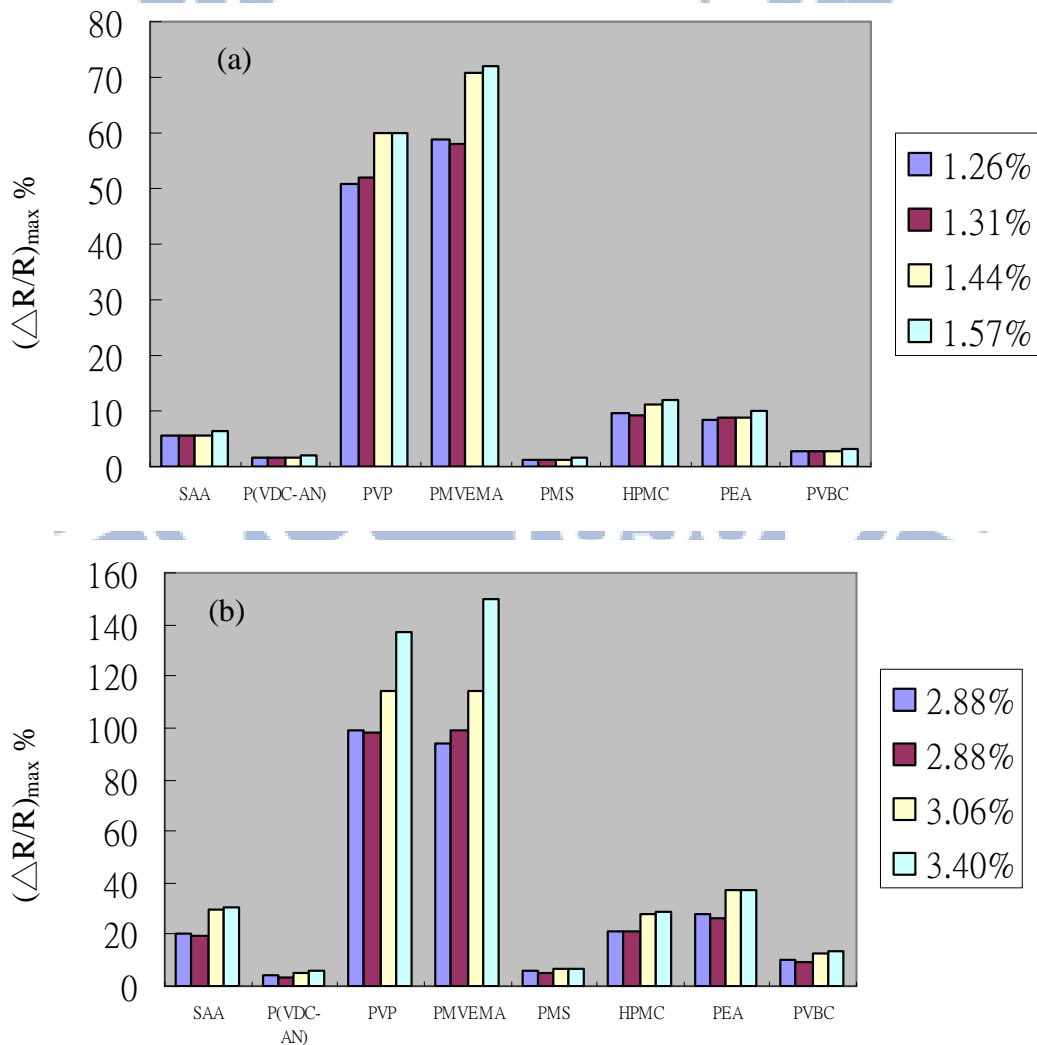
Fig. 5-18 : Bar chart of the peak sensing response, $(\triangle R/R)_{max}$), of the sensing chip under different gas concentrations for (a) Japanese sake, and (b) Kin-men sorghum gases, respectively.
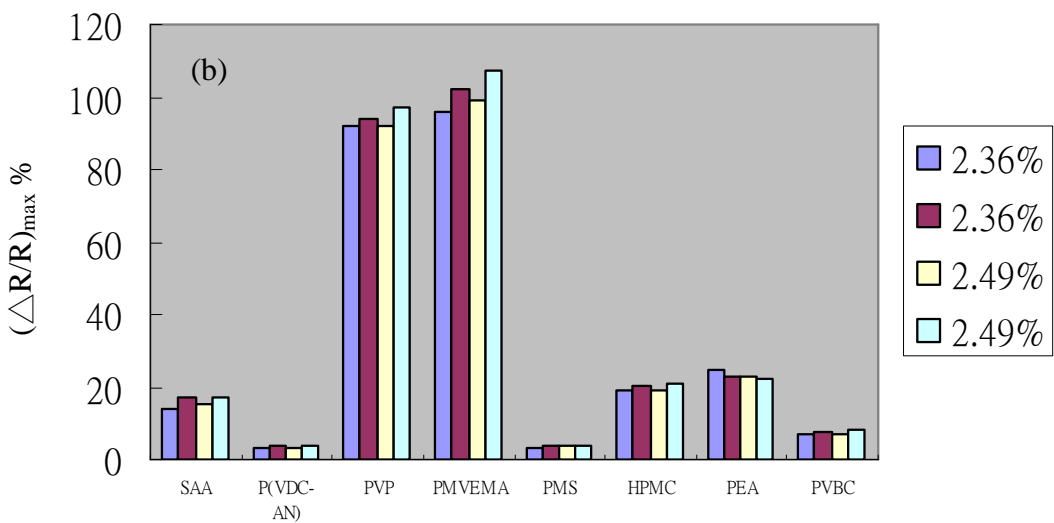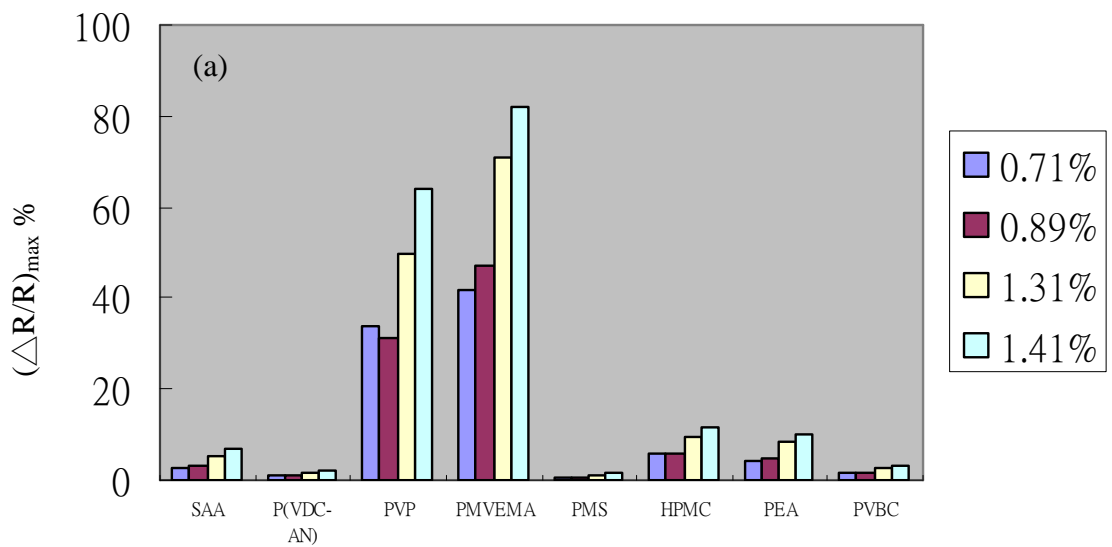
Fig. 5-19 : Bar chart of the peak sensing response, $(\triangle R/R)_{max}$, of the sensing chip under different gas concentrations for (a) medical liquor, and (b) Scotch whisky gases, respectively.
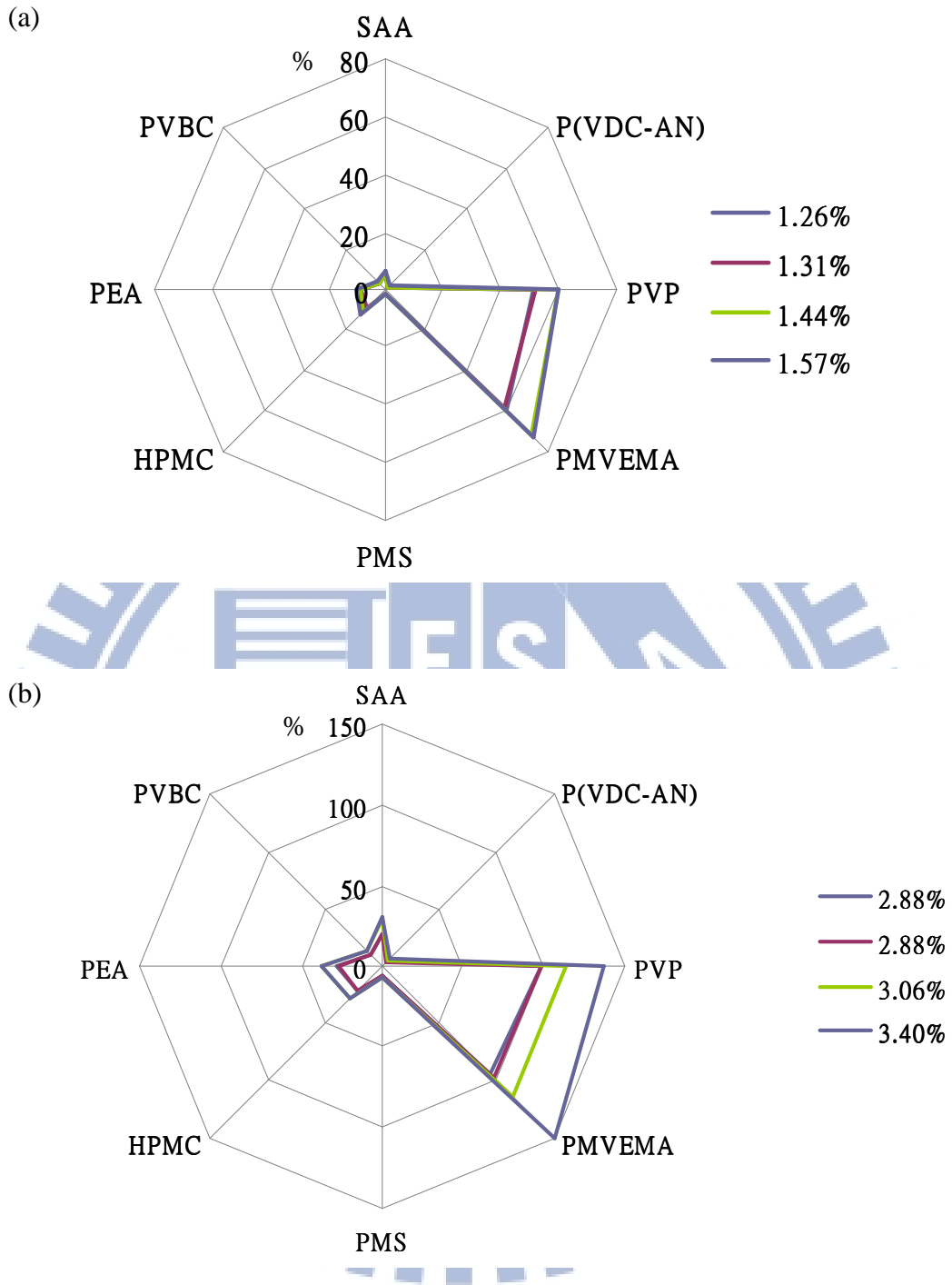
Fig. 5-20: Radar plots of the peak sensing response, $(\triangle R/R)_{max}$, of the sensing chip under different gas concentrations for (a) Japanese sake, and (b) Kin-men sorghum gases, respectively.
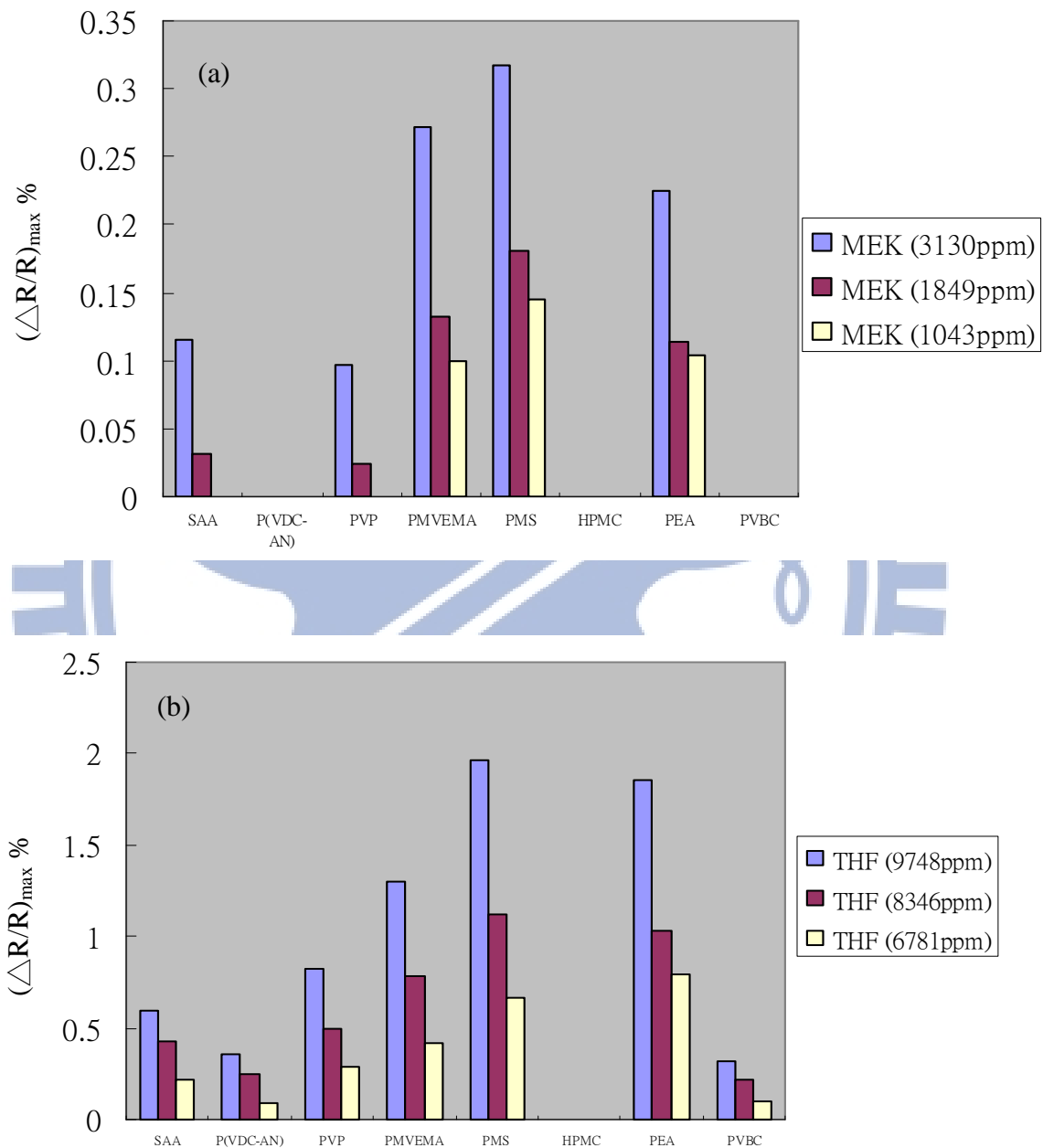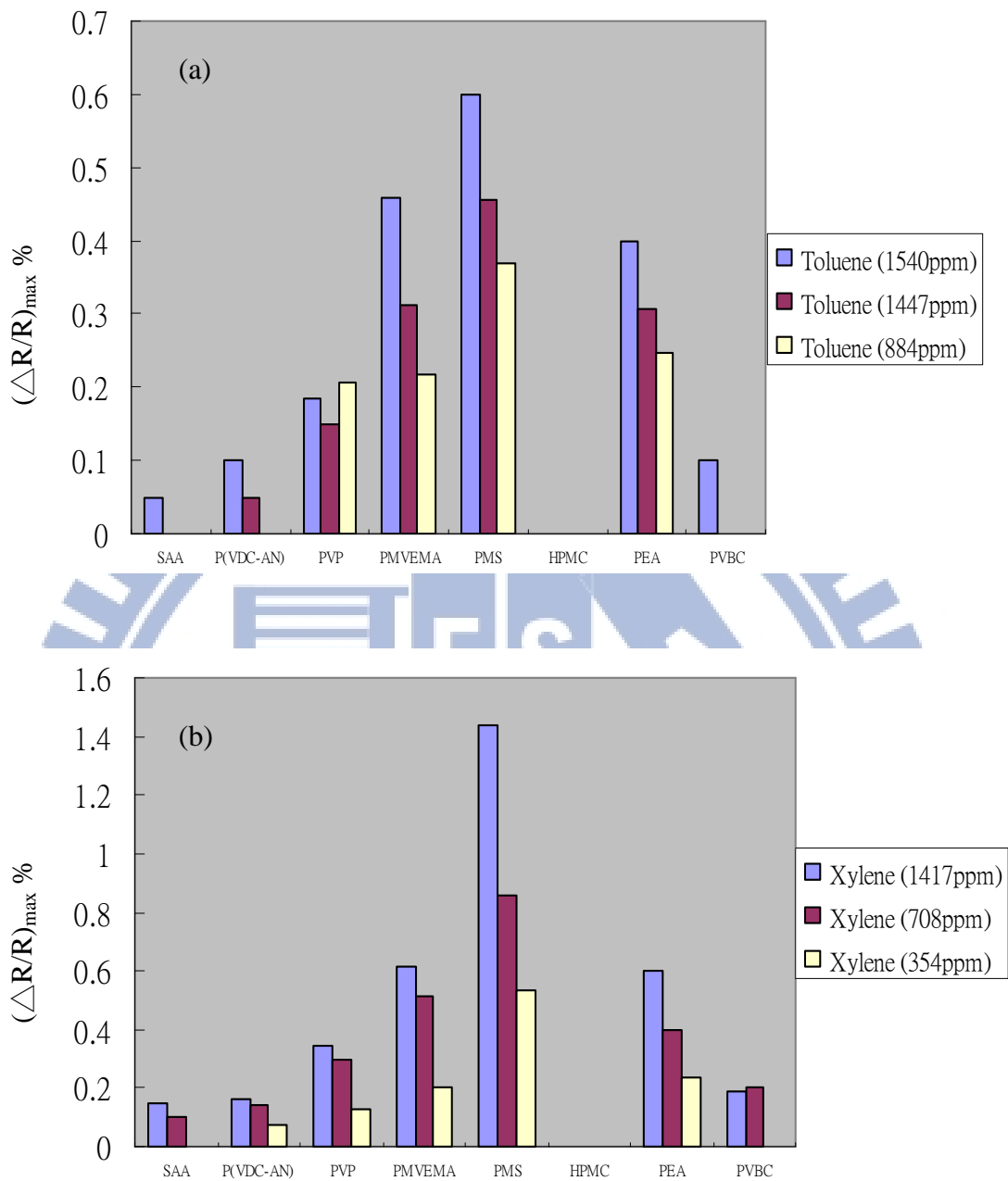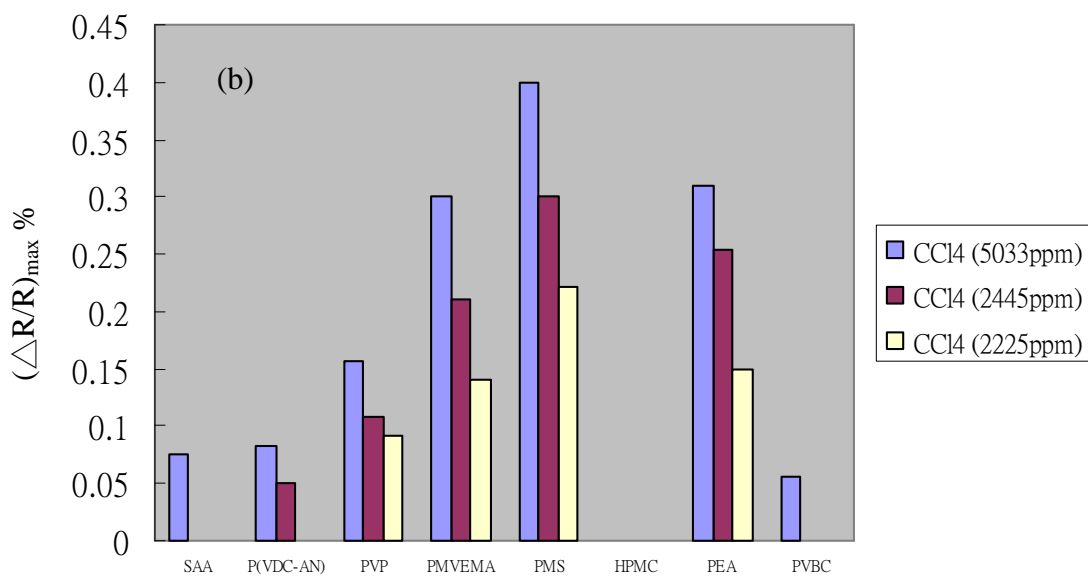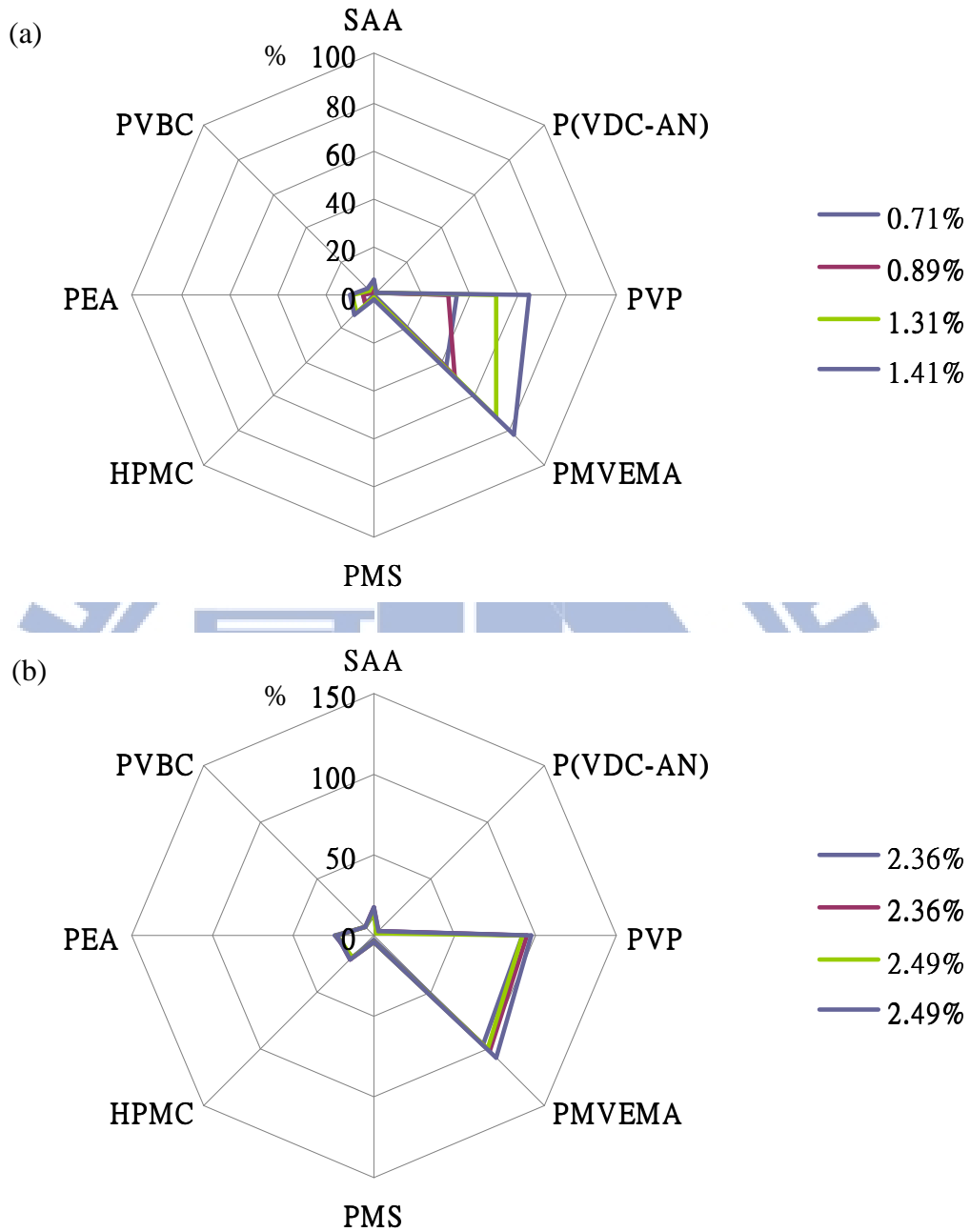
Fig. 5-21: Radar plots of the peak sensing response, $(\triangle R/R)_{max}$), of the sensing chip under different gas concentrations for (a) medical liquor, and (b) Scotch whisky gases, respectively.

By comparing with other gas groups (industrial gas group and warfare simulant gas group), these bar charts and radar plots for liquor gas group indicate that the patterns in the same gas group can be identified more easily. On the contrary, the patterns under different gas group may not be able to be identified.

In this work, three different groups of gases were examined with a chip or array with eight different polymer/MWCNT stacked sensors. It is noted that selection of polymer group takes an important role to determine the possibility of sensing the gas type and its concemtration. The solvation coefficient between gas and polymer estimated by LSER equation was one of the methods to be used to select the sensing polymer materials [Hierlemann et al. 2001; Ryan et al. 1998], as discussed in Section 3.6. Such estimation was based on the parameters of dispersive interactions, dipole interactions, hydrogen bond acidity, and hydrogen bond basicity. The solvation coefficients between ethanol gas and various polymer membranes were estimated to be in order of PMVEMA < PEA < HPMC < PVBC. A smaller solvation coefficient was proposed to be corresponding to a larger interaction between ethanol gas and polymer, resulting in a larger resistance variation. By examing the response intensity for the liquor gas group, the results show the PMVEMA polymer gives the highest sensing response due to its lowest solvation coefficient value. It is in consistant with the estimation by LSER equation. As to other two gas groups, there are no enough data to make the estimation. However, such estimation may not be able to apply to the system with the prescence of both polymer and MWCNTs, because carbon nanotubes may change the physical characteristics of the film (glass transition temperature, rigidity, and density), and possibly the chemical characteristics.

It was reported that the radar plot patterns may correlate with resident microstructural differences of these composite gas-sensing materials (CNTs + polymers), e.g. the nature of their attendant chemical functional groups. In general, the sensing behavior of polymers is related to localized molecular interactions with the analyte, including chemical bond formation, surface chemical reactivity, surface dipole interaction, and long-range van der Waals forces. At the molecular level, it was reported that

parameters like polymer backbone planarity, side chain length, conjugation length, and structural transformation energy may influence the conductivity[Hutchison et al. 2005]. The analyte-polymer interaction most likely modulates one or more of these parameters, thus influencing the surface resistivity intrinsic to the thin film polymer. This implies the possibility that multiple sensing mechanisms may act simultaneously. Upon exposure of a specific polymer to a particular analyte, one mechanism most likely dominates, resulting in the measured resistivity change. These polymers may produce a positive response to polar analytes and a negative response to non-polar analytes. One possible explanation is that the dipole–dipole electrostatic force between polar analytes with certain dipole moments and polymer dipolar alkyl side chains can compress the polymer molecules, thus reducing the hopping distance and associated activation energy.

Table 5-1: Specimen designations of polymer/MWCNT stacked sensors prepared by solution drop method, their sensing conditions, and performance at room temperature

Speci. design	Sensing gas	Gas conc. (v/v ppm)	**average $(\triangle R/R)_{max}$ value (%) of eight polymers							
			*S1	S2	S3	S4	S5	S6	S7	S8
C-1	DMMP	453	7.39	7.20	31.37	23.25	0.07	32.50	0.08	1.79
C-2	ACN	(1.5%, v/v)	4.20	9.27	12.34	18.86	0.03	13.88	0.46	1.53
C-3	DCM	(12.4%, v/v)	4.96	13.80	22.79	22.07	0.18	13.88	0.50	2.45
C-4	MEK	1043	0	0	0	0.1	0.15	0	0.10	0
		1849	0.03	0	0.02	0.13	0.18	0	0.11	0
		3130	0.12	0.00	0.10	0.27	0.32	0.00	0.23	0.00
C-5	THF	6781	0.22	0.09	0.29	0.42	0.66	0.00	0.79	0.10
		8346	0.42	0.25	0.50	0.79	1.12	0.00	1.03	0.22
		9748	0.60	0.36	0.83	1.30	1.96	0.00	1.86	0.32
C-6	toluene	884	0.00	0.00	0.21	0.22	0.37	0.00	0.25	0.00
		1447	0.00	0.05	0.15	0.31	0.46	0.00	0.31	0.00
		1540	0.05	0.10	0.18	0.46	0.60	0.00	0.40	0.10
C-7	xylene	354	0.00	0.07	0.13	0.20	0.53	0.00	0.23	0.00
		708	0.10	0.14	0.29	0.51	0.86	0.00	0.40	0.20
		1417	0.15	0.16	0.35	0.62	1.44	0.00	0.60	0.19
C-8	$CHCl_3$	2234	0.07	0.07	0.18	0.23	0.37	0.00	0.29	0.00
		3276	0.16	0.13	0.27	0.40	0.53	0.00	0.45	0.10
		4840	0.22	0.15	0.38	0.62	0.78	0.00	0.73	0.15
C-9	CCl_4	2225	0.00	0.00	0.09	0.14	0.22	0.00	0.15	0.00
		2445	0.00	0.05	0.11	0.21	0.30	0.00	0.25	0.00
		5033	0.08	0.08	0.16	0.30	0.40	0.00	0.31	0.06
C-10	Japanese sake	1.26%, v/v	5.6	1.6	51	59	1.31	9.5	8.6	2.7
		1.31%, v/v	5.7	1.5	52	58	1.3	9.3	8.8	2.7
		1.44%, v/v	5.7	1.8	60	71	1.4	11.3	9	3
		1.57%, v/v	6.3	2	60	72	1.48	12	10	3.3
C-11	Kin-men sorghum	2.88%, v/v	20.5	4.4	99	94	6.1	21.5	28.2	9.9
		2.88%, v/v	19.6	3.8	98	99	5.5	21.2	26.5	9
		3.06%, v/v	29.8	4.8	114	114	6.8	28.3	37.2	13
		3.40%, v/v	30.4	5.9	137	150	6.6	28.5	37	13.7
C-12	medicinal liquor	0.71%	2.4	1.1	34	42	0.4	5.7	4.3	1.5
		0.89%	3	1	31	47	0.7	5.8	4.6	1.6
		1.31%	5.55	1.4	50	71	1.17	9.6	8.7	2.7

Speci. design	Sensing gas	Gas conc. (v/v ppm)	**average $(\triangle R/R)_{max}$ value (%) of eight polymers							
			*S1	S2	S3	S4	S5	S6	S7	S8
		1.41%, v/v	6.7	2	64	82	1.5	11.5	10.2	3.2
C-13	Scotch whisky	2.36%	14	3.4	92	96	3.35	19	24.7	7.1
		2.49%	17	3.6	94	102	3.7	20.3	23	7.7
		2.36%	15	3.3	92	99	3.56	19.2	23	7.3
		2.49%, v/v	17	3.7	97	107	3.9	20.8	22.5	8.1

*the eight sensing polymer materials used in the stacked sensors are corresponding to the polymers listed in Table 3-2.

**the cycling duration times of one cycle to introduce dry air (t_1 = 500 sec), testing gas (t_2 = 300 sec) and dry air (t_3 = 600 sec), respectively.
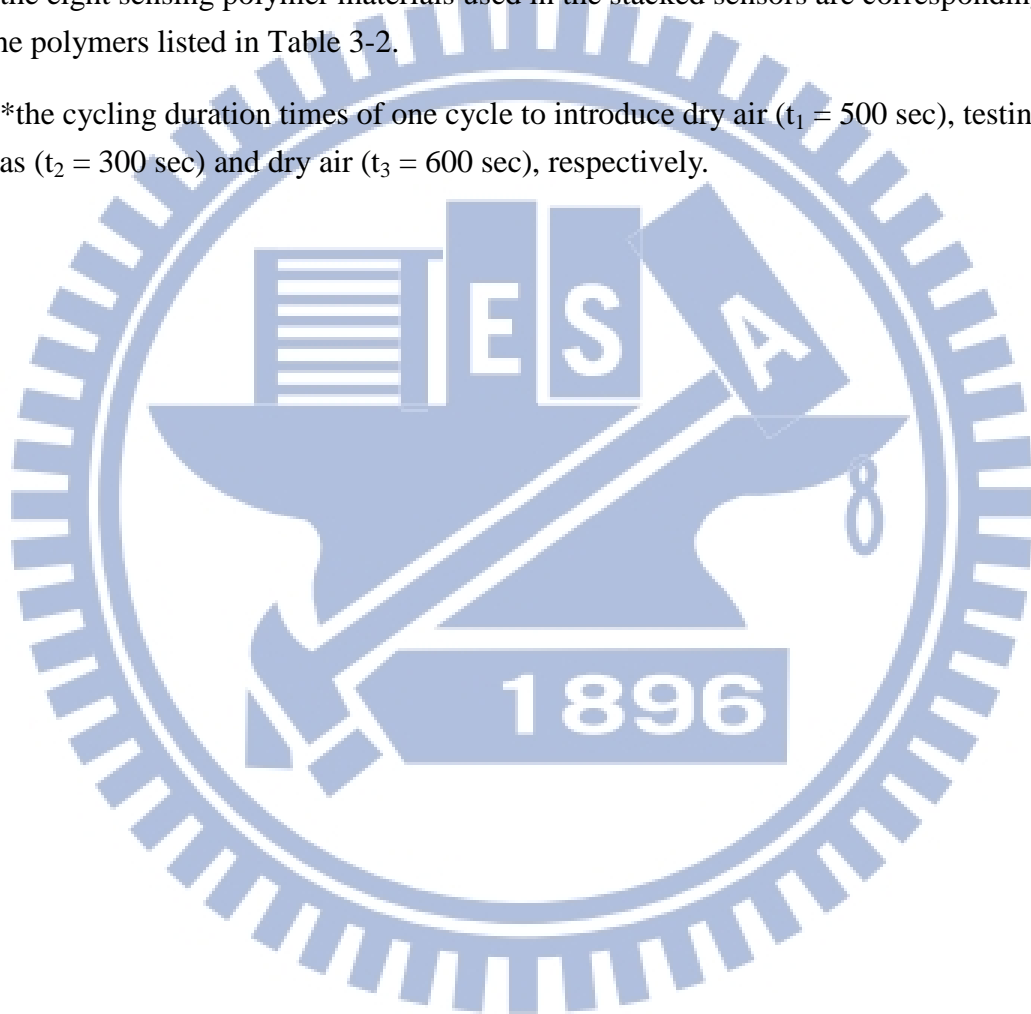
5.4. Gas specificity by mathematical PCA analysis on sensing data

In order to simplify the pattern identification for a great amount of data with PC or laptop, two mathermatical methods were used.. The two approaches were called the principal component analysis (PCA) method and the k-nearest neighbor (k-NN) classification algorithm. The latter method is essentially to show the results in a pocket size computer to reduce the size of the overall sensor system.

Principal component analysis (PCA) is a mathematical procedure that uses an orthogonal transformation to convert a set of observations of possibly correlated variables into a set of values of uncorrelated variables called principal components. The number of principal components is less than or equal to the number of original variables. PCA was invented in 1901 by Karl Pearson[Pearson 1901]. Now it is mostly used as a tool in exploratory data analysis and for making predictive models. The principal component analysis method can reduce a large number of correlated channels (variables) to fewer numbers of independent linear combination variables. This maximizes the component variance obtained through linear combination, and allows the tested gas to show maximum difference among different component channels. Figure 5-24 shows the 2-D PCA plot for sensing responses of eight sensors on a chip to three different gas types (i.e. ACN, DCM and DMMP gases) Therefore, simply glancing at the plots obtained by PCA analysis easily confirms successful classification. Figure 5-25 shows the recognition boundaries of the three simulants in PCA plots displayed with the two main principal PC1 and PC2 axes. The first principal components on the two horizontal axes of Fig. 5-24 show a high cumulative variance of 75.9%.
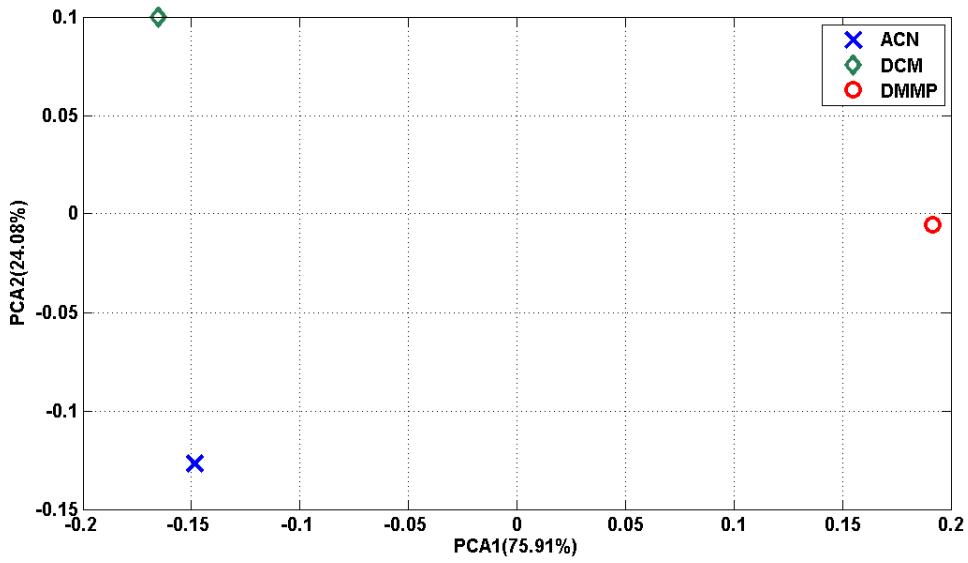
Fig. 5-22 The 2-D PCA plot for sensing responses of eight sensors on a chip to three different gas types (i.e. ACN, DCM and DMMP gases)
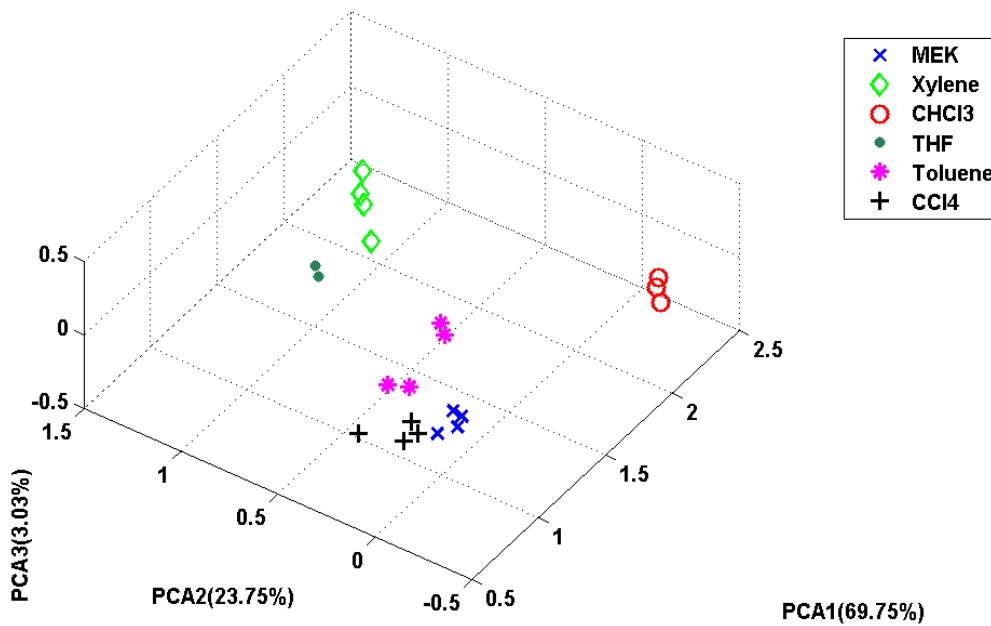
Fig. 5-23 The 3-D PCA plot for sensing responses of eight sensors on a chip to six different gas types (i.e. MEK, THF, toluene, xylene, $CHCl_3$, and CCl_4 gases)

Figure 5-25 shows 3-D PCA plots for six analytes. They clearly demonstrate that

the six tested gases are characterized by their own well-defined boundaries, and that the data scatter around at less three points in each gas boundary is relatively small. In other words, results signify that excellent gas specificity and sensing reproducibility can be achieved for the six tested gases. The first two principal components on the two horizontal axes of Fig. 5-25 show a high cumulative variance of 94.5%.
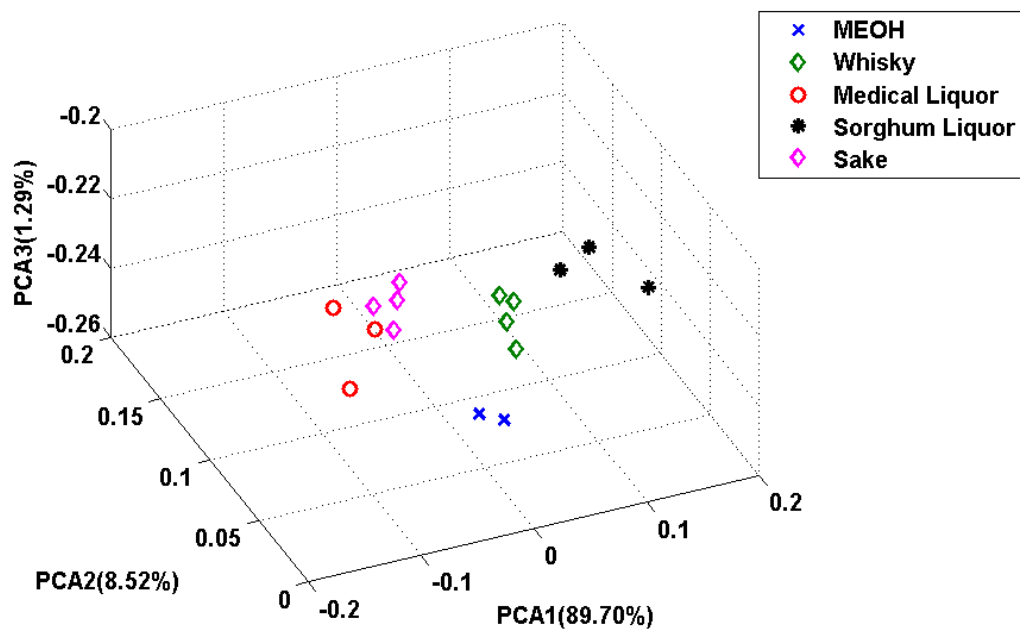
Fig. 5-24 The 3-D PCA plot for sensing responses of eight sensors on a chip to five different gas types (i.e. Japanese sake, Kin men sorghum, medicinal liquor, Scotch whisky and methanol gases)

Figure 5-26 shows 3-D PCA plots for four commercial liquors Japanese sake, Kin men sorghum, medicinal liquor, Scotch whisky and methanol gas. They clearly demonstrate that the five tested gases are characterized by their own well-defined boundaries, and that the data scatter around three points in each gas boundary is relatively small. In other words, results signify that excellent gas specificity and sensing reproducibility can be achieved for the five tested gases. The first two principal components on the two horizontal axes of Fig. 5-26 show a high cumulative variance of 98.22%.

5.5. Performance of sensing chip installed on a portable
E-Nose system

The E-Nose system used for this work was designed in this work by using the k-nearest neighbor algorithm (k-NN). It mainly consists of three major parts: sample delivery, detection and computing systems. The sample delivery system is basically a pumping system to deliver the testing gas into the reaction chamber. The detection system consists of the testing stand with a sensor array chip to record gas sensing response (resistivity variation) value after the desired gas exposure time (generally, 60 s) for each sensor on the chip. The computing system is a data acquisition microprocessor embedded with k-NN classification algorithm to fulfill the size limitation of a portable system, as described in detail elsewhere [Tang et al., 2010]. In others words, the recorded database are used by the computing system to store the sensor radio plots for each sensor and to analyze the gas specificity through k-NN method.

In pattern recognition, the k-nearest neighbor algorithm (k-NN) is a method for classifying objects based on closest training examples in the feature space[Fukunage and Narendra 1975; Keller 1985]. k-NN is a type of instance-based learning, or lazy learning where the function is only approximated locally and all computation is deferred until classification. The k-nearest neighbor algorithm is amongst the simplest of all machine learning algorithms: an object is classified by a majority vote of its neighbors, with the object being assigned to the class most common amongst its k nearest neighbors (k is a positive integer, typically small). If k = 1, then the object is simply assigned to the class of its nearest neighbor. The same method can be used for regression, by simply assigning the property value for the object to be the average of

the values of its k nearest neighbors. The k-nearest neighbor algorithm is sensitive to the local structure of the data. [Bremner et al. 2005] Nearest neighbor rules in effect compute the decision boundary in an implicit manner. It is also possible to compute the decision boundary itself explicitly, and to do so in an efficient manner so that the computational complexity is a function of the boundary complexity. The k-NN algorithm is a classical method of performing the classification task in electronic nose technology. [Blatt et al. 2010; Shaffer et al. 1999] The k-NN voting rule classifies an unlabeled test example by finding the k nearest neighbors and assigning the label of that class represented by a majority among the k neighbors.

The designed E-Nose system is powered by two 9-V batteries and is about $28 \times 18 \times 12$ cm^3 in size and 540 g in weight, as shown in Figs. 5-27(a) and (b) for the whole system and its control panel, respectively.

Fig. 5-25: Optical pictures of a portable E-Nose system: (a) the whole equipment, and (b) its control panel. (P = power On/Off, I = system initialization, S = training/testing mode selection, E = enter)

The performance of this system was used to sense specificity of four commercial liquors (Japanese sake, Kin-men sorghum, medicinal liquor, and Scotch whisky, respectively).   Under system training condition, the sensing experiments of liquor were repeatly conducted ten times to collect the required training database of the system. Under gas testing condition, the gas sensing experiments were conducted 30 times of all the liquors samples. Although the odor patterns for these four liquor odors were alike because of their similar chemical compositions, the portable E-Nose system successfully classified each alcohol odor, verifying the correct operation of the portable E-Nose system.
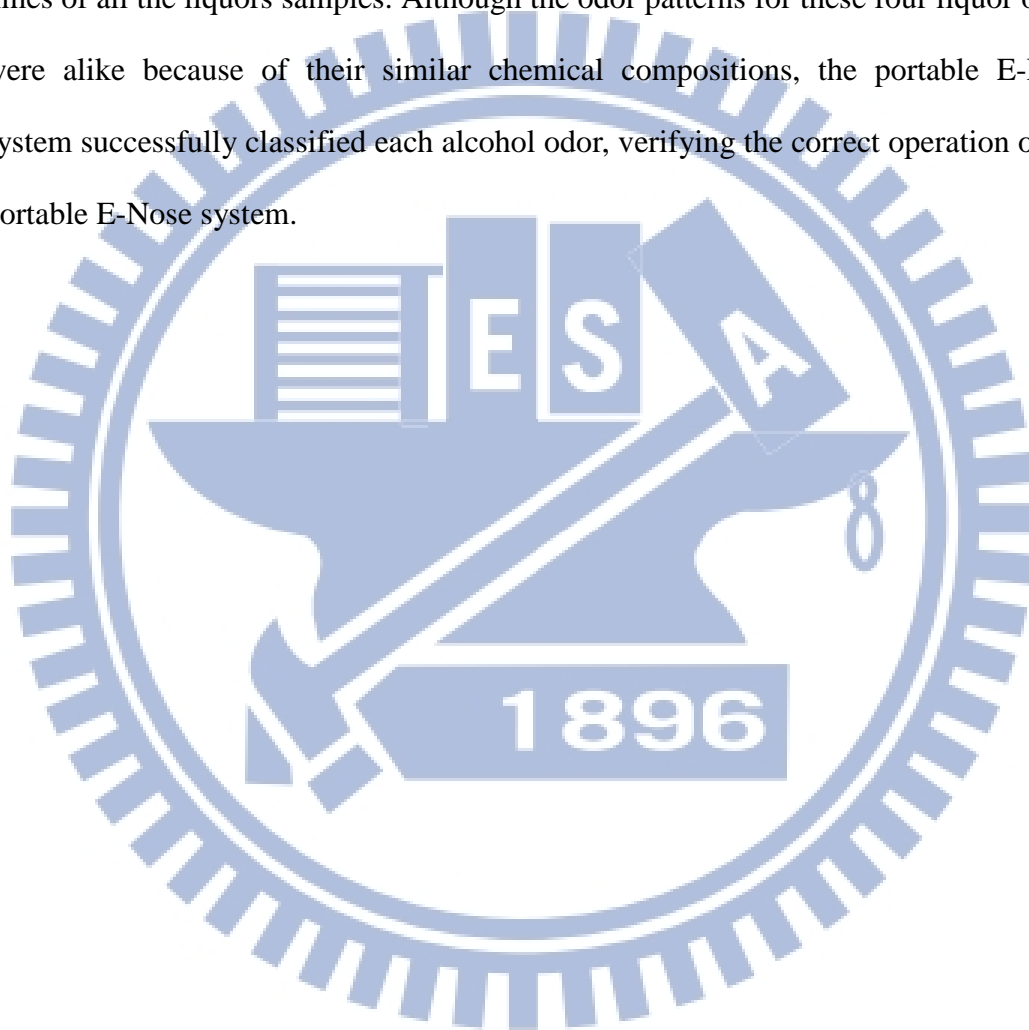
Chapter 6

Conclusions

The thermal CVD-grown MWCNTs powders and the eight different selected polymer types were used as gas sensing materials to develop the sensor chip to sense each of three groups of 14 different analytes at room temperature. The performances of the chips with the composite and the stacked sensors were compared. The chips was also be installed on a gas testing stand to form a portable E-Nose system. From the experimental results, the following conclusions can be drawn.

(a) By comparing the sensors with the MWCNTs+PVP composite and PVP polymer/CNTs stacked sensing configurations, the latter shows a greater gas sensitivity and better device life. This may be due to the fact that the stacked sensors have a polymer overlayer above the MWCNT layer to protect the MWCNTs from direct interaction with the gas.

(b) With one testing run, a chip with eight different stacked sensor types were successfully used to sense the specificity for each of three different groups of gases (six toxic industrial compound gas, three simulants of chemical warfare agents, and four commercial liquor gases) through the radar plot pattern recognition. This is due to the fact that the sensing responses of eight different sensor types can be different for each gas in the group, i.e. forming different radar plot patterns within a gas group. In other words, the radar plot pattern is essentially a fingerprint within the gas group.

(c) The gas sensitivity of the HPMC/MWCNTs stacked sensor could reach the value of the $\triangle R/R)_{max} = 32.5\%$ at room temperature under 453 ppm DMMP gas may suggest that the sensor sensitivity is high enough for general gas concentration

sensing. By monitoring the S/N ratio of the resistance response and carefully controlling the process and environment, the sensitivity can likely be improved.

(d) The PCA and k-NN analysis methods can be a good technique to read the radar plot pattern for a potable sensing system application.

(e) Solution drop casting method was demonstrated to be a good process to simplify the sensor chip fabrication.
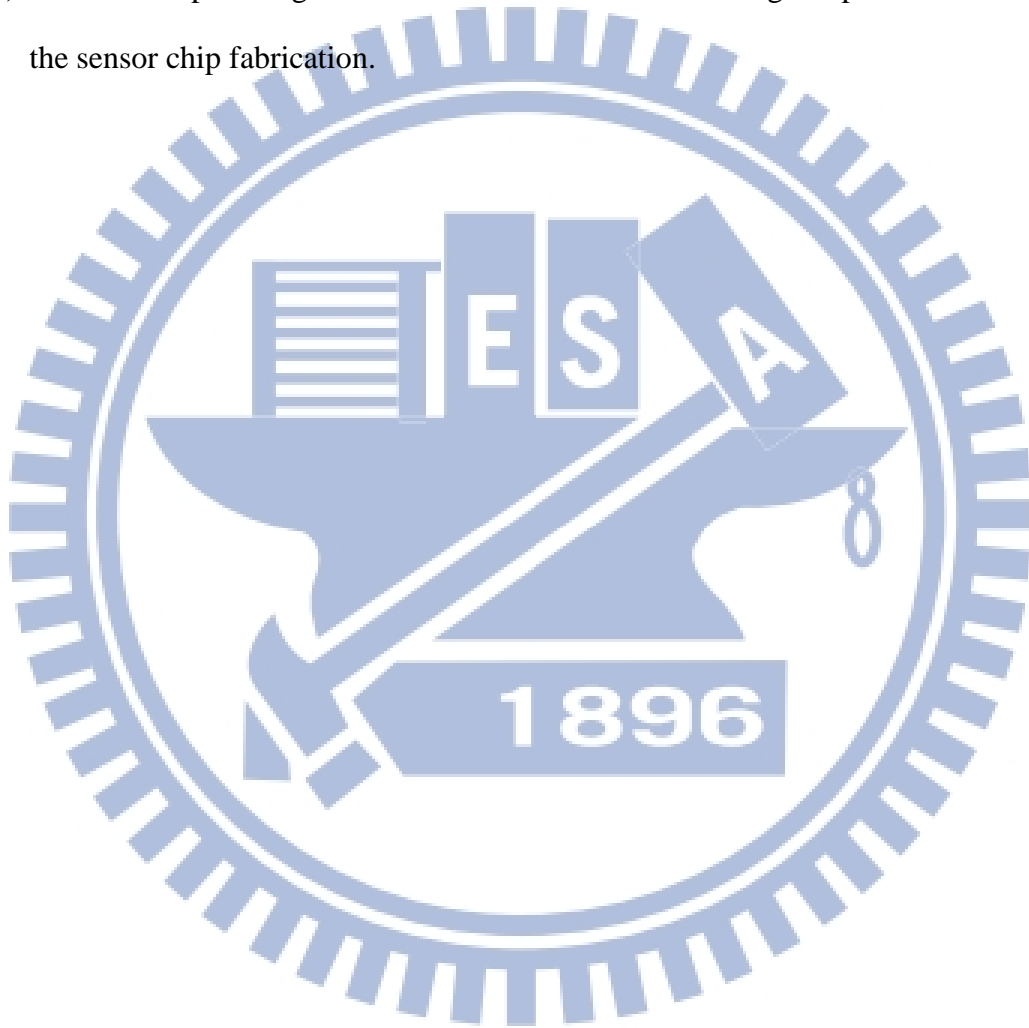
Chapter 7

Future outlooks

Development of sensitive and selective gas sensing systems for the detection of various chemical vapors is necessary, and, to develop a portable, easy-to-use, and durable gas sensing device for on-site monitoring, needs continuous research in the sensing materials, readout circuits, microprocessors, and so on. This dissertation not only exposes the potentials of CNTs on application of gas sensing material, but also explores the factor dominating the polymer/MWCNT stacked film. However, there are some subject should be further studied.

1. This E-Nose system has shown the ability to recognition of each gas through specific algorithm successfully. It could be concluded that there are differences between the reactions of the array sensors to those different gases. As the number of sensor array extended, the pattern of each target gas would be more different to others, the higher identification rate through specific algorithm could be achieved.

2. A conductive polypeptide/MWCNTs composite sensing material by a two layers approach should be done. The idea of exploiting polypeptides as the outer membrane for gas sensing derived from the knowledge of olfactory organ structure. The mucus layer produced by the mucous cells in parts of our body, such as the nose, comprises a lot of substances that play different roles in the olfactory system. The secreted mucous membrane acts to protect the body by creating a barrier and keeping the inside of the body from drying out. Furthermore, it could also facilitate gas exchange and absorption. Starting out

from this concept to adopt biomaterial as our sensing components, we should fabricate a polypeptide-based sensor by a two-step approach.

3.   Even though CNTs are good conductive materials in this chemiresistor gas sensor. However, further study on how to well disperse nano particles like nano gold on carbon nanotube materials should be able to get two advantages together in gas sensing performance.

References

<u>A</u>

1. Abdi, Y., Koohsorkhi, J., Derakhshandeh, J., Mohajerzadeh, S., Hoseinzadegan, H., Robertson, M.D., Bennet, J.C., Wu, X., Radamson, H., 2006. PECVD-grown carbon nanotubes on silicon substrates with a nickel-seeded tip-growth structure. Mater. Sci. Eng. C 26.

2. Albert, K.J., Lewis, N.S., Schauer, C.L., Sotzing, G.A., Stitzel, S.E., Vaid, T.P., Walt, D.R., 2000. Cross-reactive chemical sensor arrays. Chemical Reviews 100(7), 2595-2626.

3. Alig, I., Lellinger, D., Dudkin, S.M., Potschke, P., 2007. Conductivity spectroscopy on melt processed polypropylene-multiwalled carbon nanotube composites: Recovery after shear and crystallization. Polymer 48(4), 1020-1029.

4. Amelinckx, S., Zhang, X.B., Bernaerts, D., Zhang, X.F., Ivanov, V., Nagy, J.B., 1994. A Formation mechanism for catalytically grown helix-shaped graphite nanotubes Science 265, 635.

5. Arshak, K., Moore, E., Lyons, G., Harris, J., Clifford, S., 2004. A review of gas sensors employed in electronic nose applications. Sensor Review 24(2), 181-198.

6. Artzi-Gerlitz, R., Benkstein, K.D., Lahr, D.L., Hertz, J.L., Montgomery, C.B., Bonevich, J.E., Semancik, S., Tarlov, M.J., 2009. Fabrication and gas sensing performance of parallel assemblies of metal oxide nanotubes supported by porous aluminum oxide membranes. Sensors and Actuators B-Chemical 136(1), 257-264.

7. Avouris, P., 2002. Molecular electronics with carbon nanotubes. Accounts of Chemical Research 35(12), 1026-1034.

<u>**B**</u>

1. Baby, R., Cabezas, M., Walsoe de Reca, E., 2000. Electronic nose: a useful tool for monitoring environmental contamination. Sensors and Actuators B: Chemical 69(3), 214-218.

2. Balasubramanian, S., Panigrahi, S., Logue, C., Doetkott, C., Marchello, M., Sherwood, J., 2008. Independent component analysis-processed electronic nose data for predicting Salmonella typhimurium populations in contaminated beef. Food Control 19(3), 236-246.

3. Bartlett, P.N., Blair, N., Gardner, J.W., Assoc Sci Int, C., 1993. ELECTRONIC NOSES - PRINCIPLES, APPLICATIONS AND OUTLOOK.

4. Bernabei, M., Pennazza, G., Santonico, M., Corsi, C., Roscioni, C., Paolesse, R., Di Natale, C., D'Amico, A., 2008. A preliminary study on the possibility to diagnose urinary tract cancers by an electronic nose. Sensors and Actuators B: Chemical 131(1), 1-4.

5. Bethune, D.S., Kiang, C.H., Devries, M.S., Gorman, G., Savoy, R., Vazquez, J., Beyers, R., 1993. Cobalt- Catalysed growth of carbon nanotubes with single-atomic-layer wall. Nature 363, 605.

6. Blatt, R., Bonarini, A., Matteucci, M., 2010. Pattern Classification Techniques for Lung Cancer Diagnosis by an Electronic Nose. Computational Intelligence in Healthcare 4, 397-423.

7. Bower, C., Zhou, O., Zhu, W., Werder, D.J., Jin, S., 2000. Nucleation and growth of carbon nanotubes by microwave plasma chemical vapor deposition. Applied Physics Letters 77, 2767.

8. Bremner, D., Demaine, E., Erickson, J., Iacono, J., Langerman, S., Morin, P., Toussaint, G., 2005. Output-sensitive algorithms for computing nearest-neighbour

decision boundaries. Discrete & Computational Geometry 33(4), 593-604.

9. Buck, L., Axel, R., 1991. A novel multigene family may encode odorant receptors: a molecular basis for odor recognition. Cell 65(1), 175-187.

C

1. Capone, S., Siciliano, P., Quaranta, F., Rella, R., Epifani, M., Vasanelli, L., 2000. Analysis of vapours and foods by means of an electronic nose based on a sol-gel metal oxide sensors array. Sensors and Actuators B: Chemical 69(3), 230-235.

2. Chang, C.P., Chao, C.Y., Huang, J.H., Li, A.K., Hsu, C.S., Lin, M.S., Hsieh, B.R., Su, A.C., 2004. Fluorescent conjugated polymer films as TNT chemosensors. Synthetic Metals 144(3), 297-301.

3. Chang, C.P., Yuan, C.L., 2009. The fabrication of a MWNTs¡Vpolymer composite chemoresistive sensor array to discriminate between chemical toxic agents. Journal of materials science 44(20), 5485-5493.

4. Che, G., Lakshmi, B.B., Fisher, E.R., Martin, C.R., 1998. Carbon nanotubule membranes for electrochemical energy storage and production. Nature 393(6683), 346-349.

5. Chen, P.L., 2005. Anodic aluminum oxide template assisted growth and electron field emission of carbon nanotubes and titnium oxide nanodots. Ph. D. Dissertation, NCTU.

6. Chen, P.L., Chang, J.K., Kuo, C.K., Pan, F.M., 2004. Anodic aluminum oxide template assisted growth of vertically aligned carbon nanotube arrays by ECR-CVD. Diam Relat Mater 13, 1949.

7. Chen, Y., Shaw, D.T., Guo, L., 2000. Field emission of different oriented carbon nanotubes. Applied Physics Letters 76, 2469.

8. Cheung, C.L., Kurtz, A., Park, H., Lieber, C.M., 2002. Diameter-controlled synthesis of carbon nanotubes. The Journal of Physical Chemistry B 106(10), 2429-2433.

9. Choi, G.S., Cho, Y.S., Hong, S.Y., Park, J.B., Son, K.H., Kim, D.J., 2002. Carbon nanotubes synthesized by Ni-assisted atmospheric pressure thermal chemical vapor deposition. Journal of Applied Physics 91, 3847.

10. Choi, K.S., Cho, Y.S., Hong, S.Y., Park, J.B., Kim, D.J., 2001. Effects of ammonia on the alignment of carbon nanotubes in metal-assisted thermal chemical vapor deposition. J. Eur. Ceram. Soc. 21, 2095.

11. Choi, W., Chung, D., Kang, J., Kim, H., Jin, Y., Han, I., Lee, Y., Jung, J., Lee, N., Park, G., 1999. Fully sealed, high-brightness carbon-nanotube field-emission display. Applied Physics Letters 75(20), 3129-3131.

12. Chopra, S., Pham, A., Gaillard, J., Parker, A., Rao, A., 2002. Carbon-nanotube-based resonant-circuit sensor for ammonia. Applied Physics Letters 80, 4632.

13. Collins, P.G., Bradley, K., Ishigami, M., Zettl, A., 2000. Extreme oxygen sensitivity of electronic properties of carbon nanotubes. Science 287(5459), 1801.

14. Craven, M.A., Gardner, J.W., Bartlett, P.N., 1996. Electronic noses - Development and future prospects. Trac-Trends in Analytical Chemistry 15(9), 486-493.

<u>D</u>

1. D'Amico, A., Pennazza, G., Santonico, M., Martinelli, E., Roscioni, C., Galluccio, G., Paolesse, R., Di Natale, C., 2010. An investigation on electronic nose diagnosis of lung cancer. Lung cancer 68(2), 170-176.

2. Dai, H., 2002. Carbon nanotubes: synthesis, integration, and properties. Accounts

of Chemical Research 35(12), 1035-1044.

3. Dai, H., Rinzler, A.G., Nikolaev, P., Thess, A., Colbert, D.T., Smalley, R.E., 1996. Single-wall nanotubes produced by metal-catalyzed disproportionation of carbon monoxide. Chemical Physics Letters 260(3), 471-475.

4. Dekker, C., 1999. Carbon nanotubes as molecular quantum wires. Physics Today 52, 22-30.

5. Delzeit, L., McAninch, I., Cruden, B.A., Hash, D., Chen, B., Han, J., Meyyappan, M., 2002. Growth of multiwall carbon nanotubes in an inductively coupled plasma reactor. Journal of Applied Physics 91(9), 6027.

6. Derycke, V., Martel, R., Appenzeller, J., Avouris, P., 2002. Controlling doping and carrier injection in carbon nanotube transistors. Applied Physics Letters 80, 2773.

7. Doleman, B.J., Severin, E.J., Lewis, N.S., 1998. Trends in odor intensity for human and electronic noses: Relative roles of odorant vapor pressure vs molecularly specific odorant binding. Proceedings of the National Academy of Sciences of the United States of America 95(10), 5442-5447.

8. Dresselhaus, M., Dresselhaus, G., Jorio, A., Souza Filho, A., Saito, R., 2002. Raman spectroscopy on isolated single wall carbon nanotubes* 1. Carbon 40(12), 2043-2061.

9. Dresselhaus, M.S., Dresselhaus, G., Saito, R., Jorio, A., 2005a. Raman spectroscopy of carbon nanotubes. Phys. Rep. 409.

10. Dresselhaus, M.S., Dresselhaus, G., Saito, R., Jorio, A., 2005b. Raman spectroscopy of carbon nanotubes. Physics Reports 409(2), 47-99.

11. Dupuis, A.C., 2005. The catalyst in the CCVD of carbon nanotubes - a review. Prog. Mater. Sci. 50, 929.

12. D'Amico, A., Pennazza, G., Santonico, M., Martinelli, E., Roscioni, C., Galluccio, G., Paolesse, R., Di Natale, C., 2010. An investigation on electronic nose diagnosis of lung cancer. Lung cancer 68(2), 170-176.

F

1. Fan, S., Chapline, M.G., Franklin, N.R., Tombler, T.W., Cassell, A.M., Dai, H., 1999. Self-oriented regular arrays of carbon nanotubes and their field emission properties. Science 283, 512.

2. Fukunage, K., Narendra, P.M., 1975. A branch and bound algorithm for computing k-nearest neighbors. Computers, IEEE Transactions on 100(7), 750-753.

G

1. Gardner, J.W., 2004. Review of conventional electronic noses and their possible application to the detection of explosives. In: Gardner, J.W., Yinon, J. (Eds.), Electronic Noses & Sensors for the Detection of Explosives, pp. 1-28.

2. Gardner, J.W., Bartlett, P.N., 1994. A BRIEF-HISTORY OF ELECTRONIC NOSES. Sensors and Actuators B-Chemical 18(1-3), 211-220.

3. Gardner, J.W., Bartlett, P.N., 1995. Application of conducting polymer technology in microsystems. Sensors and Actuators a-Physical 51(1), 57-66.

4. Gardner, J.W., Bartlett, P.N., Dodd, G.H., Shurmer, H.V., 1987. 8th Int. Congress of European Chemoreception Research Organisation, University of Warwick, UK.

5. Gardner, J.W., Covington, J.A., 2007. Towards an artificial olfactory mucosa for improved odour classification. Proceedings of the Royal Society a-Mathematical Physical and Engineering Sciences 463(2083), 1713-1728.

6. Ge, M., Sattler, K., 1994. Scanning tunneling microscopy of single-shell

nanotubes of carbon. Applied Physics Letters 65(18), 2284.

7. Gomez, A.H., Hu, G., Wang, J., Pereira, A.G., 2006. Evaluation of tomato maturity by electronic nose. Computers and Electronics in Agriculture 54(1), 44-52.

8. Gopel, W., Schierbaum, K.D., 1995. SnO2 sensors: current status and future prospects. Sensors and Actuators B: Chemical 26(1-3), 1-12.

9. Grate, J.W., Kaganove, S.N., Bhethanabotla, V.R., 1998. Comparisons of polymer/gas partition coefficients calculated from responses of thickness shear mode and surface acoustic wave vapor sensors. Analytical Chemistry 70(1), 199-203.

10. Grate, J.W., Patrash, S.J., Abraham, M.H., 1995. Method for estimating polymer-coated acoustic wave vapor sensor responses. Analytical Chemistry 67(13), 2162-2169.

11. Guerin, J., Aguir, K., Bendahan, M., Lambert-Mauriat, C., 2005. Thermal modelling of a WO3 ozone sensor response. Sensors and Actuators B: Chemical 104(2), 289-293.

12. Gulino, G., Vieira, R., Amadou, J., Nguyen, P., Ledoux, M.J., Galvagno, S., Centi, G., Pham-Huu, C., 2005. C2H6 as an active carbon source for a large scale synthesis of carbon nanotubes by chemical vapour deposition. Appl. Cata. A: General 279, 89.

13. Guo, T., Nikolaev, P., Thess, A., Colbert, D.T., Smalley, R.E., 1995. Catalytic growth of single-walled nanotubes by laser vaporization. Chemical Physics Letters 243, 49.

H

1. Hagleitner, C., Hierlemann, A., Lange, D., Kummer, A., Kerness, N., Brand, O.,

Baltes, H., 2001. Smart single-chip gas sensor microsystem. Nature 414(6861), 293-296.

2. Hart, A.J., Boskovic, B.O., Chuang, A.T.H., Golovko, V.B., Robertson, J., Johnson, B.F.G., Slocum, A.H., 2006. Uniform and selective CVD growth of carbon nanotubes and nanofibres on arbitrarily microstructured silicon surfaces. Nanotechnology 17, 1397.

3. Hierlemann, A., Zellers, E.T., Ricco, A.J., 2001. Use of linear solvation energy relationships for modeling responses from polymer-coated acoustic-wave vapor sensors. Analytical Chemistry 73(14), 3458-3466.

4. Hofmann, S., Sharma, R., Ducati, C., Du, G., Mattevi, C., Cepek, C., Cantoro, M., Pisana, S., Parvez, A., Cervantes-Sodi, F., 2007a. In situ observations of catalyst dynamics during surface-bound carbon nanotube nucleation. Nano Letters 7(3), 602-608.

5. Hofmann, S., Sharma, R., Ducati, C., Du, G., Mattevi, C., Cepek, C., Cantoro, M., Pisana, S., Parvez, A., Cervantes-Sodi, F., Ferrari, A.C., Dunin-Borkowski, R., Lizzit, S., Petaccia, L., Goldoni, A., Robertson, J., 2007b. In situ observations of catalyst dynamics during surface-bound carbon nanotube nucleation. Nano Letters 7, 602.

6. Hsu, C.M., Lin, C.H., Chang, H.L., Kuo, C.T., 2002. Growth of the large area horizontally-aligned carbon nanotubes by ECR-CVD. Thin Solid Films 420, 225.

I

1. Iijima, S., 1991. Helical microtubules of graphic carbon. Nature 354, 56.

2. Iijima, S., Ichihashi, T., 1993. Single-shell carbon nanotubes of 1-nm diameter. Nature 363, 603.

<u>J</u>

1. Jorio, A., Pimenta, M., AG Filho, S., Saito, R., Dresselhaus, G., Dresselhaus, M., 2003. Characterizing carbon nanotube samples with resonance Raman scattering. New Journal of Physics 5, 139.

<u>K</u>

1. Kato, T., Jeong, G.H., Hirata, T., Hatakeyama, R., 2004. Structure control of carbon nanotubes using radio-frequency plasma enhanced chemical vapor deposition. Thin Solid Films 457(1), 2.

2. Keller, J.M., 1985. A Fuzzy^-Nearest Neighbor Algorithm JAMES M. KELLER, MICHAEL R. GRAY, and JAMES A. GIVENS, JR. IEEE Transactions on Systems, Man, and Cybernetics 15(4), 581.

3. Kim, Y.S., Ha, S.C., Yang, Y., Kim, Y.J., Cho, S.M., Yang, H., Kim, Y.T., 2005. Portable electronic nose system based on the carbon black-polymer composite sensor array. Sensors and Actuators B: Chemical 108(1-2), 285-291.

4. Kong, J., Franklin, N.R., Zhou, C.W., Chapline, M.G., Peng, S., Cho, K.J., Dai, H.J., 2000. Nanotube molecular wires as chemical sensors. Science 287(5453), 622-625.

5. Kuo, C.T., Lin, C.H., Lo, A.Y., 2003. Feasibility studies of magnetic particle-embedded carbon nanotubes for perpendicular recording media. Diam Relat Mater 12(3-7), 799.

L

1. Lala, N.L., Thavasi, V., Ramakrishna, S., 2009. Preparation of surface adsorbed and impregnated multi-walled carbon nanotube/nylon-6 nanofiber composites and investigation of their gas sensing ability. Sensors 9(1), 86-101.

2. Lamagna, A., Reich, S., Rodriguez, D., Boselli, A., Cicerone, D., 2008. The use of an electronic nose to characterize emissions from a highly polluted river. Sensors and Actuators B: Chemical 131(1), 121-124.

3. Lau, A.K.-T., Hui, D., 2002. The revolutionary creation of new advanced materials-carbon nanotube composites. Comp. Pt. B 33(4), 263.

4. Lee, C.J., Kim, D.W., Lee, T.J., Choi, Y.C., Park, Y.S., Lee, Y.H., Choi, W.B., Lee, N.S., Park, G.S., Kim, J.M., 1999. Synthesis of aligned carbon nanotubes using thermal chemical vapor deposition. Chemical Physics Letters 312, 461.

5. Lee, C.J., Lyu, S.C., Cho, Y.R., Lee, J.H., Cho, K.I., 2001. Diameter-controlled growth of carbon nanotubes using thermal chemical vapor deposition. Chemical Physics Letters 341(3-4), 245.

6. Lee, C.J., Park, J., 2000. Growth model of bamboo-shaped carbon nanotubes by thermal chemical vapor deposition. Applied Physics Letters 77(21), 3397.

7. Lee, W.Y., Liao, T.X., Juang, Z.Y., Tsai, C.H., 2004. Patterned aligned growth of carbon nanotubes on porous structure templates using chemical vapor deposition methods. Diam Relat Mater 13, 1232.

8. Li, J., Lu, Y., Ye, Q., Cinke, M., Han, J., Meyyappan, M., 2003. Carbon nanotube sensors for gas and organic vapor detection. Nano Letters 3(7), 929-933.

9. Lin, C.H., Chang, H.L., Hsu, C.M., Lo, A.Y., Kuo, C.T., 2003. The role of nitrogen in carbon nanotube formation. Diam. Relat. Mater. 12(10-11), 1851.

10. Lin, Y.J., Guo, H.R., Chang, Y.H., Kao, M.T., Wang, H.H., Hong, R.I., 2001.

Application of the electronic nose for uremia diagnosis. Sensors and Actuators B: Chemical 76(1-3), 177-180.

11. Liron, Z., Kaushansky, N., Frishman, G., Kaplan, D., Greenblatt, J., 1997. The polymer-coated SAW sensor as a gravimetric sensor. Analytical Chemistry 69(14), 2848-2854.

12. Lonergan, M.C., Severin, E.J., Doleman, B.J., Beaber, S.A., Grubb, R.H., Lewis, N.S., 1996. Array-based vapor sensing using chemically sensitive, carbon black-polymer resistors. Chemistry of Materials 8(9), 2298-2312.

M

1. Meixner, H., Gerblinger, J., Lampe, U., Fleischer, M., 1995. Thin-film gas sensors based on semiconducting metal oxides. Sensors and Actuators B: Chemical 23(2-3), 119-125.

2. Melechko, A.V., Merkulov, V.I., Lowndes, D.H., Guillorn, M.A., Simpson, M.L., 2002. Transition between 'base' and 'tip' carbon nanofiber growth modes. Chemical Physics Letters 356, 527.

3. Melechko, A.V., Merkulov, V.I., McKnight, T.E., Guillorn, M.A., Klein, K.L., Lowndes, D.H., Simpson, M.L., 2005. Vertically aligned carbon nanofibers and related structures: Controlled synthesis and directed assembly. Journal of Applied Physics 97(4), 041301.

4. Modi, A., Koratkar, N., Lass, E., Wei, B., Ajayan, P.M., 2003. Miniaturized gas ionization sensors using carbon nanotubes. Nature 424(6945), 171-174.

5. Morvan, M., Talou, T., Gaset, A., Beziau, J., 2000. Electronic-nose systems for control quality applications in automotive industry. Sensors and Actuators B: Chemical 69(3), 384-388.

6. Murakami, H., Hirakawa, M., Tanaka, C., Yamakawa, H., 2000. Field emission from well-aligned, patterned, carbon nanotube emitters. Applied Physics Letters 76, 1776.

7. Murugaraj, P., Mainwaring, D., Khelil, N.A., Peng, J.L., Siegele, R., Sawant, P., 2010. The improved electromechanical sensitivity of polymer thin films containing carbon clusters produced in situ by irradiation with metal ions. Carbon 48(15), 4230-4237.

P

1. Pan, Z.W., Xie, S.S., Chang, B.H., Sun, L.F., Zhou, W.Y., Wang, G., 1999. Direct growth of aligned open carbon nanotubes by chemical vapor deposition. Chemical Physics Letters 97, 299.

2. Panigrahi, S., Balasubramanian, S., Gu, H., Logue, C., Marchello, M., 2006. Neural-network-integrated electronic nose system for identification of spoiled beef. LWT-Food Science and Technology 39(2), 135-145.

3. Park, J.H., Park, H.H., Park, T.H., 2010. Cellular engineering for the high-level production of recombinant proteins in mammalian cell systems. Korean Journal of Chemical Engineering 27(4), 1042-1048.

4. Park, Y., Dong, K.Y., Lee, J., Choi, J., Bae, G.N., Ju, B.K., 2009. Development of an ozone gas sensor using single-walled carbon nanotubes. Sensors and Actuators B: Chemical 140(2), 407-411.

5. Pathange, L.P., Mallikarjunan, P., Marini, R.P., O'Keefe, S., Vaughan, D., 2006. Non-destructive evaluation of apple maturity using an electronic nose system. Journal of food engineering 77(4), 1018-1023.

6. Pavlou, A.K., Magan, N., McNulty, C., Jones, J.M., Sharp, D., Brown, J., Turner,

A.P.F., 2002. Use of an electronic nose system for diagnoses of urinary tract infections. Biosensors and Bioelectronics 17(10), 893-899.

7. Pearce, T.C., Schiffman, S.S., Nagle, H.T., Gardner, J.W., 2003. Handbook of machine olfaction: electronic nose technology. Handbook of Machine Olfaction: Electronic Nose Technology, by Tim C. Pearce, Susan S. Schiffman, H. Troy Nagle, Julian W. Gardner, pp. 624. ISBN 3-527-30358-8. Wiley-VCH, February 2003. 1.

8. Pearson, K., 1901. On lines and planes of closest fit to systems of points in space: Phil. Mag 2, 559-572.

9. Penza, M., Alvisi, M., Rossi, R., Serra, E., Paolesse, R., D'Amico, A., Di Natale, C., 2011. Carbon nanotube films as a platform to transduce molecular recognition events in metalloporphyrins. Nanotechnology 22(12).

10. Pillai, S.K., Ray, S.S., Moodley, M., 2007. Purification of single-walled carbon nanotubes. Journal of Nanoscience and Nanotechnology 7, 3011.

11. Postma, H.W.C., Teepen, T., Yao, Z., Grifoni, M., Dekker, C., 2001. Carbon nanotube single-electron transistors at room temperature. Science 293(5527), 76.

R

1. Ren, Z.F., Huang, Z.P., Xu, J.W., Wang, J.H., Bush, P., Siegal, M.P., Provencio, P.N., 1998. Synthesis of large arrays of well-aligned carbon nanotubes on glass. Science 282, 1105.

2. Romero, H., Sumanasekera, G., Mahan, G., Eklund, P., 2002. Thermoelectric power of single-walled carbon nanotube films. Physical Review B 65(20), 205410.

3. Rosenblatt, S., Yaish, Y., Park, J., Gore, J., Sazonova, V., McEuen, P.L., 2002. High performance electrolyte gated carbon nanotube transistors. Nano Letters 2(8), 869-872.

4. Ryan, M.A., Homer, M.L., Buehler, M., Manatt, K.S., Lau, B., Karmon, D., Jackson, S., 1998. Monitoring space shuttle air for selected contaminants using an electronic nose.

5. Ryan, M.A., Lewis, N.S., 2001. Low power, lightweight vapor sensing using arrays of conducting polymer composite chemically-sensitive resistors. Enantiomer 6(2-3), 159-170.

S

1. Saito, R., Dresselhaus, G., Dresselhaus, M.S., 2004. Physical properties of carbon nanotubes. Imperial College Press.

2. Saito, R., Fujita, M., Dresselhaus, G., Dresselhaus, M.S., 1992. Electronic-structure of chiral graphene tubules. Applied Physics Letters 60, 2204.

3. Saito, Y., Nishikubo, K., Kawabata, K., Matsumoto, T., 1996. Carbon nanocapsules and single-layered nanotubes produced with platinum-group metals (Ru, Rh, Pd, Os, Ir, Pt) by arc discharge. Journal of Applied Physics 80, 3062.

4. Satio, Y., 1995. Nanoparticles and filled nanocapsules. Carbon 33, 979.

5. Severin, E.J., Doleman, B.J., Lewis, N.S., 2000. An investigation of the concentration dependence and response to analyte mixtures of carbon black/insulating organic polymer composite vapor detectors. Analytical Chemistry 72(4), 658-668.

6. Shaffer, R.E., Rose-Pehrsson, S.L., McGill, R.A., 1999. A comparison study of chemical sensor array pattern recognition algorithms. Analytica Chimica Acta

384(3), 305-317.

7. Slater, J.M., Paynter, J., Watt, E., 1993. Multi-layer conducting polymer gas sensor arrays for olfactory sensing. Analyst 118(4), 379-384.

8. Snow, E., Novak, J., Campbell, P., Park, D., 2003. Random networks of carbon nanotubes as an electronic material. Applied Physics Letters 82, 2145.

9. Snow, E., Perkins, F., Houser, E., Badescu, S., Reinecke, T., 2005. Chemical detection with a single-walled carbon nanotube capacitor. Science 307(5717), 1942.

10. Sobanski, T., Szczurek, A., Nitsch, K., Licznerski, B., Radwan, W., 2006. Electronic nose applied to automotive fuel qualification. Sensors and Actuators B: Chemical 116(1-2), 207-212.

11. Someya, T., Small, J., Kim, P., Nuckolls, C., Yardley, J.T., 2003. Alcohol vapor sensors based on single-walled carbon nanotube field effect transistors. Nano Letters 3(7), 877-881.

12. Star, A., Joshi, V., Skarupo, S., Thomas, D., Gabriel, J.C.P., 2006. Gas sensor array based on metal-decorated carbon nanotubes. The Journal of Physical Chemistry B 110(42), 21014-21020.

T

1. Tang, H., Yan, M., Zhang, H., Li, S., Ma, X., Wang, M., Yang, D., 2006. A selective NH3 gas sensor based on Fe2O3-ZnO nanocomposites at room temperature. Sensors and Actuators B: Chemical 114(2), 910-915.

2. Tang, K.T., Chiu, S.W., Pan, C.H., Hsieh, H.Y., Liang, Y.S., Liu, S.C., 2010. Development of a Portable Electronic Nose System for the Detection and Classification of Fruity Odors. Sensors 10(10), 9179-9193.

3. Tsai, S.H., Chao, C.W., Lee, C.L., Shih, H.C., 1999. Bias-enhanced nucleation and growth of the aligned carbon nanotubes with open ends under microwave plasma synthesis. Applied Physics Letters 74(23), 3462.

V

1. Valentini, L., Cantalini, C., Armentano, I., Kenny, J.M., Lozzi, L., Santucci, S., 2004. Highly sensitive and selective sensors based on carbon nanotubes thin films for molecular detection. Diam. Relat. Mat. 13(4-8), 1301-1305.
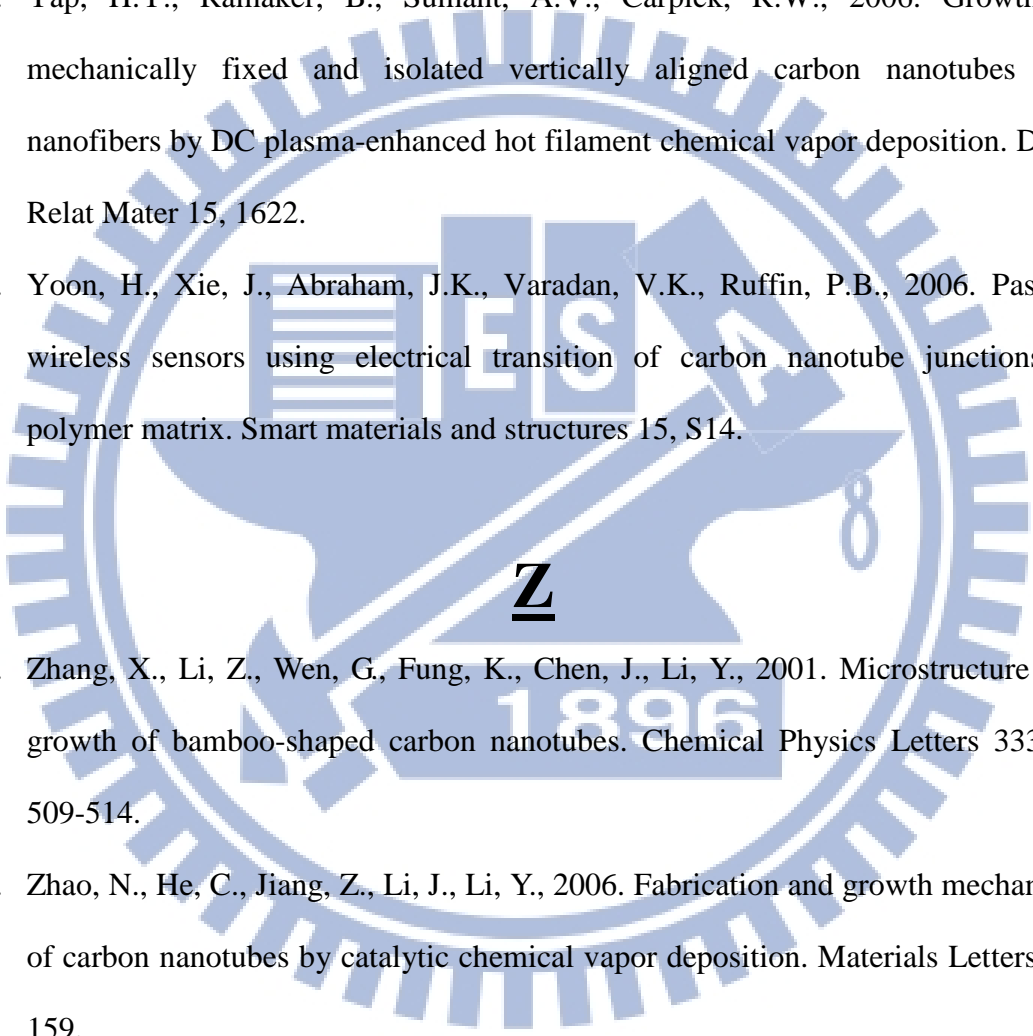
W

1. Wang, L.C., Tang, K.T., Kuo, C.T., Ho, C.L., Lin, S.R., Sung, Y., Chang, C.P., 2010. Portable electronic nose system with chemiresistor sensors to detect and distinguish chemical warfare agents. Journal of Micro-Nanolithography Mems and Moems 9(3).

2. Wei, J., Jiang, B., Zhang, X., Zhu, H., Wu, D., 2003. Raman study on double-walled carbon nanotubes. Chemical Physics Letters 376, 753.

3. Wu, T.M., Lin, Y.W., 2006. Doped polyaniline/multi-walled carbon nanotube composites: Preparation, characterization and properties. Polymer 47(10), 3576-3582.

Y

1. Yamaguchi, N., Yang, M., 2004. Development and evaluation of a micro chemical gas sensor with an inner-circulation diffuser pump. Sensors and Actuators B: Chemical 103(1-2), 369-374.

2. Yang, Q., Bai, S., Fournier, T., Li, F., Wang, G., Cheng, H., Bai, J., 2003. Direct

growth of macroscopic fibers composed of large diameter SWNTs by CVD. Chemical Physics Letters 370(1), 274-279.

3. Yang, Q., Xiao, C., Chen, W., Hirose, A., 2004. Selective growth of diamond and carbon nanostructures by hot filament chemical vapor deposition. Diam Relat Mater 13(3), 433.

4. Yap, H.Y., Ramaker, B., Sumant, A.V., Carpick, R.W., 2006. Growth of mechanically fixed and isolated vertically aligned carbon nanotubes and nanofibers by DC plasma-enhanced hot filament chemical vapor deposition. Diam Relat Mater 15, 1622.

5. Yoon, H., Xie, J., Abraham, J.K., Varadan, V.K., Ruffin, P.B., 2006. Passive wireless sensors using electrical transition of carbon nanotube junctions in polymer matrix. Smart materials and structures 15, S14.

Z

1. Zhang, X., Li, Z., Wen, G., Fung, K., Chen, J., Li, Y., 2001. Microstructure and growth of bamboo-shaped carbon nanotubes. Chemical Physics Letters 333(6), 509-514.

2. Zhao, N., He, C., Jiang, Z., Li, J., Li, Y., 2006. Fabrication and growth mechanism of carbon nanotubes by catalytic chemical vapor deposition. Materials Letters 60, 159.

Vita

姓名：王立群 (Li-Chun Wang)

出生年月日： 民國 62 年 12 月 5 日

聯絡電話：0910678120

通訊住址：桃園縣龍潭鄉民治三街 76 巷 2 號

電子郵件信箱：rubisco@ms28.hinet.net

學歷：

博士：國立交通大學材料科學與工程學系　　民國 93 年 9 月 ~ 民國 101 年 1 月

碩士：國立中山大學化學研究所　　　　　　民國 86 年 9 月 ~ 民國 88 年 6 月

大學：國立成功大學化學系　　　　　　　　民國 82 年 9 月 ~ 民國 86 年 6 月

經歷：

1.　中山科學研究院　化學研究所　　　　　民國 89 年 1 月 ~ 民國 101 年 1 月
　　助理研究員

期刊論文(與本論文相關&已發表者)：

1. **L.C. Wang**, K.T. Tang, C.T. Kuo, C.L. Ho, S.R. Lin, Yuh Sung, C.P. Chang, "A Portable Electronic Nose System with Chemiresistor sensors to detect and distinguish chemical warfare agents", Journal of Micro/Nanolithography, MEMS, and MOEMS (JM3) 9(3) 031010-1~031010-6 (July-Sep 2010).)

2. **L.C. Wang**, K.T. Tang, S.W. Chiu, S.R. Yang, C.T. Kuo, "A Bio-inspired Two-Step Multiple-walled Carbon Nanotubes-Polymer Composite Sensor Array and a Bio-inspired Fast-adaptive Readout Circuit for a Portable Electronic Nose", Biosensors and Bioelectronics, 26 (2011), pp.4301-4307.

3. **L.C. Wang**, I-Ju Teng, C. T. Kuo, C. L. Ho, H. W. Kuo, T. H. Su, K. T. Tang, S. R. Young, G. N. Shi, C. P. Chang, "A single-walled carbon nanotube network gas sensing device", Sensors, 11 (2011), 7763-7772.

期刊論文(與本論文相關&投稿中):

4. **L.C. Wang**, C. T. Kuo, Y. M. Wang, C. L. Ho, H. W. Kuo, T. H. Su, K. T. Tang, S. W. Chu, G. N. Shi, C. P. Chang, "Development a Portable E-Nose System via Nanocomposite Thin Film Sensor Array" , Sensors, (preparing)(2012).

其它期刊論文(與本論文無關)：

1. I-Ju Teng, K. L. Chen, H. L. Hsu, S. R. Jian, **L. C. Wang**, J. H. Chen, W. H. Wang and C. T. Kuo "Highly graphitized laterally interconnected SWCNT network

synthesis via a sandwich-grown method" J. Phys. D: Appl. Phys. 44(2011) 145401

2. S. F. Tang, H. H. Hsieh, H. Y. Tu, T. H. You, S. Y. Lin, **L. C. Wang**, C. D. Chiang, "Investigations for InAs/GaAs multilayered quantum-dot structure treated by high energy proton irradiation", Thin Solid Films 518 (2010) 7425－7428.

3. H. L. Hsu, J. M. Jehng, Yuh Sung, **L. C. Wang**, S. R. Yang, "The synthesis, characterization of oxidized multi-walled carbon nanotubes, and application to surface acoustic wave quartz crystal gas sensor" Materials Chemistry and Physics 109 (2008) 148–155.

4. M. Y. Hsu, S. F. Tang, C. D. Chiang, C. C. Su, **L. C. Wang**, C. T. Kuo, "Optical recombination-emission characteristics and surface morphologies of InAs quantum dots grown on misoriented GaAs substrate by MOCVD", Thin Solid Films 498 (2006) 183－187.

5. I-Ju Teng, H. L. Hsu, S. R. Jian, **L. C. Wang**, K. L. Chen, C. T. Kuo, F. M. Pan, W. H. Wang, J. Y. Juang, "Temperature-dependent electrical and photo-sensing properties of horizontally-oriented CNT networks synthesized by MPCVD sandwich-grown method ", Thin Solid Films (under review).

6. I-Ju Teng, H. L. Hsu, **L. C. Wang**, C. L. Ho, K. L. Chen, S. R. Jian, J. H. Chen, W. H. Wang, C. T. Kuo, "Multifunctional gas sensors based on horizontally-networked CNTs and polymer composites", Nanotechnology (preparing)(2012)

國內期刊論文:
1. 王立群、何政隆、郭瀚文、蘇增雄、王雅梅 "奈米薄膜氣體感測器研製" 工程 84 (2011) 101 - 108

國際研討會論文：
1. I-Ju Teng, H. L. Hsu, S. R. Jian, **L. C. Wang**, K. L. Chen, Terry T. J. Wang, J. H. Chen, W. H. Wang, C. T. Kuo, "Electrical properties and photo-sensing capabilities of laterally networked SWCNTs synthesized by a sandwich-grown method in MPCVD", International Thin Films Conference (2011).

2. I-Ju Teng, **L. C. Wang**, H. L. Hsu, Terry Wang, K. L. Chen, S. R. Jian, C. T. Kuo, "Optical and electrical response of self-assembled single-walled carbon nanotube networks", 37th International Conference on Metallurgical Coatings & Thin Films (2010).

3. **L. C. Wang**, W. D. Chen, C. T. Kuo, Y. Sung, Y. M. Liu, M.D. Ger "Simple and easy method to synthesis very long and high density carbon nanotubes by thermal chemical vapor deposition", TACT International Thin Films Conference, Taipei, Taiwan, Dec. 14-16, 2009

4. I-Ju Teng, H. L. Hsu, **L. C. Wang**, K. L. Chen, C. T. Kuo, "Controlled growth single-walled carbon nanotube networks for electrical and optical applications", TACT International Thin Films Conference, Taipei, Taiwan, Dec. 14-16, 2009.

5. **L. C. Wang**, K. T. Tang, C. T. Kuo, C. L. Ho, S. R. Lin, Y. Sung, C. P. Chang, " A Portable Electronic Nose System with Chemiresistor Sensors to Detect and Distinguish Chemical Warfare Agents", IEEE-Nanomed 2009, Tainan, Taiwan. (EI)

6. **L. C. Wang**, K. T. Tang, C. T. Kuo, S. R. Yang, Y. Sung, H. L. Hsu, J. M. Jehng, "A High-Performance Nanocomposite Material Based on Functionalized Carbon Nanotube and Polymer for Gas Sensing Applications", International Symposium on Olfaction and Electronic Nose (ISOEN 2009), Brescia, Italy. (EI)

7. **L. C. Wang**, K. T. Tang, C. T. Kuo, S. R. Yang, Y. Sung, H. L. Hsu, J. M. Jehng "A High-Performance Nanocomposite Material Based on Functionalized Carbon Nanotube and Polymer for Gas Sensing Applications" AIP Conference Proceeding "Olfaction and Electronic Nose: Proceedings of the 13 International Symposium", 1137 (1) (2009) 369-372. (2009)

8. **L. C. Wang**, I-Ju Teng, K. L. Chen, C. T. Kuo, "A simple manipulation and high performance gas sensor device with single wall carbon nanotube networks", 2nd International Conference on New Diamond and Nano Carbons Conference (2008).

9. **L. C. Wang**, C. T. Kuo, W. D. Chen, M. D. Ger, Y. Sung, Y. M. Liu, "Effects of oxide buffer layers on the catalyst-assisted carbon nanotubes growth by thermal chemical vapor deposition", New Diamond and Nano Carbons(NDNC)conference, Osaka, Japan, 2007 **(Oral)**

專利:

1. 鄭桂忠, 施崇鴻, 王立群, "The electronic nose chip places in respirator to diagnose disease", 美國發明專利, 2011/11/30 申請中。

2. 王立群, 何政隆, 郭瀚文, 蘇增雄 "Conductive polymer composite material and Method for making a conductive polymer composite material", 美國發明專利, 2011/11/30 申請中。

3. 王立群, 何政隆, 郭瀚文, 蘇增雄 "一種製備奈米複合材料薄膜之方式", 中華民國發明專利, 2011/11/30 申請中。

4. 王立群, 何政隆, 郭瀚文, 林孝瑞 "用於偵測氣體之可導電的高分子複合材料元件", 中華民國新型專利, 2011/03/01, 專利證號: M399320

5. 王立群, 何政隆, 郭瀚文, 林孝瑞 "Conductive polymer composite material and Method for making a conductive polymer composite material", 美國發明專利, 2010/06/16 申請中。

6. 王立群, 何政隆, 郭瀚文, 林孝瑞 "可導電之高分子複合材料元件及製造

可導電之高分子複合材料元件的方法”，中華民國發明專利，2010/06/16 申請中。

7. <u>王立群</u>，何政隆，郭瀚文，林孝瑞 “ Method for Fabrication Carbon nanotube, wafer for growing carbon nanotube, and carbon nanotube device ”，美國發明專利，2009/06/30 答辯中。

8. <u>王立群</u>，何政隆，郭瀚文，林孝瑞 “一種成長高準直性奈米碳管膜的方法”，中華民國發明專利，2009/06/30 答辯中。

9. <u>王立群</u>，何政隆，郭瀚文，林孝瑞 “表面聲波氣體感測裝置及其製造方法” 中華民國發明專利，2008/02/16 申請中

10. 劉如熹，王健源，徐敏瑜，<u>王立群</u>，張錦泉，“一種製作夜光磁磚之方法”，中華民國發明專利，2006/02/01. 專利證號:I238154

11. 康佳正，劉如熹，徐敏瑜，王立群，張錦泉，“橘黃色磷光粉體之配方及其製備方法” 中華民國發明專利，2005/08/21. 專利證號:I248463